

For Reference

NOT TO BE TAKEN FROM THIS ROOM

For Reference

NOT TO BE TAKEN FROM THIS ROOM

Ex LIBRIS
UNIVERSITATIS
ALBERTAENSIS



A faint, light-colored watermark of a classical building with four columns and a pediment is visible in the background.

Digitized by the Internet Archive
in 2019 with funding from
University of Alberta Libraries

<https://archive.org/details/Fenton1965>

THE UNIVERSITY OF ALBERTA

MAGNETOACOUSTIC OSCILLATIONS IN METALS

BY

EDWARD WARREN FENTON

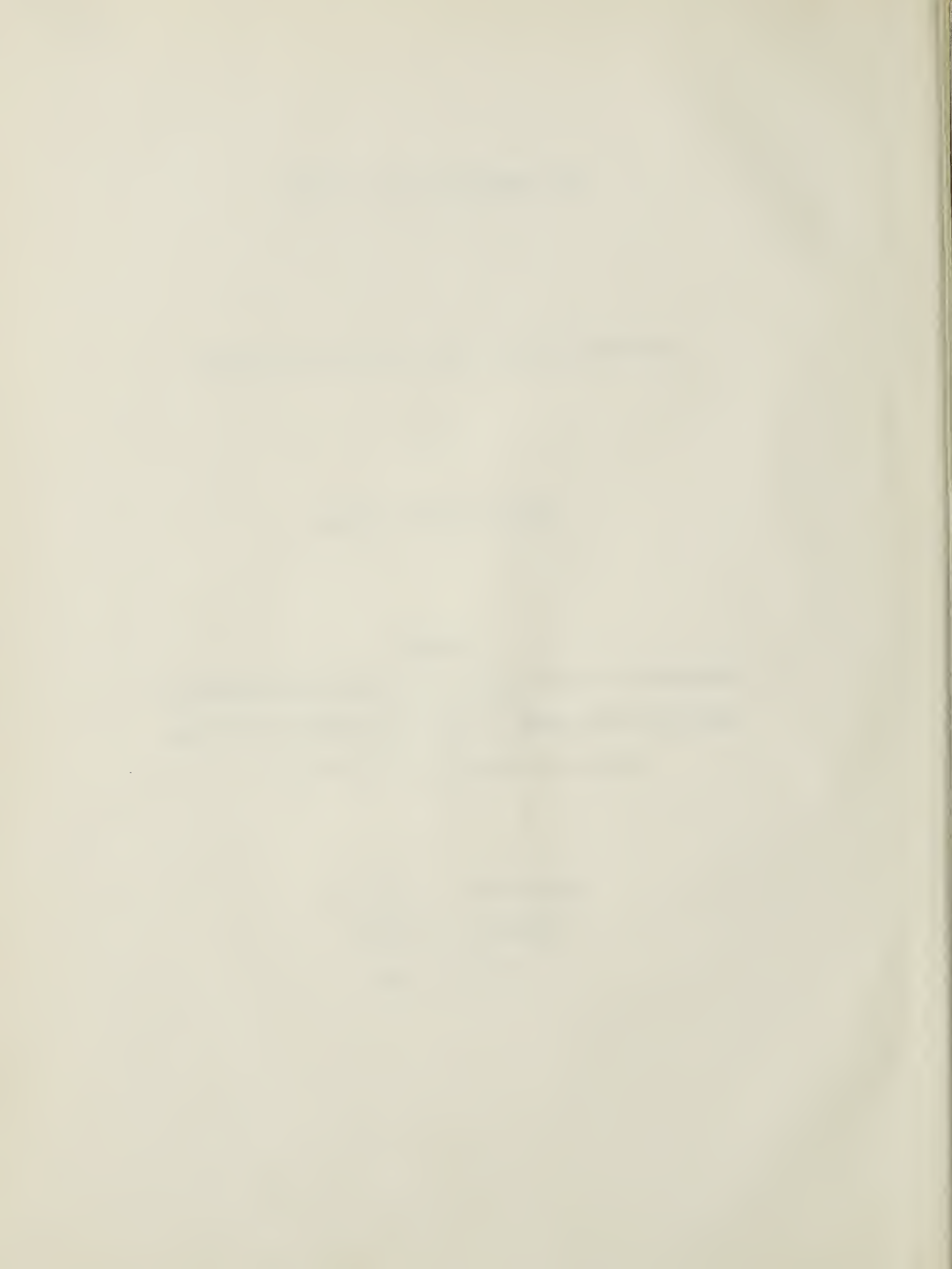
A THESIS

SUBMITTED TO THE FACULTY OF GRADUATE STUDIES IN
PARTIAL FULFILMENT OF THE REQUIREMENTS FOR THE
DEGREE OF DOCTOR OF PHILOSOPHY

DEPARTMENT OF PHYSICS

EDMONTON, ALBERTA

OCTOBER, 1965



UNIVERSITY OF ALBERTA
FACULTY OF GRADUATE STUDIES

The undersigned certify that they have read, and
recommend to the Faculty of Graduate Studies for acceptance,
a thesis entitled "MAGNETOACOUSTIC OSCILLATIONS IN METALS",
submitted by Edward Warren Fenton in partial fulfilment of
the requirements for the degree of Doctor of Philosophy.

ABSTRACT

Oscillations of the ultrasonic attenuation that are periodic in the reciprocal of an applied magnetic field have been observed in copper, magnesium and zinc. In copper, oscillations well known as "geometric oscillations" have been observed at magnetic fields less than five kilogauss. Observations of the geometric oscillations agree in all respects with theory of the effect discussed in the literature. In magnesium and zinc, at magnetic fields between five and twenty kilogauss, quantum oscillations have been observed. The observed amplitude, periodicity, line-shape and temperature dependence of the amplitude of quantum oscillations depend strongly on the relaxation time and mean-free-path of conduction electrons.

The theory of these oscillations is reviewed. For quantum oscillations two cases exist:

- (1) When the relaxation time of the electrons is comparable to or greater than the period of the ultrasonic vibrations, and the mean-free-path of the electrons is several hundred times greater than the ultrasonic wavelength, and
- (2) When the relaxation time of the electrons is much less than the period of the ultrasonic vibrations and the mean-free-path of the electrons is comparable to or somewhat greater than the wavelength of the ultrasound.

In addition intermediate regimes occur. Theory of the first case has been developed to a considerable extent in the literature, however no extensive treatments of the second case have been made.

Quantum oscillations observed in magnesium and zinc correspond to the second case. Discrepancies and agreement between experimental observations and the limited amount of theory which exists are discussed. In addition shortcomings and flaws of the existing theory are noted.

ACKNOWLEDGEMENTS

It is a pleasure to acknowledge the assistance and encouragement of my supervisor, Dr. S. B. Woods, who gave freely of his time despite pressing demands from many other responsibilities.

The assistance of members of the technical staff was invaluable, and in particular I would like to thank Mr. P. Alexander and Mr. H. McClung.

I would like to express my appreciation to both the University of Alberta and the National Research Council of Canada for assistantships and scholarships which made this period of my education possible. In addition it should be mentioned that some of the expenses of the research project were borne by the National Research Council.

TABLE OF CONTENTS

	Page
CHAPTER I. INTRODUCTION	1
CHAPTER II. THEORY OF ELECTRONS IN METALS	2
A. Wave vector space and Brillouin zones	2
B. Electron states in a metal	4
C. The Fermi surface	6
CHAPTER III. EXPERIMENTAL METHODS FOR MAPPING FERMI SURFACES	9
A. The de Haas-van Alphen effect	9
B. The anomalous skin effect	15
C. Cyclotron resonance	19
D. Galvanomagnetic effects	20
CHAPTER IV. THEORY OF MAGNETOACOUSTIC EFFECTS	22
A. Geometric oscillations	23
B. Giant quantum and de Haas-van Alphen oscillations	36
CHAPTER V. APPARATUS AND PROCEDURE	50
A. The cryostat	50
B. The magnet	51
C. Ultrasonic generator and receiver	53
D. Specimen preparation	57
E. Specimen chamber	59

	Page
CHAPTER VI. RESULTS	64
A. Geometric oscillations in copper	64
B. Quantum oscillations in magnesium	72
(i) Periods of the oscillations	73
(ii) Amplitudes of the oscillations	82
(iii) Character of the D-oscillations	87
C. Quantum oscillations in zinc	90
(i) Periods of the oscillations	92
(ii) Amplitudes of the oscillations	96
(iii) Effect of electron spin	106
CHAPTER VII. SUMMARY AND CONCLUSIONS	109
BIBLIOGRAPHY	112

LIST OF FIGURES

	Page
3.1 The de Haas-van Alphen effect.	13
4.1 S_{33} vs. qR (Attenuation for longitudinal waves vs $1/\lambda H$).	34
4.2 S_{11} and S_{22} vs qR (Attenuation for transverse waves vs $1/\lambda H$).	35
4.3 Electron energy levels in a quantizing magnetic field for a parabolic band.	39
5.1 Block diagram of ultrasonic circuitry.	54
5.2 Specimen chamber.	60
5.3 Tuned circuit in specimen chamber.	62
6.1 Echo amplitude vs. magnetic field for "dog's bone" orbit.	66
6.2 Echo amplitude vs. magnetic field for central body orbit.	67
6.3 Extremal orbits of the Fermi surface of copper.	69
6.4 Absorption extrema vs. magnetic field for the "dog's bone" orbit.	70
6.5 Absorption extrema vs. magnetic field for the central body orbit.	71
6.6 Chart recording of the acoustic attenuation in magnesium.	74
6.7 Chart recording of the acoustic attenuation in magnesium.	75
6.8 Chart recording of the acoustic attenuation in magnesium.	76

	Page
6.9 Periods of the B-oscillations in magnesium.	78
6.10 Periods of the D-oscillations in magnesium.	79
6.11 Periods of the A, B and C-oscillations in magnesium.	80
6.12 Fermi surface of magnesium.	81
6.13 α/T vs. T (B-oscillation).	83
6.14 α vs. T (D-oscillation).	86
6.15 Fermi surface of divalent hexagonal close-packed metal in the second band when spin-orbit coupling is taken into account.	89
6.16 Chart recording of the acoustic attenuation in zinc.	93
6.17 Chart recording of the acoustic attenuation in zinc.	94
6.18 Chart recording of the acoustic attenuation in zinc.	95
6.19 Periods of the A-oscillations in zinc.	97
6.20 Periods of the B-oscillations in zinc.	98
6.21 Periods of the C-oscillations in zinc.	99
6.22 Fermi surface of zinc.	100
6.23 Dependence of amplitude on angle θ between \bar{q} and \bar{H} .	103
6.24 α/T vs. T .	107

CHAPTER I

INTRODUCTION

During the past decade, to facilitate description of electron behaviour in metals, alloys and semiconductors, one of the major tasks of solid state physics has been investigation of Fermi surface topology. There are many methods of obtaining such information, and since 1959 studies of the absorption of ultrasound in the presence of magnetic fields have been important in this regard. More recently, quantum oscillations of absorption in magnetic fields have yielded additional information with respect to effective masses and g-factors of electrons, and hold promise of important information concerning electron-phonon interactions.

The original motivation for the work described in this thesis was the possibility of obtaining Fermi surface information by studying ultrasonic absorption. It has since been found that the most important results obtained have not been Fermi surface measurements but have been in connection with quantum effects in the absorption mechanism. There are few published results concerning these effects, the theory is in an unsatisfactory state, and the phenomena are thus poorly understood and a fruitful field for research.

CHAPTER II

THEORY OF ELECTRONS IN METALSA. Wave Vector Space and Brillouin Zones

The study of the motion of an electron in a periodic potential has led to the recognition that electrons must be in certain quantum states. To each quantum state there corresponds a wave function and one direction of spin. To characterize the wave function a set of three quantum numbers is sufficient. The three quantum numbers can be considered as three components of a wave-vector, and the two possible spin directions can be described by means of a fourth quantum number. The study of the motion of an electron then becomes a study of the probability of the electron going from one quantum state to another. For a collection of such electrons the distribution among available quantum states must be considered. This leads to the definition of a wave vector space which, for each crystal structure, is found to be divided into a set of Brillouin zones. In each zone the electron energy E is a quasi-continuous function of the wave vector. The boundary of each zone consists of a number of planes where E experiences a discontinuity. These planes are defined by the points in wave-vector

space where the electrons experience Bragg reflection#. The region cut off by those planes nearest to the origin is called the first Brillouin zone and is simply connected. The second Brillouin zone is made up of several smaller regions lying immediately outside the first zone, so as to just cover all its faces. The third zone then covers all exterior faces of the second zone, and can have contact with the first zone only along lines and not across surfaces. The Brillouin zones constructed by this process are unique.

Brillouin zones above the first can be represented by a "folded-in" scheme in which segments of a particular zone are displaced in k -space so that a zone identical to the first is formed. This process corresponds to the fact that an electron in some segment of a higher zone will be reflected at the outer boundaries of the zone such that the wave vector \bar{k} becomes $-\bar{k}$, which will place the electron in the opposite segment of the same zone. The energy of the electron remains unchanged in the reflection, and the process can be visualized as a continuous trajectory through the folded-in zone.

#NOTE: The structure factor familiar from the theory of X-rays in crystals may be zero for a particular plane. However in real metals there is still a Bragg reflection since the electron wave functions are never plane waves.

There are only fourteen types of Brillouin zones for electrons, as for phonons, corresponding to the fourteen Bravais lattices, though if the lattice has a basis, symmetry may lead to zones "sticking together" in pairs, as in the hexagonal close-packed structure.

B. Electron States in a Metal

An electron will be described by a wave packet rather than by a single plane wave even when there is no crystalline field. This wave packet has extensions Δx_i in real space and Δk_i in wave-vector space which satisfy Heisenberg's uncertainty principle $\Delta x_i \Delta k_i \geq 1/2$. Omitting the spin, and if the wave function $\psi_{\bar{k}}(\bar{r})$ is associated with the quantum state \bar{k} , the wave function $\psi(\bar{r})$ of a particular electron is

$$\psi(\bar{r}) = \int g(\bar{k}) \psi_{\bar{k}}(\bar{r}) d^3\bar{k} \quad (2.1)$$

The integration is carried out over the entire wave vector space. The integrand is non-zero only over a region of order Δk_i and vanishes everywhere else. The function $g(\bar{k})$ is a normalized distribution function which gives the probability of finding the electron in the particular quantum

state \bar{k} . The set of functions $\psi_{\bar{k}}(\bar{r})$ are orthonormal and complete. Therefore

$$g(\bar{k}) = \int \psi_{\bar{k}}(\bar{r}) \psi_{\bar{k}}^*(\bar{r}) d^3\bar{r} \quad (2.2)$$

Integration is over the entire volume of the crystal, but the integrand is non-vanishing only over a region of order Δx_i . The quantity $\bar{p} = \hbar \bar{k}$, which is often referred to as the momentum of an electron in a crystal, has all the properties of the wave-vector, that is those of a set of good quantum numbers, but is not the actual momentum of an electron. \bar{p} satisfies the equation $\frac{d\bar{p}}{dt} = \bar{F}$ where \bar{F} is the externally applied force, which outside the crystal would be identical with Newton's law of motion, but in the crystal it is not. The momentum is obtained by applying the momentum operator to the wave function of the electron, yielding a result different from \bar{p} . However during interactions in the crystal the quantity \bar{p} is conserved, and may be referred to as the quasi-momentum.

The group velocity v_g of the wave $\psi(\bar{r})$ is obtained from the average derivative of the frequency of the wave with respect to the wave vector

$$\bar{v}_g = \left\langle \frac{d\omega}{d\bar{k}} \right\rangle \quad (2.3)$$

Since the energy E of an electron is $\hbar\omega$,

$$\bar{v}_g = \frac{1}{\hbar} \left\langle \frac{dE}{dk} \right\rangle \quad (2.4)$$

The group velocity is the velocity of the wave packet describing the electron, and so is actually the average velocity of the electron.

C. The Fermi Surface

Instead of considering the individual electrons of a crystal, each of which is described by a complicated wave packet, it is much easier to consider the individual quantum states \bar{k} . In this case the important factors are the average degree of occupancy f of a given quantum state, and the way in which f is influenced by external forces. f is not directly a function of \bar{k} , but is a universal function of the energy $E(\bar{k})$, called the Fermi-Dirac distribution function:

$$f(E) = \frac{1}{1 + e^{(E - E_f)/kT}} \quad (2.5)$$

Here E_f is the Fermi energy, and $f(E)$ can vary only between 1 and 0, these limits encompassing states that are on the average always occupied to always unoccupied.

At $T = 0$, in the ground state of the system all quantum states with energy less than the Fermi energy will be occupied and all those with greater energies will be unoccupied. At temperatures above zero the distribution function will be similar except for a region of width $\sim kT$ centred at the Fermi energy. The distribution will no longer be a step function but will change smoothly from 1 to 0 in this region. In a metal, at temperatures of a few hundred degrees or less the region will be very narrow in comparison to the Fermi energy.

At low temperatures ($kT \ll E_f$) only those electrons very near the Fermi surface can participate in interactions where the energy gained or lost is considerably less than the Fermi energy. With the exception of electron-electron interactions this is almost always the case. A great deal of theoretical work has been done in the last decade which shows that electron-electron interactions do not seriously limit the one-electron theory. Thus the topology of the Fermi surface is an important factor in determining transport properties of metals.

Since the electron energy E is a function of the wave vector \vec{k} , in general E_f is a function of direction in wave vector space as well as of $|k|$. In addition discontinuities

in energy occur at the Brillouin zone boundaries in \bar{k} -space, and the Fermi surface may separate into several sheets, each contained within a particular Brillouin zone.

In discussing the topology of Fermi surfaces, it is convenient to think of the energy surfaces $E(\bar{k})$ in each band as extending periodically through the whole of \bar{k} -space, and not simply confined within a Brillouin zone centred about $\bar{k} = 0$. Thus each Brillouin zone may be regarded as repeated periodically to fill \bar{k} -space completely, so that when an electron approaches the boundary of a zone it passes through into the adjacent repetition of the same zone, corresponding to Bragg reflection of the electron to the opposite boundary.

If a given sheet of the Fermi surface lies entirely within the boundaries of a zone, it must clearly form a closed surface. If it consists of sections localized on separate zone faces or around separate corners, these sections will again combine in the extended zone scheme to form simple closed surfaces, containing electrons or holes. But if sections extend from one face of the zone to another, or from one corner to another, the resultant structure in the extended zone scheme will be a multiply connected or open surface which extends throughout \bar{k} -space.

CHAPTER III

EXPERIMENTAL METHODS FOR MAPPING FERMI SURFACES

In this chapter four methods of making Fermi surface measurements, exclusive of measurements of ultrasonic absorption, will be discussed briefly.

A. The De Haas-Van Alphen Effect

The de Haas-van Alphen effect was discovered during experiments measuring the magnetic susceptibility of single crystals of bismuth at liquid helium temperatures¹. Since that time the characteristic oscillatory variations with magnetic field have been used extensively for Fermi surface measurements. The theoretical basis of the effect will be described below.

In a magnetic field, the electrons of a single crystal will travel on a surface of constant energy in \bar{k} -space. Due to quantization of the generalized angular momentum (actually the quasi-momentum), allowable momentum states will not be the same as those when the field is not present, and in fact decrease in number and increase in degeneracy as the field increases. As shown by Onsager², if

the field is in the z -direction, then the allowed orbits in \vec{k} -space are those for which A , the area of the orbit in the k_x - k_y plane, is given by

$$A = (n + \gamma) 2\pi eH/\hbar c \quad (3.1)$$

where n is an integer and γ is an undetermined phase factor.

If we consider the case of an empty lattice (for which the Fermi surface is a sphere), in a magnetic field the allowable states occur on a discrete set of cylinders with a common axis in the k_z -direction. Each of the quantized states is of such degeneracy that the total number of states previously available within the Fermi surface is now available on the cylinders and within the confines of the same Fermi surface.

The total energy W of the electrons is given by

$$\begin{aligned} W &= \int_{-\infty}^{\infty} \sum_n \left(\frac{2\pi eH}{\hbar c} \right) E_n(H, k_z) \frac{(2v dk_z)}{(2\pi)^3} \\ &= \frac{eHv}{2\pi^2 \hbar c} \int_{-\infty}^{\infty} \sum_n E_n(H, k_z) dk_z \end{aligned} \quad (3.2)$$

E_n is the energy of the n^{th} permitted state given H and k_z , and v is the volume of the metal. The factor $2\pi eH/\hbar c$, which

is the area between permitted orbits, when multiplied by $2\pi dk_z/(2\pi)^3$ gives the number of states for a given H , k_z . The upper limit of the summation is determined by the fact that $E_n(H, k_z) < E_f$.

As H increases, a term drops out of the integrand whenever successive $E_n(H, k_z)$ become equal to E_f , or whenever $A_n(E_n)$ equals $A(E_f)$. Consider the magnetic field H_1 , which makes $A_n(E_n)$ equal to $A(E_f)$. Then

$$A_n(E_n, H_1, k_z) = (n + \gamma)2\pi e H_1 / \hbar c \quad (3.3)$$

Then if H_2 makes $A_{n-1}(E_{n-1})$ equal to $A(E_f)$,

$$A_{n-1}(E_{n-1}, H_2, k_z) = (n - 1 + \gamma)2\pi e H_2 / \hbar c \quad (3.4)$$

Then equating left hand sides,

$$\Delta\left(\frac{1}{H}\right) = \frac{1}{H_1} - \frac{1}{H_2} = \frac{2\pi e}{\hbar c A(E_f, 0, k_z)} \quad (3.5)$$

if we assume that $A(E_f, 0, k_z) = A(E_f, H, k_z)$, which is valid for magnetic fields which can be realized experimentally.

The integrand of equation 3.2 then has discontinuities spaced $\Delta\left(\frac{1}{H}\right)$ apart, and the energy W will in general be an oscillatory function of H .

Consider the Fermi surface of a real metal. As H increases, the cylinders in \bar{k} -space containing the permissible orbits will expand. The expansion of most of the cylinders will vary W only smoothly, as the only change is a smooth variation of the z -extension of the cylinder contained within the Fermi surface. There are just two conditions for which expansion of a cylinder can cause a discontinuity in the integrand of equation 3.2. Either the tube is tangent to a minimum cross-section of the Fermi surface, in which case the cylinder splits into two cylinders, or it is tangent to a maximum cross section of the Fermi surface, in which case the cylinder vanishes entirely. (See Figure 3.1). If one of these extremal cross sections is denoted by A' , then W , and therefore $\chi = -\partial^2 W / \partial H^2$ will oscillate with period $\Delta(\frac{1}{H})$ given by

$$\Delta(\frac{1}{H}) = \frac{2\pi e}{\hbar c A'} \quad (3.6)$$

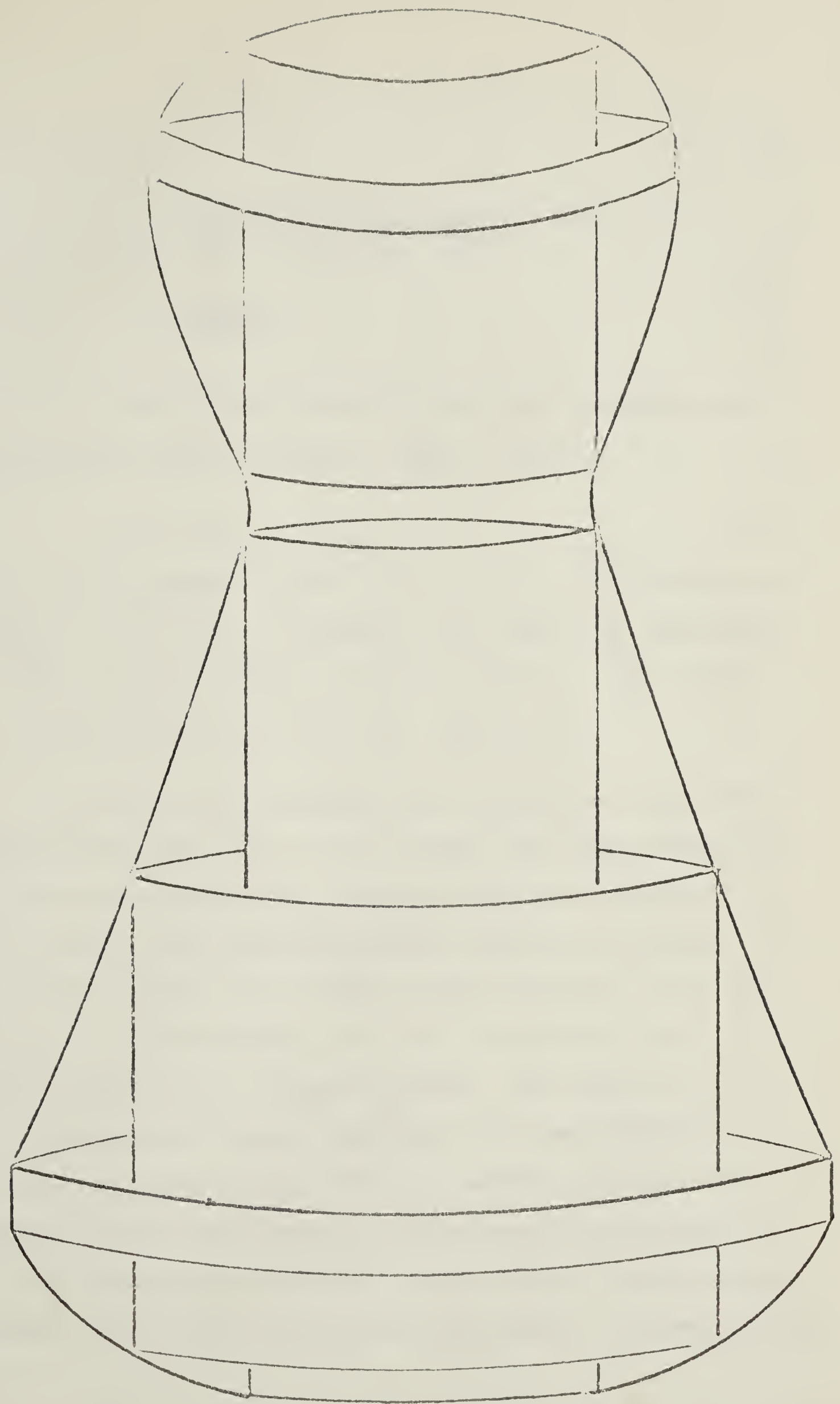
If several extremal cross sections exist for a given crystal orientation, then χ will oscillate with several periods which will beat with each other.

The difference in energy $E_n - E_{n-1}$ when A is near A' is given approximately by

FIGURE 3.1

The de Haas-van Alphen Effect

The two cylinders at the local maxima of the cross-sectional area will disappear with increasing magnetic field. The minimum in the cross-sectional area of the Fermi surface has just caused one cylinder to break into two.



$$\begin{aligned}\Delta E &= \frac{dE(A')}{dA} \Delta A = \frac{2\pi eH}{\hbar c} \frac{dE(A')}{dA} \\ &= \frac{eH\hbar}{m^*(A')c}\end{aligned}\quad (3.7)$$

where m^* is the effective mass of electrons averaged over the cyclotron orbit. Since $\omega_c = \frac{eH}{m^*c}$, then

$$\Delta E = \hbar\omega_c \quad (3.8)$$

For $H = 30$ kilogauss, and $m^* = m$, $\omega_c \approx 5 \times 10^{11}$ radians/sec, and $\hbar\omega_c \approx 4 \times 10^{-3}$ ev. Evidently then there are approximately 10^3 cylinders within the Fermi sphere at this field and the oscillations will be very rapid in H .

In the above analysis the temperature T has been assumed to be zero. If T is not zero, but large enough so that kT is approaching $\hbar\omega_c$, then as the cross sectional area A' of an orbit increases with H through a somewhat fuzzy Fermi surface, the change in the integrand of W will no longer be discontinuous, but will nevertheless be markedly great if T is small enough. The period of W will be unaffected but the amplitude will be reduced as the temperature is raised. For the magnetic field of 30 kilogauss quoted above, $\hbar\omega_c$ is approximately equivalent to 5^0K , and quite clearly fields of this order of magnitude are necessary so that $kT \ll \hbar\omega_c$ may be satisfied, and oscillations occur.

One expects the amplitude of the oscillations of χ ($= \frac{\partial^2 F}{\partial H^2}$ for $T \neq 0$, where F is the free energy) to depend on

$\frac{kT}{\hbar\omega} = \frac{kTm^*(A')c}{eH\hbar}$. Lifshitz and Kosevich³ have shown this to be true, and find for the oscillatory variation of F

$$F_{\text{osc}} \propto TH^{3/2} \cos[(\hbar c A' / eH) + \delta] e^{-[2\pi^2 kTm^*(A')c / eH\hbar]} \quad (3.9)$$

Thus from measurements of the period $\Delta(\frac{1}{H})$ of the oscillations of χ , the extremal cross-sections A' of the Fermi surface can be determined, and from the variation of the amplitude with temperature, $m^*(A')$ or $\frac{dA'}{dE}$ can be deduced. To achieve the results experimentally, the procedure must be carried out at liquid helium temperatures, and the specimens must be sufficiently pure so that the mean free path of the electrons is much longer than the cyclotron orbit, or $\omega_c \tau > 1$, where τ is the relaxation time of the electrons.

B. The Anomalous Skin Effect

Consider the surface of an infinite slab of an isotropic metal, with the surface of the metal as the x-y plane. Current is induced by an electric field of frequency ω , plane polarized in the x-direction and normal to the surface of the metal. If electrons which collide with the surface

of the metal are reflected with k_x and k_y unchanged, and k_z replaced by $-k_z$, Pippard⁴ has shown that the surface impedance Z in the x -direction is given by

$$Z = 8i\omega \int_0^\infty \frac{dv}{v^2 + 4\pi i\omega\sigma(v)} \quad (3.10)$$

The conductivity is defined by

$$J_\nu = \sigma(v) \mathcal{E}_\nu$$

and \mathcal{E}_ν and J_ν are the Fourier components of $\mathcal{E}(Z)$ and the current density $J(Z)$ (both in the x -direction).

$$\mathcal{E}(Z) = \int_{-\infty}^{\infty} \mathcal{E}_\nu e^{i\nu Z} dv$$

and

$$J(Z) = \int_{-\infty}^{\infty} J_\nu e^{i\nu Z} dv$$

If the mean free path ℓ of the electrons is very short the only values of v which contribute appreciably to Z are those for which $v\ell \ll 1$. In this case $\sigma(v)$ is constant over the range with a value equal to the direct current conductivity σ , and the normal skin effect is obtained:

$$Z_n = (1 + i) \sqrt{2\pi \omega/\sigma} \quad (3.11)$$

If the mean free path of the electrons is long enough so that $v\ell \gg 1$, then as shown by Pippard

$$\sigma(v) = \frac{e^2}{4\pi^2 \hbar v} \int R(k_y) dk_y \quad (3.12)$$

$R(k_y)$ and the range of integration are determined as follows. Consider the curve formed by the intersection of the Fermi surface $E(\vec{k}) = E_f$ and a plane normal to k_y . $R(k_y)$ is the sum of the absolute values of the radii of curvature of all points on this curve where the tangent is parallel to the k_z axis. The minimum and maximum values k_y are given by the extremities of the Fermi surface in the k_y direction. In this case, if $v\ell \rightarrow \infty$ (the extreme anomalous limit), Z is given by

$$Z = 8i\omega \int_0^\infty \frac{v dv}{v^3 + is^3} \quad , \quad (3.13)$$

where

$$s = \frac{\omega e^2}{\pi \hbar} \int R(k_y) dk_y \quad . \quad (3.14)$$

Equation 3.13 can be integrated to give

$$Z_\infty = \frac{8\pi\omega}{3^{3/2} s} (1 + i\sqrt{3}) \quad . \quad (3.15)$$

As shown by Reuter and Sondheimer⁵, assuming completely diffuse scattering at the metal surface, instead of the specular reflection considered above, leads to

$$Z = \frac{4\pi^2 i \omega}{\int_0^\infty \ln [1 + 4\pi i \omega \sigma(v)] dv} \quad (3.16)$$

and in the extreme anomalous limit

$$Z_\infty = \frac{\sqrt{3}\pi\omega}{s} (1 + i\sqrt{3}) \quad (3.17)$$

The impedances given by expressions for the two types of reflection differ by a factor of 9/8. In either case Z depends only on the frequency of the applied electric field and the geometry of the Fermi surface.

Measurement of Z for a variety of crystal orientations provides $\int R(k_y) dk_y$. Reconstruction of the Fermi surface from a knowledge of this integral is not usually possible, and the anomalous skin effect is used as a tool for checking Fermi surface models derived by other means.

To achieve anomalous conditions experimentally, liquid helium temperatures and microwave frequencies must be used. Specimens must be sufficiently pure to insure that impurity scattering does not limit the mean free path of the electrons to the classical region (ℓ must be greater than the classical skin depth) and surfaces must be smooth and sufficiently strain free to approximate the bulk material.

C. Cyclotron Resonance

The determination of the energy $E_f(\bar{k})$ as a function of \bar{k} is equivalent to a determination of the effective mass tensor

$$\left(\frac{1}{m^*}\right)_{ij} = \frac{1}{\hbar^2} \left(\frac{\partial^2 E}{\partial k_i \partial k_j}\right)_{E=E_f}$$

The effective mass can be determined by cyclotron resonance experiments in which the electrons are accelerated in spiral orbits about the axis of a static magnetic field H .

According to the usual cyclotron equation

$$\omega_c = \frac{eH}{m^*c} \quad (3.18)$$

Resonant absorption of energy from an rf electric field perpendicular to the static magnetic field occurs when the field frequency is equal to the cyclotron frequency.

Detailed treatments of the interaction are given by Dresselhaus, Kip and Kittel⁶, Shockley⁷, Chambers⁸, and Pippard⁹. Since only those electrons on the Fermi surface are able to absorb energy, any m^* measured will be approximately $m^*(E_f, k_z)$. The procedure provides no means of singling out a particular k_z however, and so the measured m^* will be an average value over k_z of $m^*(E_f, k_z)$. Chambers observed that

if the applied magnetic field is almost parallel to the surface of the metal, then only those electrons for which v_z in the direction of the field is zero or very small will return to the same position in the surface layer and thus be able to resonate. Then one should be able to measure m^* for a localized group of electrons in k -space, rather than an average over the entire Fermi surface.

As in the case of the de Haas-van Alphen effect the condition $\omega_c \tau > 1$ must be satisfied. In addition the individual particle motion of the electrons must be decoupled from the plasma oscillations of the metal, requiring that $\omega_p \gg \omega_c$ and r (radius of cyclotron orbit) $\gg \delta$, the classical skin depth. This means that $\ell \gg r \gg \delta$, which are the conditions for the extreme anomalous skin effect.

D. Galvanomagnetic Effects

Since Peierls¹⁰ first pointed out that magneto-resistance effects were essentially due to departures from the isotropic free-electron model, it has been recognized that these effects might yield a great deal of information with respect to Fermi surface topology.

If $\omega_c = \frac{eH}{m^*c}$ is the usual cyclotron frequency of a representative electron in a magnetic field, and τ is as usual the relaxation time, several distinguishable cases occur:

- (i) $\omega_c\tau \ll 1$, the low field region,
- (ii) $\omega_c\tau \sim 1$, the intermediate field region,
- (iii) $\omega_c\tau \gg 1$, the classical high field region,
- (iv) $\hbar\omega_c \geq kT$, the quantum oscillation region.

The quantities observed experimentally are the resistivities $\rho(\bar{H})$, either with current flow \bar{J} parallel to \bar{H} , or perpendicular to \bar{H} . The theory of the effects is very involved and will not be discussed here, other than to say that thus far the information obtained with respect to Fermi surfaces is qualitative only. In the quantum oscillation region, oscillations of $\rho(\bar{H})$ periodic in $1/H$ are observed with periods identical to the de Haas-van Alphen effect, and having the same origin. The quantum oscillations of the electrical conductivity are of some interest since the electron orbits observed are not always the same as those observed in the magnetic susceptibility measurements. The theoretical explanation for this remains in doubt.

CHAPTER IVTHEORY OF MAGNETOACOUSTIC EFFECTS

In this chapter oscillatory variations of the ultrasonic attenuation in a magnetic field will be discussed. The oscillations occur at low temperatures where the absorption is almost entirely due to electrons. In general the phenomena are treated theoretically according to whether the frequency of the sound wave ω is much smaller than the reciprocal of the relaxation time τ of the electrons, or is comparable to or greater than τ^{-1} . In the first case ($\omega\tau \ll 1$) the sound vibrations can be considered as an external field in which the electron gas is located and which modulates the energy of the electrons. In the second case ($\omega\tau \geq 1$) the sound absorption is treated as the absorption of sound quanta of energy $\hbar\omega$ and momentum $\hbar\bar{q}$ (\bar{q} = propagation vector of sound wave), which takes place as the result of collisions of the sound quanta with the electrons. Of course, effects in the $\omega\tau \ll 1$ regime can be treated as a limiting case of calculations for the $\omega\tau \geq 1$ regime. In both regimes the condition $q\ell > 1$ is required, (ℓ is the mean free path of the electrons) for oscillations in the sound absorption to be observed experimentally.

In the semi-classical regime ($\omega\tau \ll 1$) geometric oscillations (often referred to incorrectly as geometric resonances) may occur. In the quantum region ($\omega\tau \geq 1$) cyclotron resonance and giant quantum oscillations, so named because the ratio of maximum to minimum attenuation can be greater than 10^3 , may occur. In addition to these three effects a fourth exists, de Haas-van Alphen type oscillations. This effect is properly regarded as in the semi-classical regime, however since there is a similarity to giant quantum oscillations and the theory is dealt with as a limiting case of the quantum regime, de Haas-van Alphen oscillations will be discussed together with giant quantum oscillations.

A. Geometric Oscillations

The magnetoacoustic effect most commonly used for Fermi surface measurements, geometric oscillations, are most satisfactorily treated using semi-classical methods. The electronic fields of the ultrasonic wave serve as a means of measuring the linear extension of extremal orbits of the Fermi surface. Consider the case where \vec{q} and the magnetic field \vec{H} are perpendicular. The ultrasonic attenuation will be an extremum for a particular orbit diameter such that the electron-sound wave interaction is a maximum at the two locations of the cyclotron orbit where the velocity of the

electrons in the direction of \bar{q} is zero. Increasing the diameter of the cyclotron orbit by any integral number of sound wavelengths λ will also yield an extremum. These extrema will be maxima or minima with the opposite extrema occurring in between at half integral values of λ , since the sound wave is sinusoidal.

Since real space trajectories are unambiguously related to those in momentum space, in principle the Fermi surface can be mapped out by varying the directions of \bar{q} and \bar{H} . This method was first proposed by Pippard¹¹ in 1957, and since that time has been used on many metals. The relationship between a given period in H^{-1} and the extremal momentum perpendicular to \bar{q} and \bar{H} is

$$\hbar k_{\text{ext}} = \frac{e\lambda}{2c\Delta\left(\frac{1}{H}\right)} \quad (4.1)$$

The oscillations in attenuation are typical of extremal orbits on the Fermi surface, even though non-extremal orbits contribute to the attenuation. The oscillatory contributions from non-extremal orbits cancel out almost completely.

There are other effects in the semi-classical limit than equation 4.1 such as resonant absorption by open orbits and oscillations of the absorption with \bar{q} parallel to \bar{H} . These

effects can be understood on the basis of geometric arguments if the basic mechanism of geometric oscillations is understood, and will not be discussed here.

A detailed quantitative theory of the dependence of attenuation on a magnetic field was not developed until three years after Pippard's proposal, even though Fermi surface measurements using this method had been made on several metals by then. (A great many metals have not been examined yet, particularly among the alkali and transition metals). In 1960 two theories were published, one by Gurevitch¹² and the other by Cohen, Harrison and Harrison¹³, hereafter referred to as CHH.

In both theories interactions between particles are replaced by interactions of individual particles with a self-consistent electromagnetic field. However in the Gurevitch theory the principle contribution to the attenuation arises from deformation of the Fermi surface by the sound wave, according to a "deformation tensor" which is not evaluated but only estimated. In the CHH theory the electronic current is calculated as a function of the self-consistent field by solving the Boltzmann transport equation, and then by using Maxwell's equations both the field and electronic current are obtained. The energy is dissipated as Joule heat, and a calculation of this yields the attenuation coefficient.

Physically, the absorption mechanism involves creation by the sound wave of a non-equilibrium distribution function $f(\bar{r}, \bar{v}, t)$ for the electrons, and subsequent decay toward equilibrium through electronic collisions. The CHH theory is exact to a model where a free electron gas moves through a uniform background of positive charge, where a relaxation time exists for the electron collisions, and where the self-consistent field is proportional to the particle velocity of the sound wave.

Both the Gurevitch and CHH theories produce the oscillatory variation of attenuation observed experimentally in the semi-classical regime. However the Gurevitch theory is of a somewhat phenomenological nature and does not treat the absorption mechanism in a satisfactory manner. For this reason it will not be discussed further and only the Cohen theory, which is a rather elegant treatment, will be discussed below.

Consider a gas of N_0 electrons per unit volume moving through a uniform background of positive charge of the same density. A sound wave manifests itself as a velocity field $\bar{u}(\bar{r}, t) \propto e^{i[\bar{q} \cdot \bar{r} - \omega t]}$ in the positive background. Interactions between particles are replaced by interactions of each particle with a self-consistent electromagnetic field derived from Maxwell's equations, which can be reduced to

$$E_{||} = \left(\frac{4\pi}{i\omega}\right) j_{||}, \quad \bar{E}_{\perp} = \frac{(4\pi i/\omega)(v_s/c)^2}{1 - (v_s/c)^2} \bar{j}_{\perp}.$$

\bar{E} is the electric field, \bar{j} the total current density, and v_s the phase velocity of the sound wave. Both vary as $e^{i[\bar{q} \cdot \bar{r} - \omega t]}$ and are expressed in terms of components parallel and perpendicular to the direction of sound propagation. The total current consists of a contribution \bar{j}_e from the electrons and a contribution from the positive background, $N\bar{e}$:

$$\bar{j} = \bar{j}_e + N\bar{e} \quad (4.3)$$

(It can be shown by a simple argument that the total current is close to zero).

The electronic current obeys an equation similar to Ohm's law which can be derived by solving the Boltzmann transport equation. The electronic current is given by

$$\bar{j}_e(\bar{r}, \bar{v}, t) = -e \int \bar{v} f(\bar{r}, \bar{v}, t) d\bar{v} \quad (4.4)$$

where $f(\bar{v}, \bar{r}, t)$ is the distribution function in phase space. When no sound wave is present the distribution function reduces to the thermal equilibrium Fermi-Dirac function $f_0(\bar{v}, E_f^0)$.

When a sound wave is present the distribution function is determined from Boltzmann's equation

$$\frac{\partial f}{\partial t} + \bar{v} \cdot \frac{\partial f}{\partial \bar{r}} + \frac{\bar{F}}{m} \cdot \frac{\partial f}{\partial \bar{v}} = \frac{\partial f}{\partial t} \Big|_{\text{coll.}} \quad . \quad (4.5)$$

\bar{F} is the Lorentz force:

$$\bar{F} = -e [\bar{E} + (\bar{v}/c) \times \bar{H}] . \quad (4.6)$$

\bar{H} includes a part \bar{H}_1 associated with the sound wave in addition to the static field \bar{H}_0 applied to the metal. The collision term in equation 4.5 is assumed to have the form

$$\frac{\partial f}{\partial t} \Big|_{\text{coll}} = - \frac{(f - f_s)}{\tau} \quad (4.7)$$

where τ is the relaxation time mentioned previously and f_s is the distribution of electrons after scattering:

$$f_s(\bar{r}, \bar{v}, t) = f_0(\bar{v} - \bar{u}(\bar{r}, t), E_f(\bar{r}, t)) . \quad (4.8)$$

Implicit in this form of distribution function is Pippard's concept of a local Fermi surface which varies from point to point on a relatively stationary sound wave. This relation holds since the electrons will scatter into a velocity distribution centred about the velocity of the scattering centres, which will have the local velocity of the lattice.

The Boltzmann equation can be solved by a method due to Chambers¹⁴, which will not be discussed here. The result is an expression obtained for \bar{j}_e :

$$\bar{j}_e = \bar{\sigma} \cdot (\bar{E} - m\bar{u}/e\tau) - \bar{R} N_1 e v_s . \quad (4.9)$$

The first term includes the effect of the local velocity of the lattice on the distribution function. The second term would not occur using the assumption of charge neutrality and can be shown to be much smaller than the first. Here the electron density has been represented as $N = N_0 + N_1$, and $\bar{\sigma}$ is the magneto-conductivity tensor for frequency ω and wave vector \bar{q} :

$$\bar{\sigma} = \int d\bar{v} (-e\bar{v}) \bar{J}(\bar{v}) \left(- \frac{\partial f_0}{\partial E} \right) . \quad (4.10)$$

The vector \bar{R} is given by

$$\bar{R} = \frac{2 E_f^0}{3 N_0 \tau v_s} \int \bar{v} K(\bar{v}) \frac{\partial f_0}{\partial E} d\bar{v} \quad (4.11)$$

and $\bar{J}(\bar{v})$ and $K(\bar{v})$ are given by

$$\{\bar{J}(\bar{v}); K(\bar{v})\} = \int_{-\infty}^t \{e\bar{v}; 1\} e^{i[\bar{q} \cdot (\bar{r}^1 - \bar{r}) - \omega(t^1 - t)] - \frac{(t-t^1)}{\tau}} dt^1 \quad (4.12)$$

The two points (\bar{r}^1, t^1) and (\bar{r}, t) are on the trajectory of an electron in field \bar{H}_0 , and $t^1 < t$.

It can be shown that the average rate of loss of electronic kinetic energy by way of collisions is $\langle \bar{j}_e \cdot \bar{E} \rangle_{Av.}$ per unit volume. Not all of this kinetic energy is dissipated as heat, since a certain portion is fed back coherently into the sound wave. Allowing for this, the net power dissipated per unit volume is

$$Q = \frac{1}{2} R_e [\bar{j}_e^* \cdot \bar{E} - \bar{u} \cdot N_o m (\langle \bar{v} \rangle - \bar{u}) / \tau] \quad (4.13)$$

The second term is the collision drag effect which returns energy to the sound wave.

The electric field \bar{E} is assumed to be linearly related to \bar{u} by the expression

$$\bar{E} = \bar{W} \cdot N_o e \bar{u} / \sigma_o \quad . \quad (4.14)$$

\bar{W} is a tensor which must be determined and σ_o is the zero-field conductivity. Maxwell's equations (equation 4.2) can be rewritten in the form

$$\bar{j} = -\sigma_o \bar{B} \cdot \bar{E} \quad . \quad (4.15)$$

The tensor \bar{B} has diagonal components

$$i \left(-\frac{\omega}{4\pi\sigma_o}, \frac{\omega c^2}{4\pi\sigma_o v_s^2}, \frac{\omega c^2}{4\pi\sigma_o v_s^2} \right) \quad \text{or } i(-\gamma, \beta, \beta).$$

When 4.14 is used in 4.13,

$$Q = N_0 \left(\frac{1}{2} m |\bar{u}|^2 / \tau \right) \hat{u} \cdot \bar{S} \cdot \hat{u} \quad (4.16)$$

where

$$\bar{S} = - \operatorname{Re} [(1 + \bar{B}) \cdot \bar{W}] \quad (4.17)$$

and \hat{u} is a unit vector in the direction of the polarization of the sound wave.

The attenuation coefficient α can be obtained from Q and the energy density of the sound wave. For a particular polarization the result is:

$$\alpha_i = \frac{mv_F}{Mv_S} \frac{S_{ii}}{\ell} \quad (4.18)$$

Here ℓ is the mean free path of the electron discussed previously, M is the ion mass, and v_F is the Fermi velocity.

The next step, and the heart of the problem, is explicit determination of \bar{S} . This can be done by solving the two simultaneous equations for the current density, given by equations 4.9 and 4.15 (which are derived from the Boltzmann equation, and Maxwell's equations). The result is:

$$S_{ii} = \operatorname{Re} \left\{ (1 + B_{ii})^2 \left[\left((1 - \bar{R})^{-1} \cdot \bar{\sigma}/\sigma_0 + \bar{B} \right)^{-1} \right]_{ii} \right\}^{-1} \quad (4.19)$$

The tensor \bar{R} of equation 4.19 can be shown to have the components

$$R_{ij} = R_i \delta_{1j}$$

where R_i is a component of the vector \bar{R} of equation 4.11.

It can be shown that

$$R_{il} = \frac{-i\omega\tau v_F^2}{3\sigma_0(1 - i\omega\tau)v_s^2} \sigma_{il} \quad (4.20)$$

Equations 4.18 and 4.19 are the solution to the problem since the magneto-conductivity tensor σ_{ij} can be evaluated from equations 4.10 and 4.12. To do this the equations of motion of the electron in a cyclotron orbit must be written down so that the point (\bar{r}, t) on the electron trajectory can be expressed in terms of the point (\bar{r}', t') . Suitable expressions may then be obtained and substituted into equation 4.12. Components of the magneto-conductivity tensor are obtained by substituting $\bar{J}(\bar{v})$ into equation 4.10 and integrating over the Fermi surface. (The temperature is assumed to be 0° K, but the results would be little different for temperatures of only a few degrees).

The resulting expressions for the magneto-conductivity tensor are complicated and will not be repeated here (see p. 943 of reference 13). The denominators have the form

$[1 + i(n\omega_c - \omega)\tau]$ where ω_c is the cyclotron frequency and n is a positive integer. This shows the possibility of cyclotron resonance contributing to the acoustic absorption when the magnetic field is sufficiently low that $\omega_c \leq \omega$. This feature does not occur in the Gurevitch result. The condition $\omega\tau \gg 1$, which is very difficult to obtain, must also be met for experimental observation. The numerators of the expressions are complicated functions of Bessel functions.

As is clear from the foregoing discussion, the expressions for S_{ii} , which are proportional to the attenuation coefficient, are exceedingly complicated. For the case where $\omega_c \gg \omega$, CHH show graphs of S_{11} , S_{22} and S_{33} . See figures 4.1 and 4.2. The graphs show, roughly, a sinusoidal contribution plus a monotonic increase with qR for transverse waves, and a monotonic decrease with qR for longitudinal waves (R is the diameter of the cyclotron orbit). The amplitude of the sinusoidal variation differs considerably for the three polarization directions. The Gurevitch theory does not distinguish between directions of polarization since components of the "deformation tensor" are unknown.

FIGURE 4.1

Relative Attenuation vs. qR , Longitudinal Sound Wave.

The attenuation is obtained by multiplying S_{11} by

$(Nm/\rho v_s \tau) [q^2 \ell^2 / 3 (1 + \omega^2 \tau^2)]$. The $\beta \ll 1$ curve applies when the classical skin depth is much less than the wavelength and the curve $\beta \gg 1$ when it is much greater. In both cases $\omega_c \tau \gg 1$ and $q\ell \gg 1$.

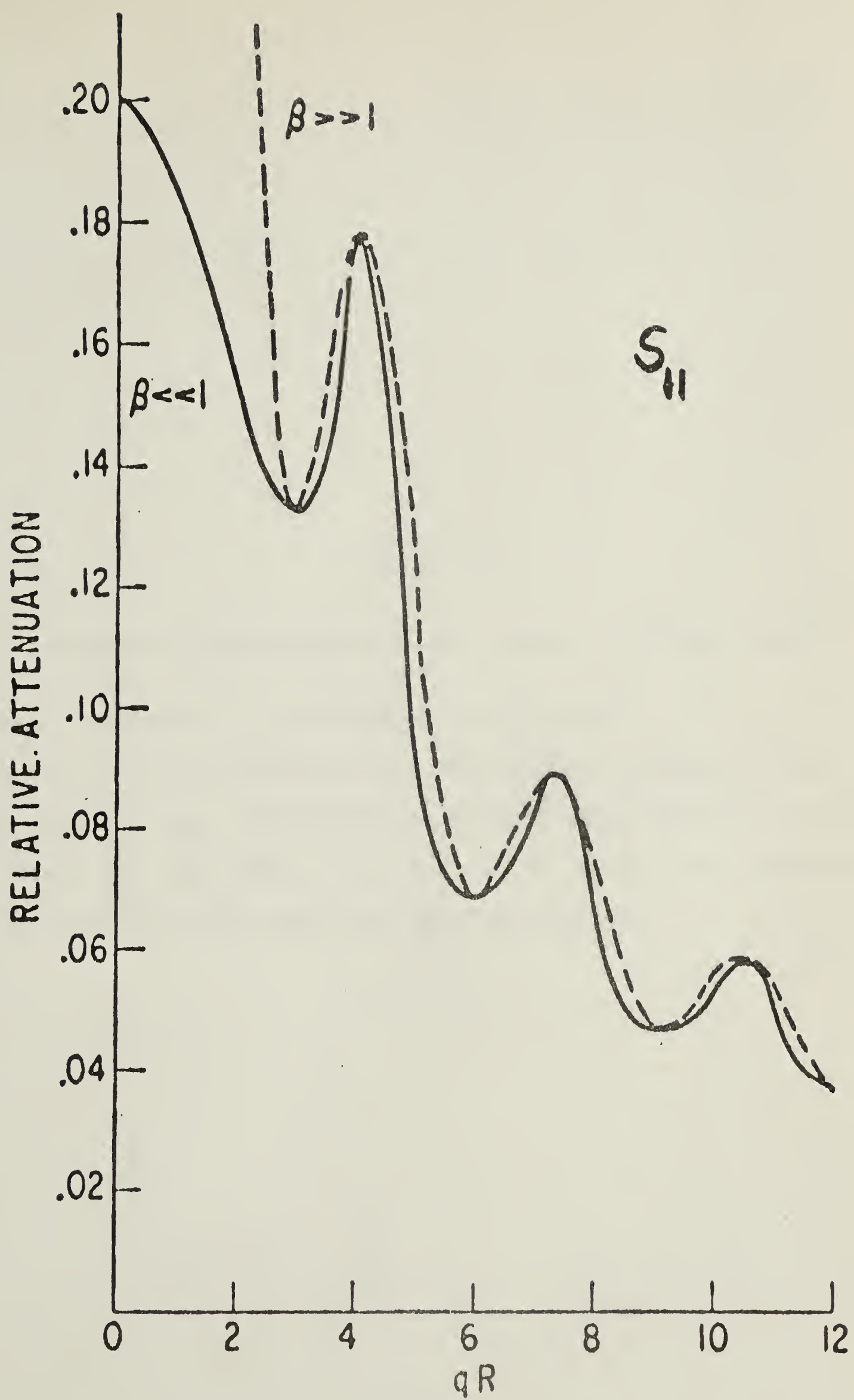
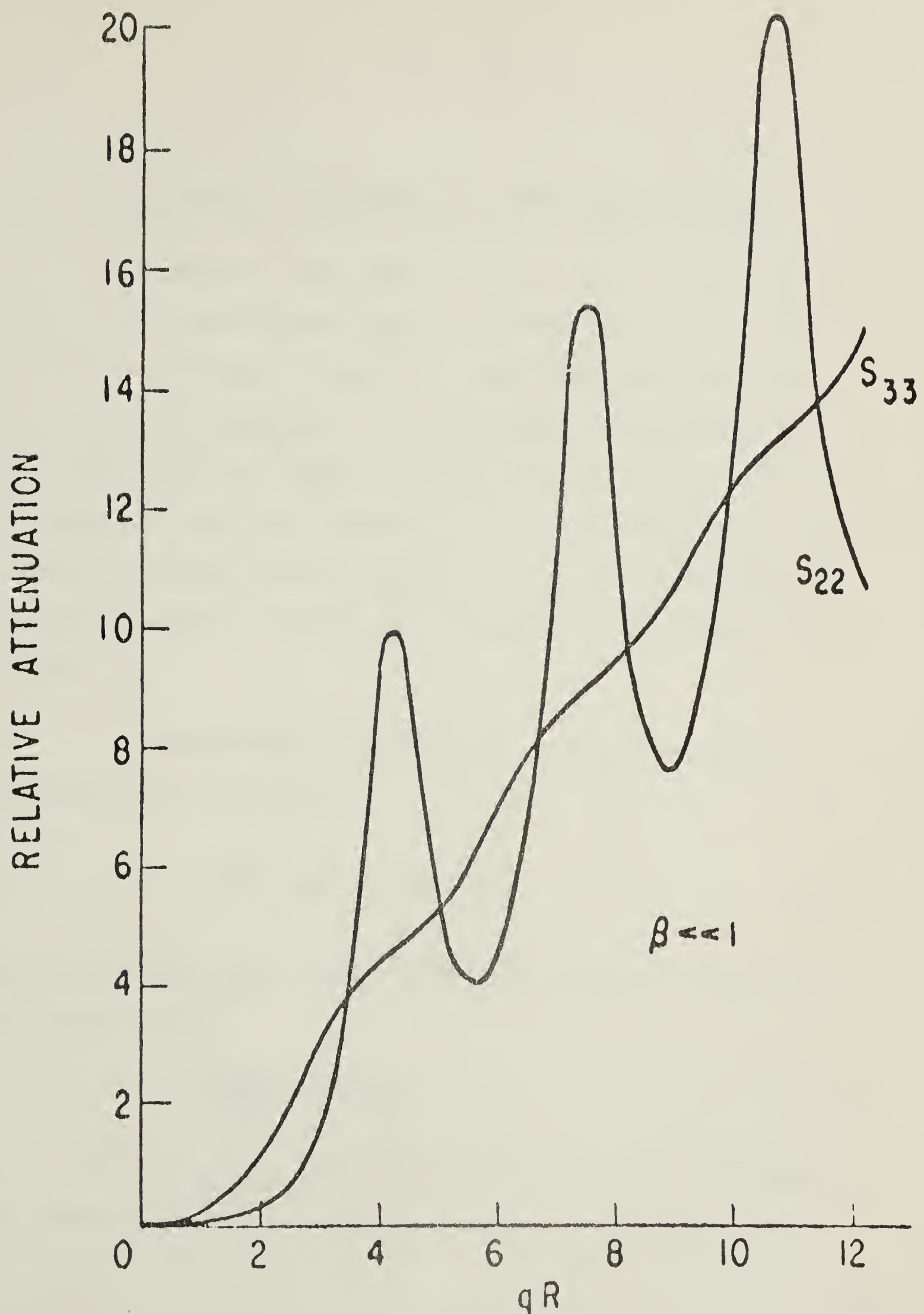


FIGURE 4.2

Relative Attenuation vs. qR , Transverse Sound Wave.

The attenuation is obtained by multiplying S_{22} or S_{33} by $Nm/\rho v_s \tau$. S_{22} corresponds to polarization perpendicular to the field; S_{33} corresponds to polarization parallel to the field. In both cases $\omega_c \tau \gg 1$, $q\ell \gg 1$, and the classical skin depth is less than the sound wavelength.



B. Giant Quantum and de Haas-van Alphen Oscillations

Consider first giant quantum oscillations which occur at low temperatures, when the mean free path of the conduction electrons in a metal is sufficiently long that $\omega\tau \geq 1$, and the absorption of sound may be considered as the direct absorption of phonons by the electrons. In the absence of a magnetic field the major role in the absorption is taken by electrons whose group velocity v_g in the direction of the acoustical wave vector \vec{q} is equal to the phase velocity of sound v_s .

Consider the conservation laws during phonon absorption by an electron:

$$E(\vec{k}) + \hbar\omega = E(\vec{k} + \vec{q}) \quad . \quad (4.21)$$

Expanding $E(\vec{k} + \vec{q})$ to first order in \vec{q} , and if \vec{q} is in the Z-direction,

$$\left(\frac{\partial E}{\partial k_Z}\right) q = \hbar v_s q \quad (4.22)$$

$v_g = v_s$ where v_{gz} is the group velocity of the electrons in the Z-direction.

An analogous situation occurs in the presence of a magnetic field. Consider a quadratic isotropic dispersion law for the electrons. The energy of an electron in the magnetic field then takes the form

$$E_n = \hbar\omega_c(n + \frac{1}{2}) + p_z^2/2m^* \quad (4.23)$$

where n is the Landau quantum number, $\omega_c = eH/m^*c$ is the cyclotron frequency, m^* is the effective mass, and p_z is the quasi-momentum in the direction of the magnetic field. Taking into account conservation of energy and of the z -component of the quasi-momentum,

$$\begin{aligned} \hbar\omega_c(n + \frac{1}{2}) + \hbar^2 k_z^2/2m^* + \hbar\omega &= \hbar\omega_c(n' + \frac{1}{2}) \\ &+ \hbar^2(k_z + q_z)^2/2m^*. \end{aligned} \quad (4.24)$$

Putting $E_n, (k_z + q_z) = E(k_z) + \hbar\omega$ the condition is obtained:

$$\omega_c(n' - n) + v_s q = v_{gz} q_z \quad (4.25)$$

Two cases arise; either $\omega_c > q_z v_F$, where v_F is the Fermi velocity, or $\omega_c \leq q_z v_F$. Consider the first case which applies at ultrasonic frequencies $\sim 10^8$ cycles/sec. Then condition 4.25 can only be satisfied for $n' = n$. Consequently the electrons which participate in the acoustical absorption in a magnetic field are those for which

$$v_{gz} = \frac{v_s}{\cos \theta} \quad (4.26)$$

where θ is the angle between \vec{q} and \vec{H} .

Quite clearly only electrons with energies lying in the energy interval where the Fermi distribution function is changing can participate in the absorption. The participating electrons describe orbits on the Fermi surface in planes perpendicular to the direction of the magnetic field and the location of the orbits in the z-direction in wave-vector space is fixed by equation 4.26. This means that the absorption electrons will not describe extremal orbits. As a rule condition 4.26 means that the orbits described will be very close to extremal orbits, however when $\cos \theta$ is small they may be markedly different in area.

The absorption of sound by electrons will be a periodic function of the magnetic field in the same manner as the de Haas-van Alphen effect, that is, absorption will occur as successive Landau cylinders appear on the Fermi surface where v_{gz} satisfies 4.26.

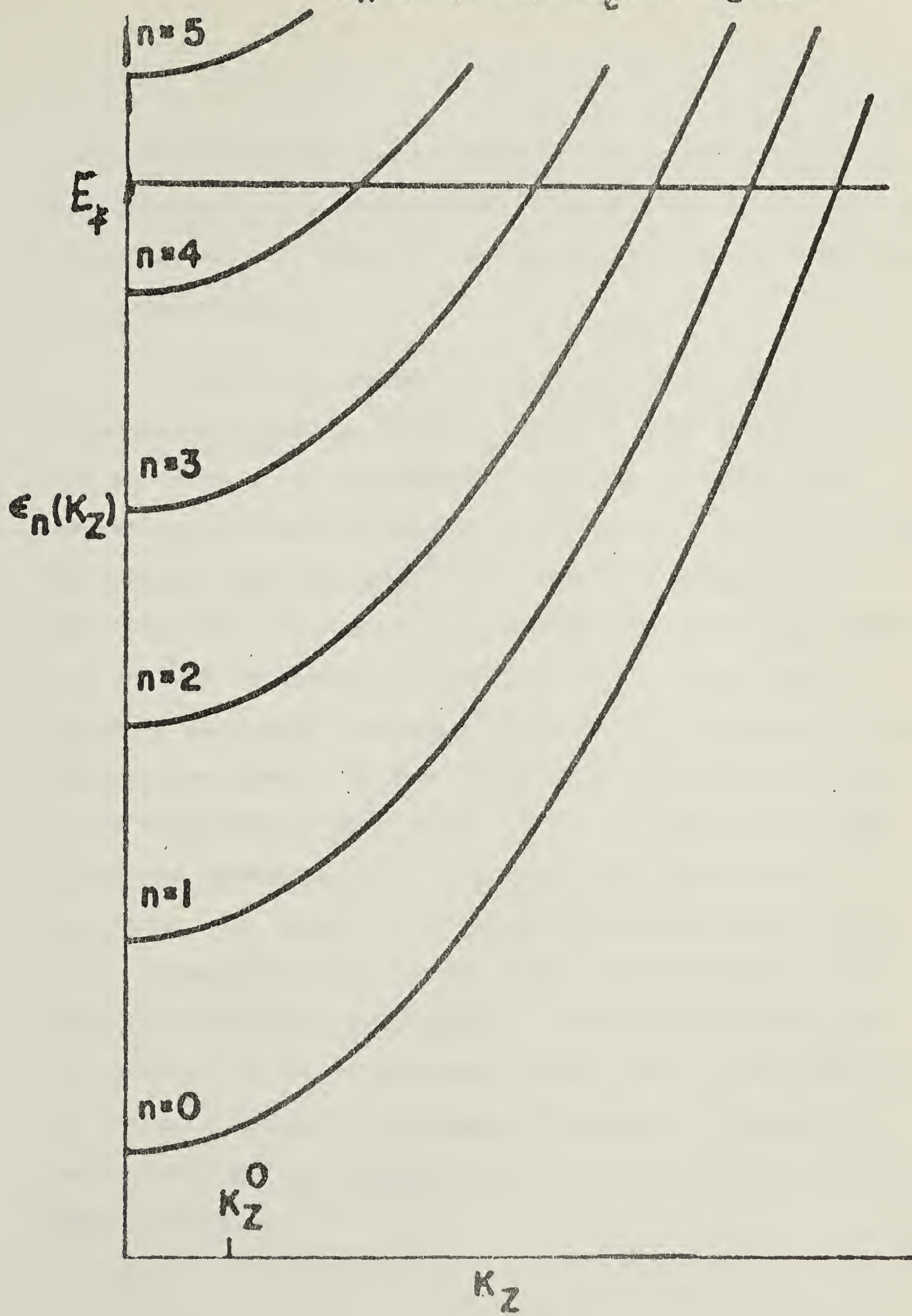
For temperatures above 0°K absorption of sound by electrons will occur if there is a Landau cylinder within $\sim kT$ of E_f at v_{gz} . See figure 4.3. In addition the range will

FIGURE 4.3

Electron Energy Levels in a Quantizing Magnetic Field for
Parabolic Band.

The energy $\epsilon_n(k_z)$ is a function of the quantum numbers n , which determines which Landau level the electron occupies, and k_z , which is the component of the electron wave-vector parallel to the applied magnetic field. k_z^0 is the value of k_z for which the electron group velocity in the direction of the magnetic field satisfies the condition $v_{gz} = v_s / \cos \theta$. Maximum absorption of ultrasonic energy occurs for values of the magnetic field such that a Landau level intersects the Fermi surface, E_f , at $k_z = k_z^0$.

$$\epsilon_n = (n + 1/2) \hbar \Omega_c + \hbar^2 k_z^2 / 2m$$



be further broadened since electrons within $\hbar\omega$ of E_f may participate at zero temperature. However $\hbar\omega \ll kT$ at a temperature of 1°K and if the sound frequency is less than a kilomegacycle/sec.

Gurevitch, Skobov and Firsov¹⁵ first calculated the energy absorbed by electrons from a longitudinal sound wave in terms of an undetermined constant matrix element describing the electron-phonon interaction. In an alternative theory Quinn and Rodriguez¹⁶ calculate the attenuation explicitly for the case of a free electron gas in the presence of a uniform background of positive ions. Quinn and Rodriguez calculate the magnetoconductivity tensor and then consider two cases. In the first case the relaxation time of the electrons is very large ($\omega\tau \gg 1$). The first case yields the resonance type of oscillations calculated by Gurevitch. The second case yields sinusoidal oscillations of the attenuation with an amplitude of order $(\hbar\omega_c/E_f)^{3/2}$ times the zero-field attenuation. These oscillations are very similar to the de Haas-van Alphen oscillations and are due to oscillations of the magneto-conductivity tensor of the electron gas as successive Landau levels emerge from the Fermi surface.

An important difference between the two theories in the quantum limit is that Gurevitch does not take the relaxation time as infinite and thus obtains a great deal more information. For this reason the Gurevitch theory is more satisfactory and will be outlined below, although it says nothing about the electron-phonon interaction, simply treating it as a parameter.

In the Gurevitch theory the energy operator for interaction of an electron with the sound wave has the form

$$V = \frac{1}{2} (U e^{-i\omega t} + U^* e^{i\omega t}) \quad (4.27)$$

where $U = \Lambda_{ik} U_{ik} e^{i\bar{q} \cdot \bar{r}}$. Here U_{ik} is the tensor amplitude of the deformation of the sound wave, and Λ_{ik} is an undetermined tensor, the components of which depend on the components of the quasi-momentum operator.

If the scattering of electrons is elastic, then the energy absorbed by electrons in unit time is

$$W = -\frac{1}{V_0} \frac{\pi}{2\hbar} \sum_{aa'} (f_{a'} - f_a) \hbar\omega_{aa'} \langle a | U | a' \rangle \delta(\hbar\omega_{aa'} + \hbar\omega) \quad (4.28)$$

where a and a' denote states of the electron in the field of the scatterers, $\hbar\omega_{aa'} = E_a - E_{a'}$, f_a is the Fermi function, $\langle a | U | a' \rangle$ is the matrix element of the operator U , and V_0

is the volume of the crystal. If $\hbar\omega \ll kT$, then $f_a - f_{a'} =$

$$\left(\frac{\partial f_a}{\partial E}\right)_{E_f} \hbar\omega_{aa'} = \left(\frac{\partial f_a}{\partial E}\right)_{E_f} \hbar\omega .$$

The absorption coefficient α is obtained by dividing equation 4.28 by the flux density of acoustical energy $\rho\omega^2 u_o^2 v_s / 2$, where ρ is the density of the crystal, u_o is the amplitude of the sound wave and v_s is the velocity of the sound wave.

As a zero order approximation, the effect of scatterers is neglected. Then the expression obtained for α is

$$\alpha = \frac{\pi}{V_o \rho u_o \omega} \sum_{aa'} \left(\frac{\partial f_a}{\partial E}\right)_{E_f} \langle a | U | a' \rangle \delta(\omega_{aa'} + \omega) \quad (4.29)$$

If an approximation is considered where the components of the tensor are constant (do not vary with the electron momentum or energy, or the sound frequency, or the magnetic field), the electron spectrum is quadratic and isotropic, and if $\bar{q} \parallel \bar{H}$, then

$$\langle a | U | a' \rangle = \Lambda_{ik} u_{ik} \delta_{s_z s_{z'}} \delta_{nn'} \delta_{p_z + q_z, p_{z'}} \quad (4.30)$$

where s_z is the spin, and where as before n is the Landau quantum number. The absorption coefficient is then

$$\alpha = \alpha_0 \frac{\hbar\omega_c}{8kT} \frac{q_z}{m} \sum_{n,s_z} \int dp_z \delta\left(\frac{q_z p_z}{m} + \frac{\hbar q_z^2}{2m} - \hbar\omega\right) \cosh^{-2} \left[\frac{E_f - \hbar\omega_c(n + \frac{1}{2}) - \mu_0 s_z H - p_z^2/2m}{2kT} \right] \quad (4.31)$$

where μ_0 is the Bohr magneton and α_0 , the attenuation in zero magnetic field, is given by

$$\alpha_0 = \frac{m^2 |\Lambda_{ik} u_{ik}|^2}{2\pi\hbar^2 \rho u_0^2 q_z^2 v g} \quad (4.32)$$

Integrating over p_z ,

$$\alpha = \alpha_0 \frac{\hbar\omega_c}{kT} \sum_{n,s_z} \cosh^{-2} \left[\frac{\hbar\omega_c(n + \frac{1}{2}) + s_z \mu_0 H - E_f}{2kT} \right]$$

where the small quantity $p_z^2/2m$ has been neglected.

If $\hbar\omega_c \ll kT$, this reduces to the expression α_0 . When $\hbar\omega_c \gg kT$, the function $\alpha(\frac{1}{H})$ has a series of sharp peaks, the distance between which is

$$\Delta\left(\frac{1}{H}\right) = \frac{2\pi e}{\hbar c A_0} \quad (4.33)$$

and the height of which is proportional to H , separated by wide gently sloping minima which are exponentially small in comparison. A_o is the area of the orbit on the Fermi surface for which condition 4.26 is satisfied and may be different than the extremal area measured by de Haas-van Alphen oscillations of the magnetic susceptibility.

Equation 4.32 describes the behaviour of the absorption coefficient close to the absorption maxima, however description of the minima requires some consideration of electron scattering. When scattering is considered and the behaviour of the minima established the amplitude of the quantum oscillations compared to zero-field attenuation can be estimated. The treatment by Gurevitch et al takes account of scattering by smearing out the electronic energy by \hbar/τ . This was done by replacing the δ -function of equation 4.31 by a Lorentzian function whose width is proportional to τ^{-1} . (This technique is of course questionable, however more rigorous techniques produce the same results if the relaxation time is sufficiently great). The result then obtained is

$$\alpha = \alpha_o \frac{\hbar\omega_c}{4kT} \int dy \frac{1}{\pi} \frac{B}{1+By^2} \sum_n \cosh^{-2} \left[\frac{y^2}{2} - \frac{E - \hbar\omega_c(n + \frac{1}{2})}{2kT} \right] \quad (4.34)$$

$$\text{where } B = q\ell \left(\frac{kT}{E_f}\right)^{1/2} \quad \text{and} \quad y = p_z (2mkT)^{-1/2}.$$

When $B \gg 1$, then

$$\frac{\alpha_{\max}}{\alpha_{\min}} \sim q\ell \left(\frac{\hbar\omega_c}{E_f}\right)^{1/2}, \quad \left(\frac{\hbar\omega_c}{kT}\right) \gg 1. \quad (4.35)$$

When $B \sim 1$,

$$\frac{\alpha_{\max}}{\alpha_{\min}} \sim \left(\frac{\hbar\omega_c}{kT}\right)^{3/2}. \quad (4.36)$$

Skobov¹⁷ has considered the effect of scattering by neutral impurities using a more rigorous approach. When $(q_z\ell)^2 \gg \frac{E_f}{\hbar\omega_c}$, then only one Landau level may participate in the absorption at any particular value of the magnetic field, and in this case the oscillations are giant quantum oscillations and have great amplitude. (The expression for α is in the form of an integral equation). When $(\frac{E_f}{\hbar\omega_c}) \gg (q_z\ell)^2 \gg 1$, many Landau levels participate in the absorption and the attenuation is given by

$$\alpha(H) = \alpha_0 \left[1 + q_z \ell \left(\frac{\hbar\omega_c}{E_f}\right)^{1/2} \sum_{n=1}^{\infty} (-1)^n A_n \frac{\cos[2\pi n E_f / \hbar\omega_c - \pi/4]}{\pi \sqrt{n}} \right] \quad (4.37)$$

where α_0 is the zero field attenuation and

$$A_n = \frac{2\pi^2 n k T / \hbar\omega_c}{\sinh(2\pi^2 n k T / \hbar\omega_c)}.$$

This expression for the attenuation is similar to the expression for de Haas-van Alphen oscillations of the magnetic susceptibility (equation 3.9).

The Gurevitch theory and subsequent theories by Skobov¹⁷ and by Liu and Toxen¹⁸ claim that when $q\ell\left(\frac{\hbar\omega}{E_f}\right)^{1/2} \gg 1$ but $\omega\tau \ll 1$, only a single Landau level contributes to ultrasonic absorption. In each case the effect of scattering is treated as a mechanism to relax the requirement of momentum conservation in the electron-phonon interaction through the uncertainty principle. (The uncertainty of the electron momentum is $1/q\ell$ times the phonon momentum). However, the basic consideration is not merely momentum conservation but equation 4.26 relating the group velocity of electrons at the Fermi surface to the phase velocity of the sound wave. Uncertainty of this relation will be introduced by uncertainty of the electron energy and will be equal to $1/\omega\tau$ times the sound velocity. Uncertainty of the group velocity which electrons must have to participate in ultrasonic absorption will thus be much larger than that estimated using the mean free path of the electrons. Thus if $\omega\tau < 1$ many Landau levels may contribute to ultrasonic absorption, since the electron group velocity must only be in the range $\frac{v_s}{\cos\theta} \pm \left(\frac{v_s}{\cos\theta}\right) \frac{1}{\omega\tau}$. The number of Landau levels

simultaneously satisfying this condition will be determined by the contour of the Fermi surface. In general Fermi surfaces are so shaped that when $q\ell(\frac{\hbar\omega_c}{E_f})^{1/2} \gg 1$ only one Landau cylinder will contribute to the absorption, since for small angles θ , where $v_{gz} = v_s/\cos\theta$ the change of this component of the group velocity is large proceeding from one Landau level to another on the Fermi surface. However when θ is close to 90° , or for special cases of Fermi surface topology, the Skobov theory may not be accurate.

The temperature variation of the amplitude of giant quantum oscillations has been studied by Shapira and Lax¹⁹ (using the results of Gurevitch et al) for the case $q\ell(\frac{kT}{E_f})^{1/2} \gg 1$, and $\hbar\omega_c \gg kT$. According to their calculations the amplitude is given by

$$A = \left| \frac{m_z^* e H_i \omega \bar{\Lambda}^2}{16 \pi kT \hbar^2 \rho v_s^2 c \cos \theta} \right|. \quad (4.38)$$

The results of experiments in gallium at fields of 100 kilogauss and greater confirm the reciprocal variation with temperature (although Shapira and Lax do not actually show the results). For the case of a free electron gas and no collisions Rodriguez²⁰ derived an expression for the amplitude,

disregarding scattering, but for an arbitrary ratio $\hbar\omega_c/kT$.

The result is

$$\frac{\alpha}{\alpha_0} = 1 + \sum_{n=1}^{\infty} (-1)^n \frac{4\pi kT}{\hbar\omega_c} \sin\left(\frac{\pi n \omega}{\omega_c}\right) \frac{\cos(2\pi n E_f/\hbar\omega_c)}{\sinh(2\pi^2 n kT/\hbar\omega_c)} . \quad (4.39)$$

Although the Rodriguez derivation is for the case of no scattering, it appears that inadvertently all Landau cylinders have been included and the expression is probably characteristic of de Haas-van Alphen oscillations rather than giant quantum oscillations.

Shapira and Lax¹⁹, and Rodriguez²⁰, have calculated the effect of electron spin. The result is that each absorption peak is split into two overlapping peaks, which in certain cases will have an appreciable separation. The splitting increases with magnetic field, and at sufficiently high fields effective masses and g-factors can be determined from the shape and separation of absorption peaks. If the first sub-peak at field H_1 is associated with Landau level n and spin up and the second sub-peak at field H_2 with Landau level $(n + \ell)$ and spin down, then:

$$g = 2 \frac{m_0}{m^*} \left[\frac{H_2 - H_1}{PH_1 H_2} + \ell \right] \quad (4.40)$$

Here P is the period of the oscillation.

In the preceding discourse only electron-phonon interactions in which the Landau quantum number n remains unchanged have been considered. However at very high ultrasonic frequencies (~ 10 kilomegacycles/sec) giant quantum oscillations of the absorption can occur for $\Delta n = \pm 1$. As shown by Langenberg, Quinn and Rodriguez²¹, this effect can be used as a tool for studying Fermi surface orbits at any plane perpendicular to the magnetic field, rather than just extremal orbits (de Haas-van Alphen effect) or orbits which satisfy equation 4.16 (giant quantum oscillations).

CHAPTER VAPPARATUS AND PROCEDURE

To observe oscillations of acoustic attenuation in metals the conditions $q\ell \gg 1$ or $\hbar\omega_c > kT$ or both must be satisfied. Either condition requires that measurements be performed at liquid helium temperatures. If inhomogeneities of the magnetic field are to be ignored the field must be homogeneous to one part in 10^4 or better over the dimensions of the specimen.

A. The Cryostat

A cryostat was constructed capable of operating in the range from 1 to 50°K , and with a dewar system designed to fit between magnet pole pieces separated by three inches. A similar cryostat has been described by Adler²². The operating range of the cryostat during the experiments was never required to be above 4°K and in this range temperature was controlled by pumping on the helium bath. Although the cryostat incorporates a specimen chamber which may be evacuated, the experiments were usually run with specimens in direct contact with the helium bath. Measurement of the helium vapor pressure yielded specimen temperatures accurate to considerably better than one percent.

B. The Magnet

The electromagnet used in the experiments, which was designed and constructed by the Pacific Electric Motor Co., can be rotated about a vertical axis and has pole-pieces eight inches in diameter. With a separation of three inches between the pole-pieces fields as great as twenty-three kilogauss can be obtained. Since the original pole-pieces provided very poor field homogeneity, new pole-pieces with compensating rings at the edges were designed. Nuclear magnetic resonance measurements indicate that field homogeneity was improved to one part in 10^5 or better over a one-inch diameter sphere.

The magnitude of the field is controlled by electronic circuitry which increases or decreases the current supply to field windings of a direct-current generator according to whether the difference between an adjustable reference potential and some d.c. potential monitoring the field is positive or negative. The original circuitry did not operate satisfactorily and was modified to improve the field control. (Even so the circuitry proved to be temperamental and an entirely new controller will be installed soon).

In addition further amplification was introduced so that the original control voltage supplied by a resistor in series with the magnet windings could be replaced by a Hall voltage from an indium-antimonide probe attached to one pole-face.

The indium-antimonide probe is highly insensitive to temperature changes and the direct current supplied to the probe is regulated to one part in 10^4 . The probe was calibrated using nuclear magnetic resonance to obtain about ten field readings and using a ballistic galvanometer to interpolate. In addition a highly stable 5000 gauss permanent magnet was purchased to check the calibration from day to day. The Hall probe thus calibrated yields field measurements accurate to better than 1/2 %. (The accuracy of the readings is limited primarily by the fact that the Hall voltage is displayed on a chart recorder).

A synchronous motor was used to vary the reference potential, and thus the magnetic field. Since the Hall voltage is close to a linear function of the magnetic field, varying the reference potential linearly or reciprocally with time imposes the same variation on the magnetic field. Suitable circuitry was designed so that this could be done. The speed of the synchronous motor was varied with an audio oscillator so that the magnetic field was increased or decreased at a convenient rate.

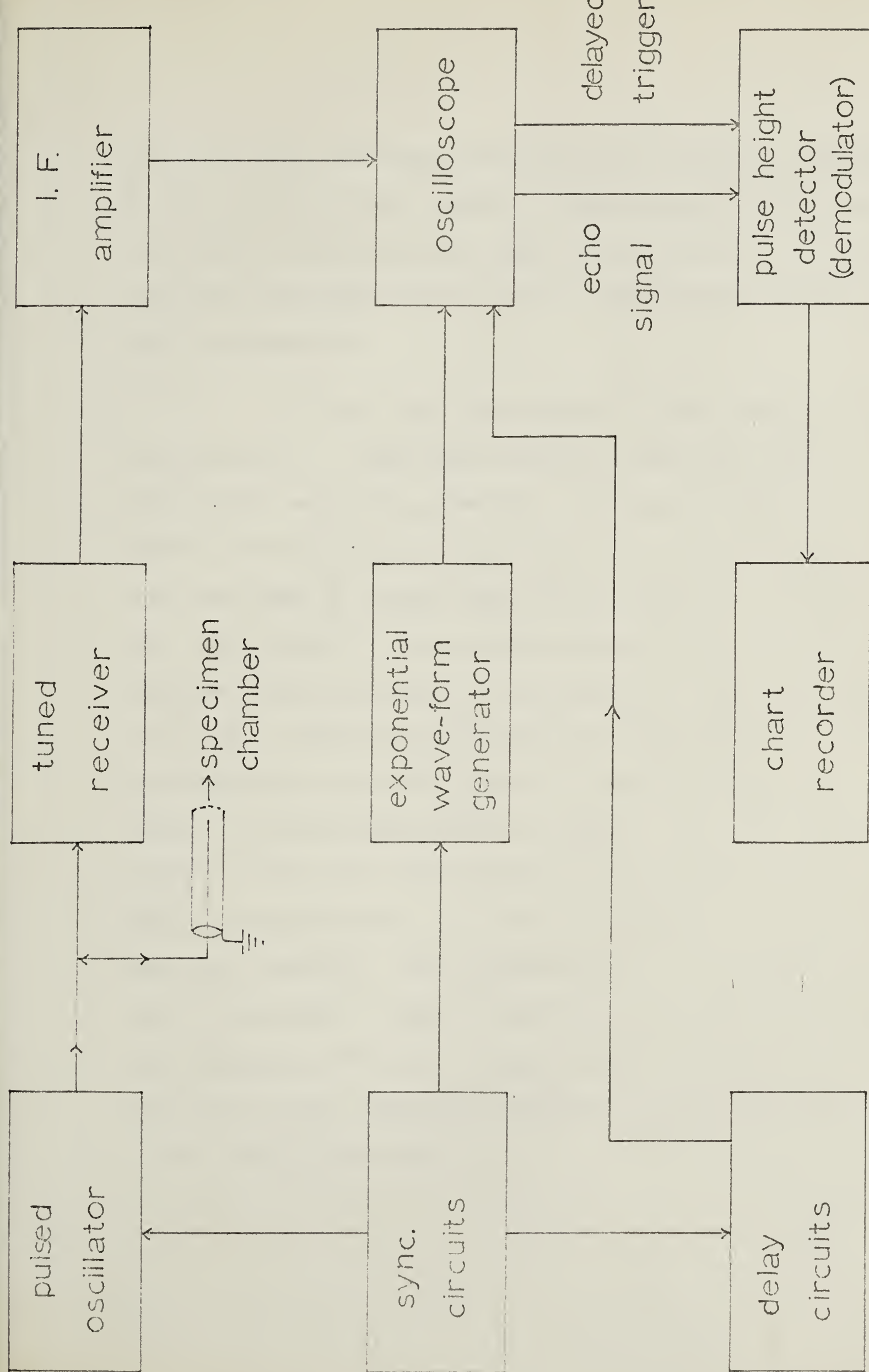
C. Ultrasonic Generator and Receiver

An ultrasonic generator, receiver and oscilloscope are incorporated in a single unit manufactured by Sperry Products, Inc. The operating range of the unit extends from 5 to 200 megacycles/sec, and the output is a 100 volt, 1 microsecond pulse matched to a 50 ohm coaxial cable. The pulse repetition rate is 100 per second, and the pulse length can be increased or decreased by a factor of two. (In addition there is a high impedance output not suitable for the frequency range 30-180 megacycles/sec used in the experiments).

The output of the pulsed oscillator is used to drive an appropriate transducer (usually a quartz crystal cut and polished to resonate at the desired frequency or some odd sub-harmonic). The mechanical output (ultrasound) of the transducer produced by the piezoelectric effect is coupled into the specimen under investigation. Reverberations or echoes in the specimen are picked up by the same transducer and coupled to a tuned receiver by a synchronization circuit which blocks out the receiver during pulse generation by the r-f oscillator. An i-f amplifier demodulates and amplifies the echo pulses which are then displayed on an oscilloscope. A block diagram of the circuit is shown in figure 5.1. As shown by the diagram an exponential wave form is provided by

FIGURE 5.1

Block Diagram of Ultrasonic Circuitry.



the circuitry which appears on the oscilloscope superimposed on the series of echo pulses. The exponent of this waveform is continuously adjustable and calibrated so that comparison with the echo pulses will yield a measurement of the ultrasonic attenuation.

In order that the series of echo pulses decrease exponentially in amplitude certain conditions must be satisfied by the specimen geometry. Ultrasound must be propagated between reflecting surfaces which are highly parallel. The surfaces must be large enough that with the transducer centrally placed on one of them negligible reflections are received from the sides of the specimen. The transducer itself is a resonant structure and this requires a certain minimum area of the two parallel transducer surfaces. The result of these requirements is that in the 10^8 cycle/sec range in which the experiments were performed the transducers must be approximately $1/4$ inch in diameter, the metal specimens must have parallel faces approximately $1/2$ square inch in area, and the distance between reflecting surfaces must be less than approximately $3/4$ inch. A more severe limitation on the thickness of the specimens is usually provided by the magnitude of the sound attenuation.

It is virtually impossible to measure the absolute magnitude of ultrasonic attenuation characteristic of the bulk material of a specimen because of uncertainties in the transducer efficiency, the efficiency of the transducer to specimen bond, and the reflection coefficients at the parallel faces of the specimen. However these factors are not functions of such variables as temperature or magnetic field, so the variation of the attenuation due to electrons with these parameters can be readily measured.

Many research groups use comparisons of an exponential waveform or calibrated pulse with echo amplitudes to obtain measurements of attenuation at constant temperature and magnetic field. The attenuation as a function of temperature or magnetic field can then be obtained only from a great many individual measurements. A quicker and more satisfactory method is to utilize a continuous recording of the amplitude of a selected echo along with a continuous recording of the other variable. For this purpose circuitry was constructed incorporating an electronic gate to select some appropriate interval from the receiver signal of the Sperry unit, and a capacitor-tube circuit which follows the echo amplitude and produces a d.c. output in the millivolt range. Suitable circuitry was incorporated to make the output a linear function of echo amplitude on two ranges and a logarithmic function on another range.

Finally, two signals proportional to echo amplitude and magnetic field strength are displayed on a two-pen Leeds and Northrup millivolt recorder. As mentioned previously, the magnetic field can be automatically varied linearly or reciprocally in time, and the sound attenuation (or echo amplitude) is displayed continuously on the chart recorder as a function of magnetic field H or $1/H$. This automatic recording technique facilitates very rapid measurements in comparison to the pulse comparison technique, and in addition the magnitude of any spurious effects or noise can be readily assessed.

D. Specimen Preparation

Since metal specimens used in the experiments must be large single crystals sufficiently pure so that $q\ell > 1$ when the sound frequency $\sim 10^8$ cycles/sec, for most metals the purity must be 99.999 % or better. Single crystals were either purchased or grown from polycrystalline material using a travelling furnace constructed for this purpose. Suitable gears and synchronous motors were used so that the travel rate could be adjusted between 0.1 and 10 cm/hr. A furnace designed to travel horizontally did not yield crystals

of sufficient quality, due to vertical mixing in the molten zone which resulted in an intolerable angular spread of the microcrystalline structure. (For de Haas-van Alphen or giant quantum oscillations the angular spread of micro-crystallites must be less than a few minutes of arc). This arrangement was replaced with one designed for vertical travel of the molten zone.

It is especially difficult to grow magnesium crystals owing to the high vapor pressure of magnesium at its melting point (~ 2 cm mercury), and to the great propensity of magnesium to oxidize and to absorb hydrogen at high temperatures. It was found that magnesium crystals grown in a hydrogen atmosphere, which is essential to avoid excessive oxidation, had to be outgassed at high temperatures for one or two days; this treatment effected a reduction of the residual resistance by a factor of two or three. The high vapor pressure contributed a great deal to the mixing in the molten zone of the horizontal apparatus. This mixing was absent with vertical travel of the furnace because then the upper portion of the molten zone serves as a vapor seal for the lower, cooler, trailing edge.

Single crystals either grown in the laboratory or purchased were oriented by x-ray diffraction and spark

machined to suitable specimen geometries. Specimens were annealed and then hand-lapped so that reflecting surfaces were parallel to within one ten-thousandth inch. Occasionally specimens were further annealed after hand-lapping.

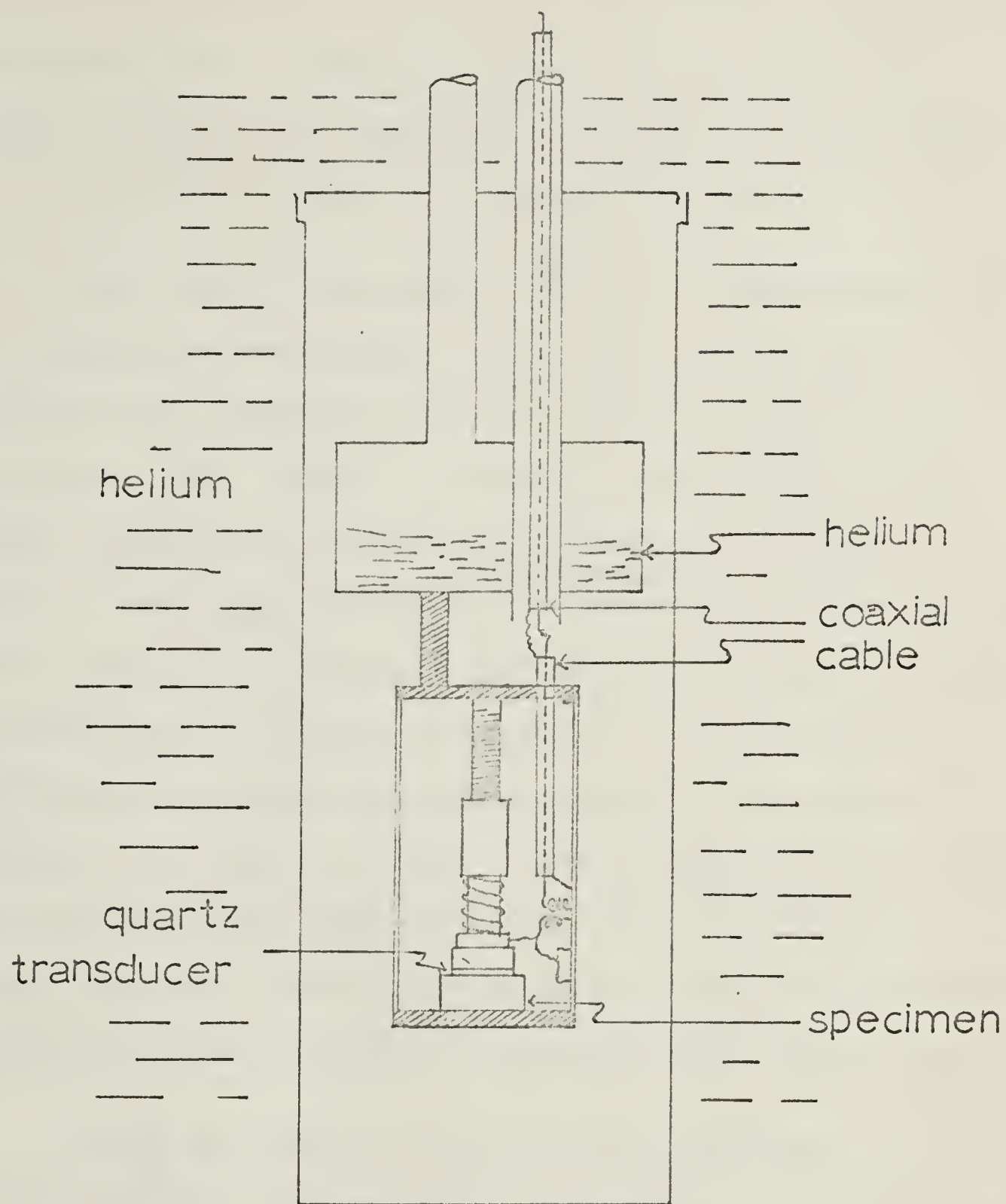
E. Specimen Chamber

The coaxial cable along which the pulses were transmitted was suitably constructed in the region between the high and low temperature sections of the cryostat to minimize heat flow. The most efficient arrangement proved to be standard 50-ohm teflon-insulated cable, separated just above the helium bath into two segments as shown in figure 5.2. Electrical connection of the two portions of the cable is effected by two fine copper wires one or two inches in length. Heat flow through these wires is negligible. The low temperature portion of the coaxial cable is connected to the tuned circuit of figure 5.3. By using various inductances L and variable capacitors C the circuit could be tuned to frequencies ranging from 10 to 180 megacycles, and matched to the 50-ohm impedance of the coaxial cable.

Transducers are most satisfactorily bonded to the specimens using silicone grease as the bonding agent. No-nac grease which is more commonly used has a tendency to fracture

FIGURE 5.2

Specimen Chamber.



at low temperatures. This is not surprising since No-nac has a water base and the recrystallization of ice can easily result in fracturing during the cooling process.

Since only longitudinal ultrasonic waves were used in the experiments, the quartz transducers were X-cut. Transducers with a primary resonant frequency of 10 to 12 megacycles/sec were found to afford the most satisfactory compromise between efficiency at the desired operating frequency (\sim 100 megacycles/sec), and ease of tuning of the circuit in figure 5.3. At higher resonant frequencies the thinner crystals introduce larger capacitance, and the efficiency of the transducer at any frequency is inversely proportional to the index of the harmonic which must be used. Thus transducers with higher resonant frequency are more efficient for a particular operating frequency (which must be an odd multiple), but make tuning more difficult because of the increased capacitance.

Tuning was difficult for several reasons:

- (1) Characteristics of the circuit components are temperature dependent. In addition, to achieve a good bond between the transducer and the specimen, different bonding agents must be used at low temperatures than at room temperature. However, the poor room temperature bond of silicone grease, which is effective at low temperatures, is adequate to tune the circuit at room temperature if applied with extreme care.

FIGURE 5.3

Tuned Circuit in Specimen Chamber.

- (2) Variable capacitors, which might facilitate tuning at liquid helium temperatures, are unreliable in this temperature range.
- (3) Stray inductance and capacitance that are an appreciable fraction of the resonant values cannot be avoided. These factors are also temperature dependent.

Tuning is thus as much an art as a science, despite the scholarly write-ups of experimental technique which appear in the literature.

RESULTSA. Geometric Oscillations in Copper

Experiments were carried out to measure geometric oscillations in copper. Since a thorough study of this effect in copper has been made by Morse et al^{23,24} and by Bohm and Easterling²⁵, the primary aim was to gain familiarity with experimental procedure and to check the operation of the apparatus. Several experiments failed before results were obtained. The causes of failure were:

- (1) fracturing of the transducer to specimen bond during cooling from room temperature to liquid helium temperatures,
- (2) mechanical breakdown of a variable capacitor in the specimen chamber during fine tuning at liquid helium temperatures, and
- (3) inadequate specimen quality.

Only after several failures with other materials was it found that silicone grease serves as a good bond at liquid helium temperatures and does not fracture during the cooling process. Difficulties with the variable capacitor were avoided by tuning the circuit of figure 5.3 entirely at room temperature, with many tests at liquid air temperature to monitor the tuning.

The first copper specimen, from which no results were obtained, was spark machined from one end of a single crystal purchased from Research Crystals Inc. The crystal was grown from 99.999% pure copper by the floating zone process. Since during the crystal growing process the equilibrium impurity concentration of the molten zone may be considerably greater or less than in the solid phase, there may be regions near each end of the crystal which have a higher concentration of impurities than elsewhere. This factor, along with the possibility that mechanical stresses may have introduced strains and lattice imperfections which were not removed by annealing, may have reduced the mean free path of the electrons below the value required for observing magneto-acoustic effects.

Geometric oscillations were obtained in the second copper specimen, which was spark machined from a more central section of the crystal. Two of the chart recordings obtained, which show the amplitude of the first echo on one pen and the strength of the magnetic field on the other (varying reciprocally with time), appear in figures 6.1 and 6.2. Since none of the echo signal has been suppressed before recording it can be seen that the amplitude of the oscillations is very large.

FIGURE 6.1

Echo Amplitude vs. Magnetic Field for "Dog's Bone" Orbit.

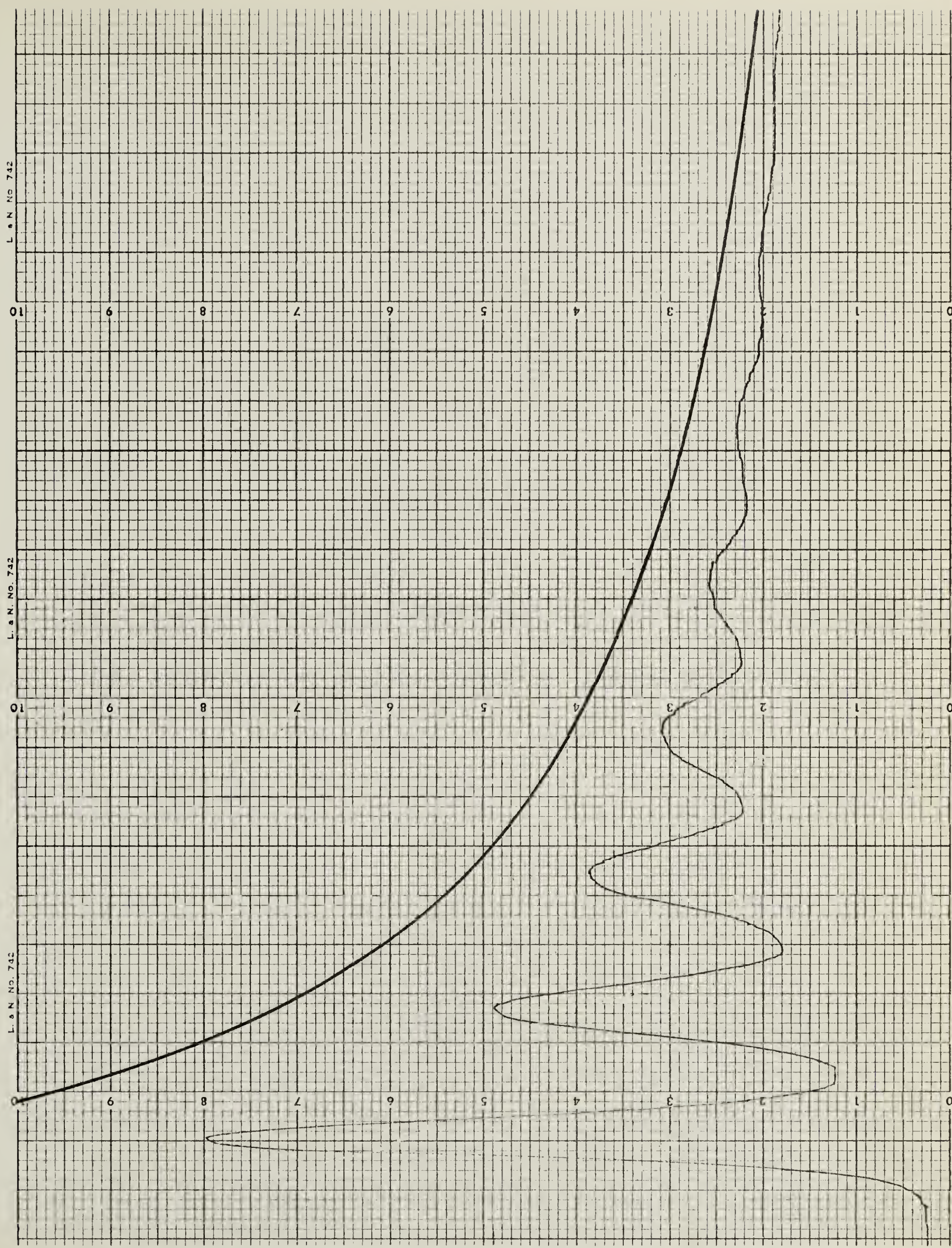
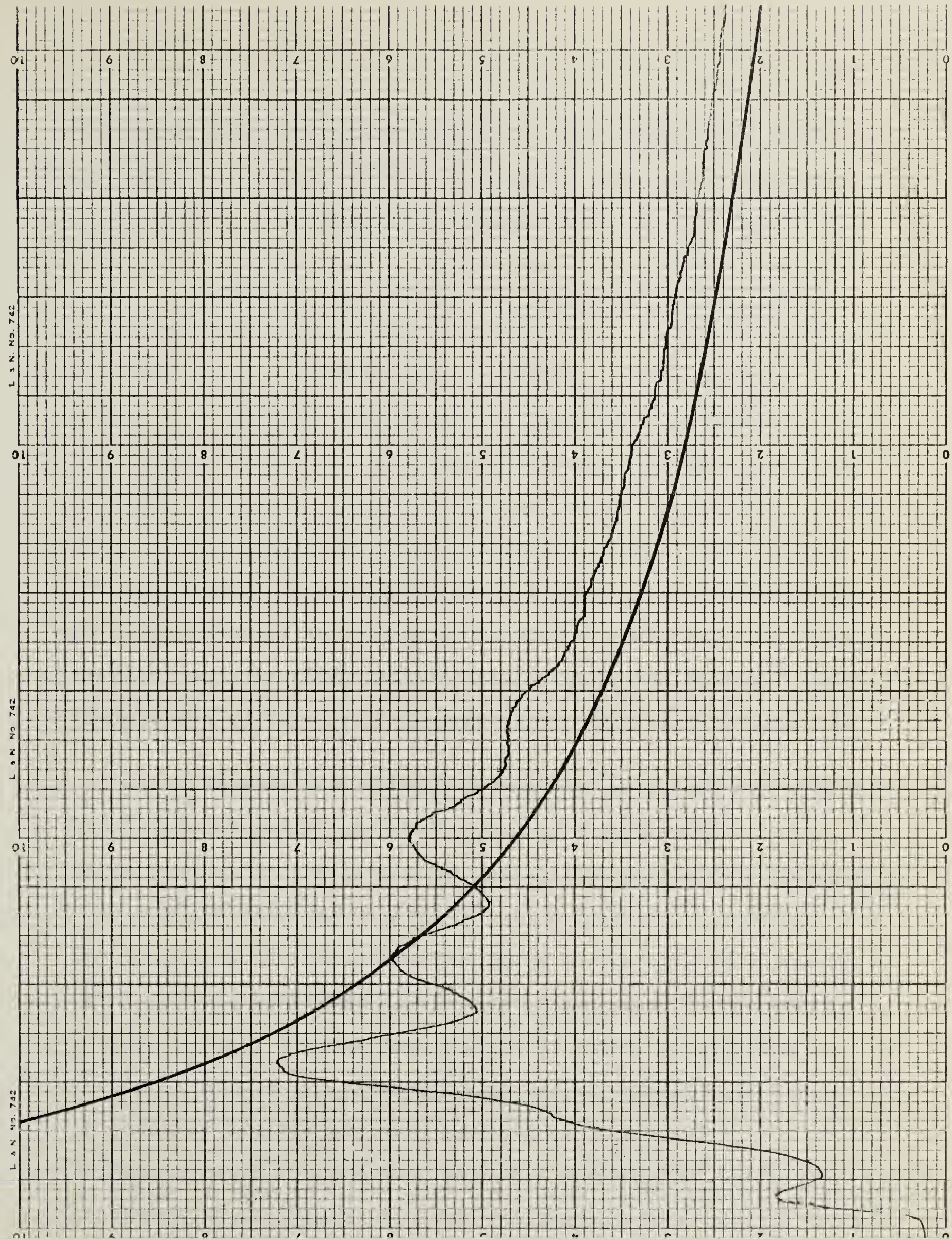


FIGURE 6.2

Echo Amplitude vs. Magnetic Field for Central Body Orbit.



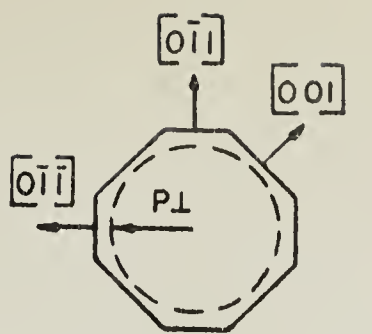
The sound waves were longitudinal and the frequency, obtained by calibrating the receiver with an r-f oscillator accurate to one part in 10^5 , was 137.3 megacycles.

Figure 6.3, showing the Fermi surface of copper in the extended zone scheme, indicates the characteristic extremal orbits contributing to geometric oscillations. Figure 6.1, showing oscillations arising from the "dog's bone" orbit, and figure 6.2, showing oscillations arising from the central body orbit, are very similar to the results of Morse²³. Oscillations arising from the central body orbit are more pronounced and greater in number than those obtained by Morse, indicating a larger $q\ell$ factor. From five to seven oscillations are observed and according to the theory²⁶ this indicates a $q\ell$ factor of between twenty-five and thirty-five.

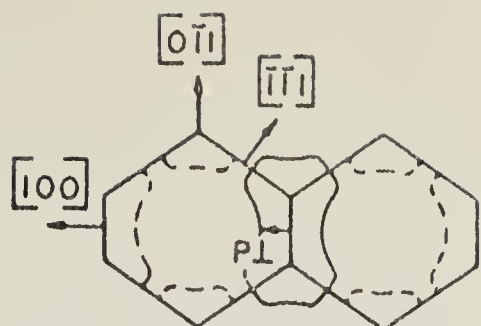
Figures 6.4 and 6.5 show plots of successive absorption extrema against the reciprocal of the magnetic field. Since scatter on the graphs is small, the accuracy of oscillation periods obtained should be better than a few percent. The sound velocity and thus the sound wavelength were obtained using elastic constants for copper measured at liquid helium temperatures by Overton and Gaffney²⁷. When the periods of the oscillations and wavelength of the ultrasound are used in equation 4.1, the extremal momenta obtained are $(1.22 \pm .03) \times 10^{-19}$ g-cm/sec for the "dog's bone" orbit and $(1.45 \pm .03) \times 10^{-19}$ g-cm/sec for the central body orbit. These

FIGURE 6.3

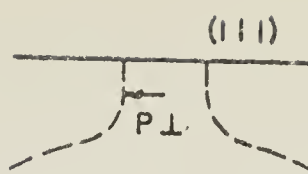
Extremal Orbits of the Fermi Surface of Copper.



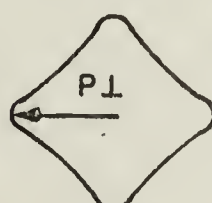
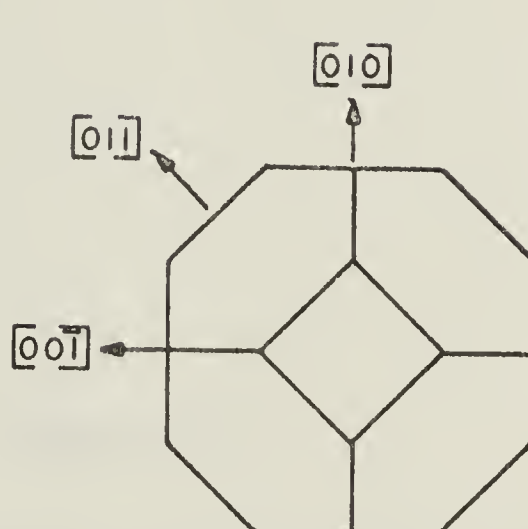
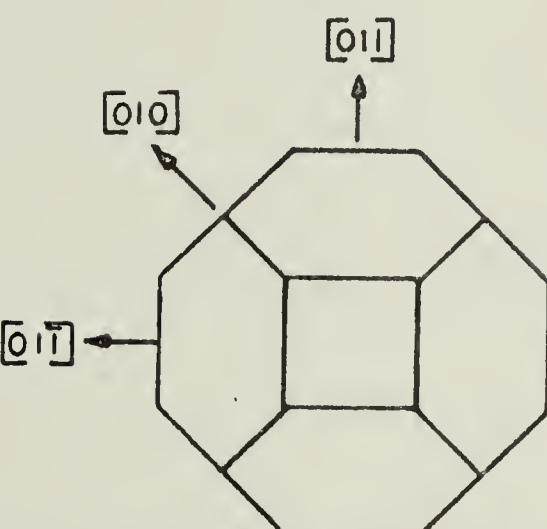
$q \parallel [011]$, $H \parallel [100]$
"BELLY" ORBIT



$q \parallel [011]$, $H \parallel [011]$
DOG'S BONE
(SHORT SIDE)

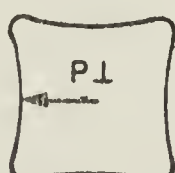


$q \parallel [1\bar{1}0]$, $H \parallel [1\bar{1}1]$
NECK ORBIT
(ALSO POSSIBLY
BELLY ORBIT)



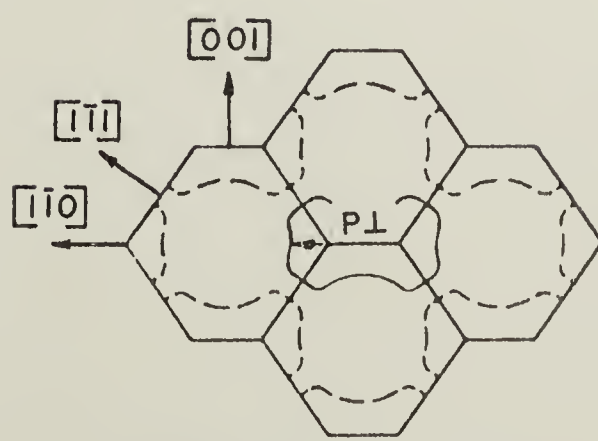
\vec{q} parallel to $[011]$

\vec{H} parallel to $[100]$

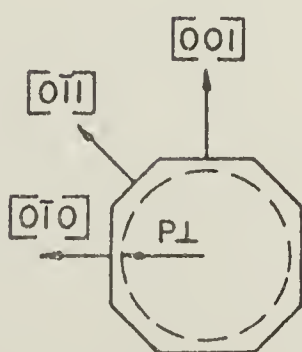


\vec{q} parallel to $[010]$

\vec{H} parallel to $[100]$



$q \parallel [001]$, $H \parallel [110]$
DOG'S BONE (LONG SIDE)



$q \parallel [001]$, $H \parallel [100]$
BELLY ORBIT
(ALSO POSSIBLY
ROSETTE)

FIGURE 6.4

Absorption Extrema vs. Magnetic Field for the "Dog's Bone" Orbit.

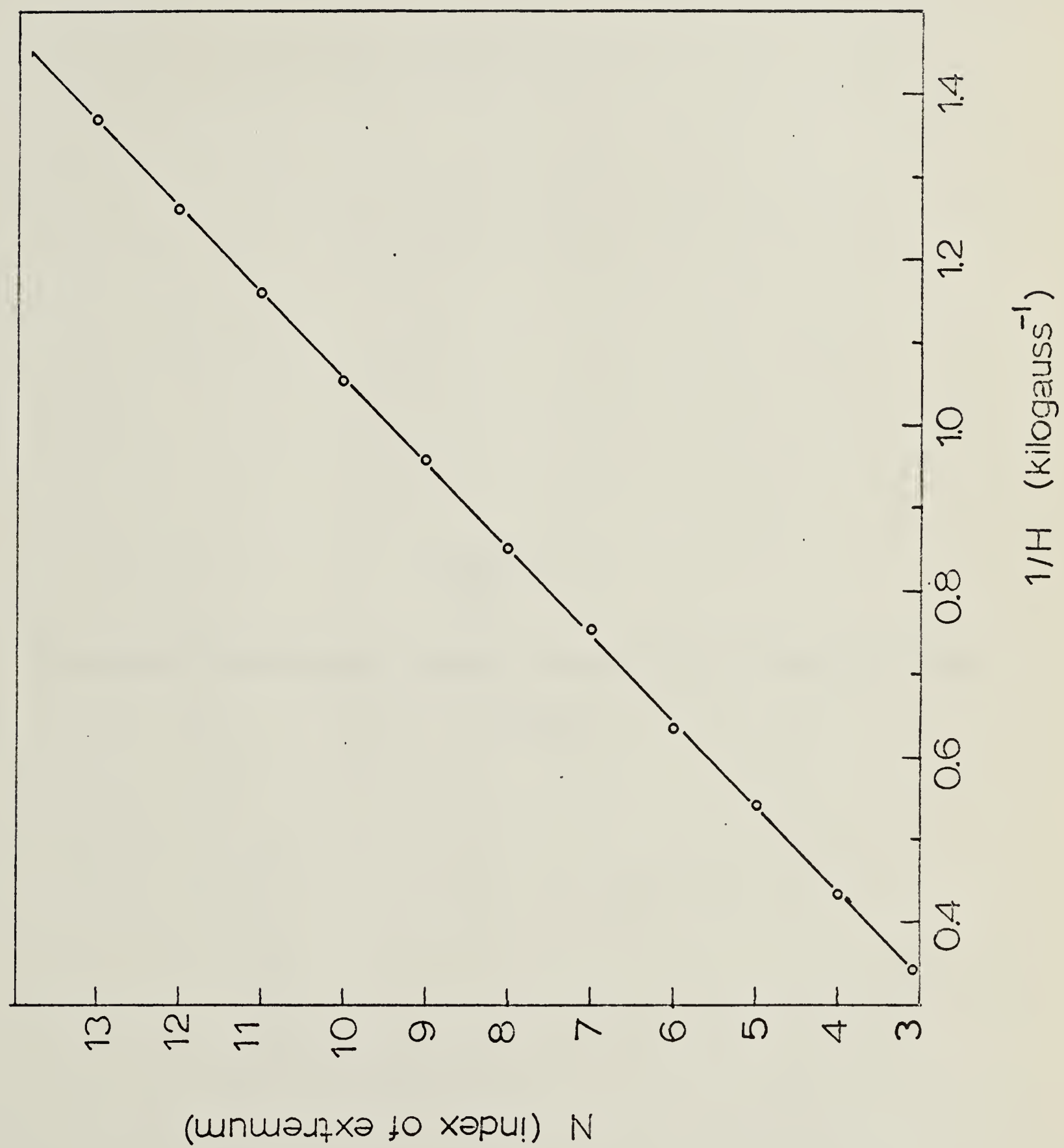
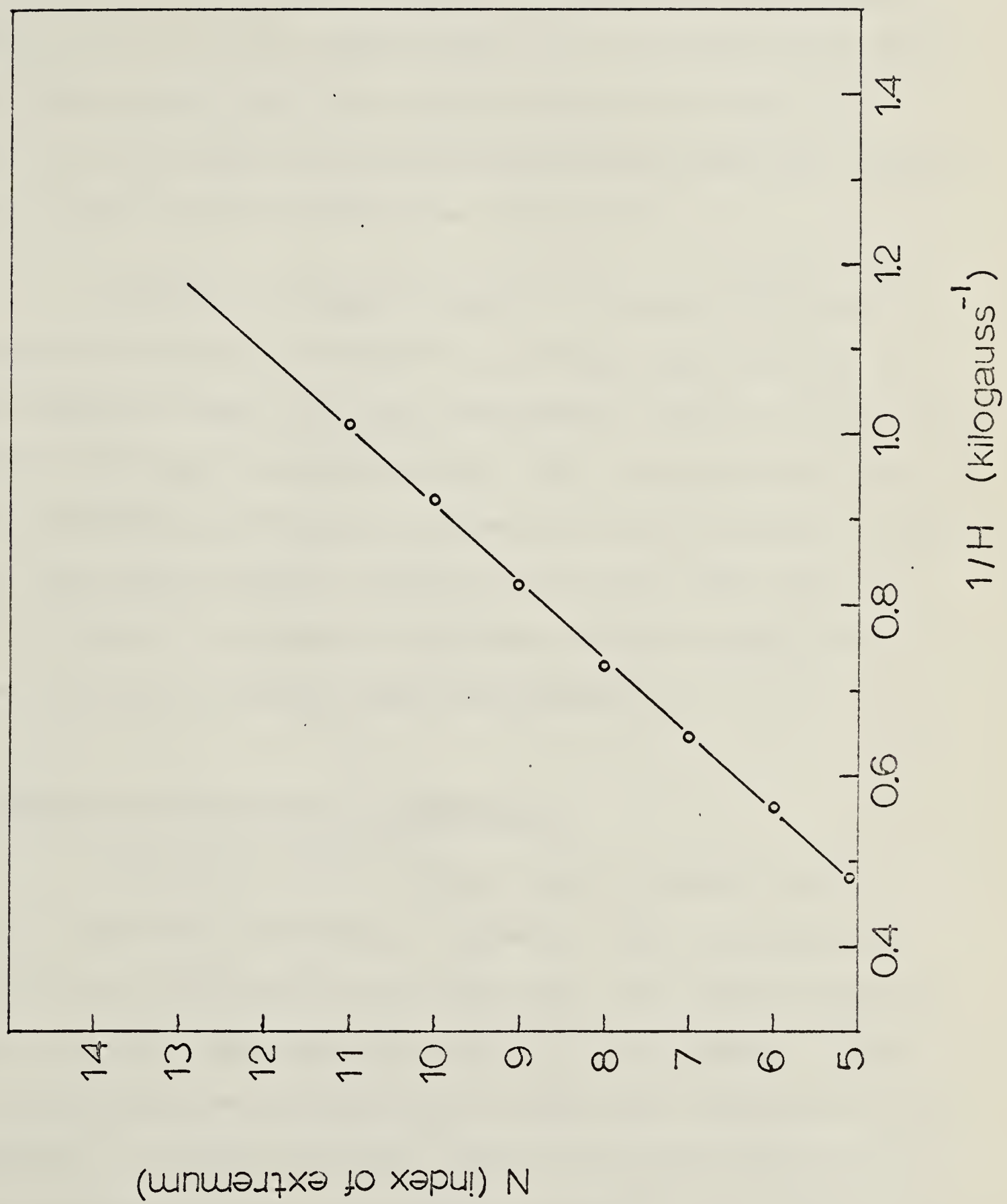


FIGURE 6.5

Absorption Extrema vs. Magnetic Field for the Central Body Orbit.



values compare with the values 1.22 and 1.41 obtained by^{23,24} Morse, and 1.22 and 1.49 obtained by Bohm and Easterling.²⁵ Morse's value for the central body orbit is based on a very weak oscillation, and the accuracy claimed by Bohm and Easterling for this orbit is 2%, which means that the results of all three investigations are compatible.

Further information can be obtained with respect to the Fermi surface of copper by propagating sound along other symmetry axes, but such measurement would only duplicate results which have been published. The primary objectives of the experiments performed on copper have been achieved, since large amplitude geometric oscillations have been observed, and the results inferred for extremal momenta agree with those of Morse et al and Bohm and Easterling.

B. Quantum Oscillations in Magnesium

Experiments were carried out on several single crystal magnesium specimens. Geometric oscillations were not observed with any of the specimens, and quantum oscillations were only observed with one of the specimens. Three of the specimens were grown from 99.99% pure polycrystalline magnesium. A fourth specimen, which was grown from 99.999% pure starting material by Cambridge Crystals Inc., yielded no results. A fifth specimen was grown in the laboratory from

99.999% pure magnesium obtained from the American Mining and Smelting Co. The residual resistance ratio of this specimen was $\frac{R_{4.2}}{R_{300}} \sim 7 \times 10^{-4}$. The absence of magnetoacoustic oscillations in any of the other specimens indicates that in these specimens the electron mean free path was considerably shorter than in the fifth specimen.

Two successful experiments were run on the fifth specimen. The direction of sound propagation for both experiments was about 10 degrees from the (10 $\bar{1}$ 0) axis in the (11 $\bar{2}$ 0) plane. The magnetic field vector was rotated in (10 $\bar{1}$ 0) and (11 $\bar{2}$ 0) planes. Figures 6.6, 6.7 and 6.8 show chart recordings typical of the results but chosen for orientations of the magnetic field where oscillations of only one or two periods in 1/H are present. The magnetic field was varied continuously and automatically from 0 to 20 kilogauss; however since oscillations of the sound absorption occurred only above 10 kilogauss most of the observations were restricted to the 10 to 20 kilogauss range.

No observations of magnetoacoustic oscillations in magnesium have been reported in the literature.

(i) Periods of the oscillations:

Four sets of oscillations periodic in 1/H were observed. Measurements were taken at two or three orientations of the magnetic field with ultrasonic frequencies of 27, 45, 63, and 81 megacycles/sec., to determine any variation of

FIGURE 6.6

Chart recording showing oscillations of the acoustic attenuation in magnesium. The magnetic field is approximately 20 kilogauss when the Hall probe trace is full scale. The magnetic field vector \bar{H} is in the $(11\bar{2}0)$ plane, 20 degrees from the (0001) axis and 60 degrees from the direction of the sound wave-vector \bar{q} . The large amplitude, long period D oscillation arises from the γ -orbits, and the short period B oscillation arises from the β -orbits, as shown in figure 6.13.

L. & N. NO. 742 L. & N. NO. 742 L. & N. NO. 742

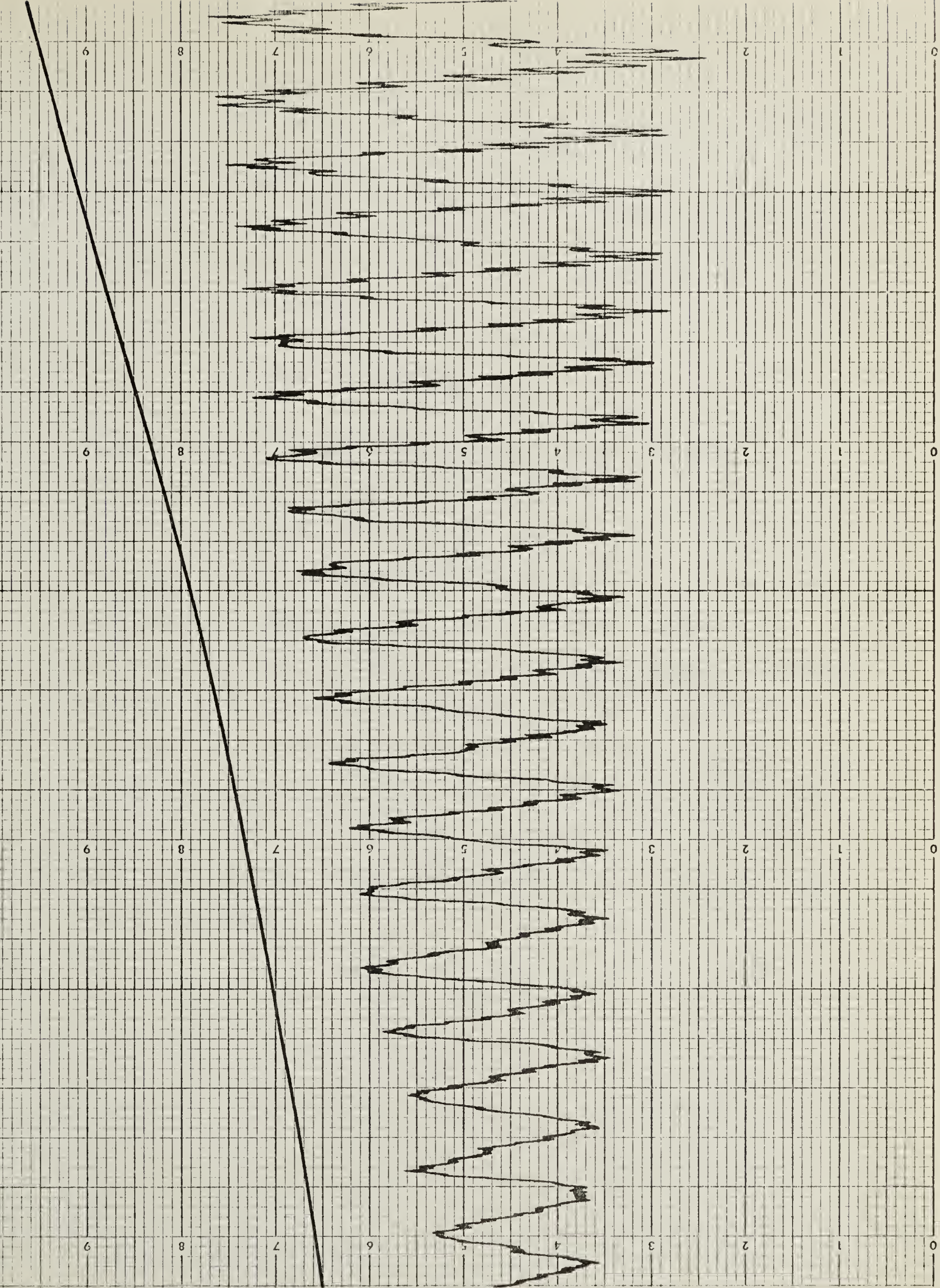


FIGURE 6.7

Chart recording showing oscillations of the acoustic attenuation in magnesium. The magnetic field is approximately 20 kilogauss when the Hall probe trace is full scale. The beat pattern is formed from B-oscillations arising from two pairs of β -orbits on the hole surface of figure 6.13. The magnetic field vector \bar{H} is in the $(11\bar{2}0)$ plane, 5 degrees from the $(10\bar{1}0)$ axis, and 5 degrees from the direction of the sound wave-vector \bar{q} . The beats arise from a shift in the direction of magnetic field of the planes of the two pairs of β -orbits from extremal orbit positions. For one pair of orbits the period increases, for the other pair the period decreases.

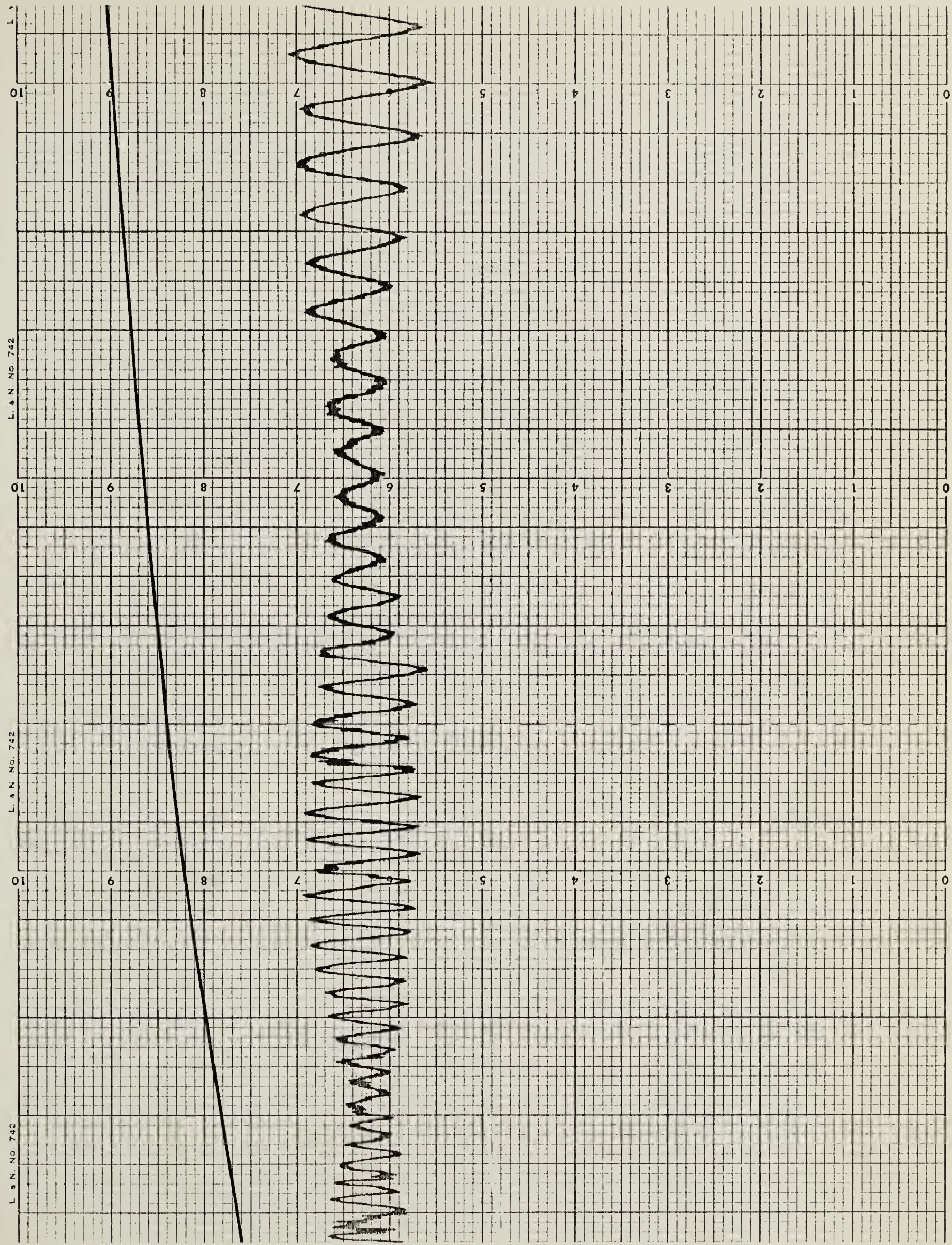


FIGURE 6.8

Chart recording showing oscillations of the acoustic attenuation in magnesium. The magnetic field is approximately 20 kilogauss when the Hall probe trace is full scale. The magnetic field vector \bar{H} is in the $(10\bar{1}0)$ plane, parallel to the (0001) axis. The sound wave-vector \bar{q} is 10 degrees from the $(10\bar{1}0)$ axis in the $(11\bar{2}0)$ plane. The long period A-oscillations arise from the α -orbits, and the short period C-oscillations arise from the λ -orbits, shown in figure 6.13.

L.S.N. NO. 742

10

9

8

7

6

5

4

3

2

1

0

L.S.N. NO. 742

10

9

8

7

6

5

4

3

2

1

0

L.S.N. NO. 742

10

9

8

7

6

5

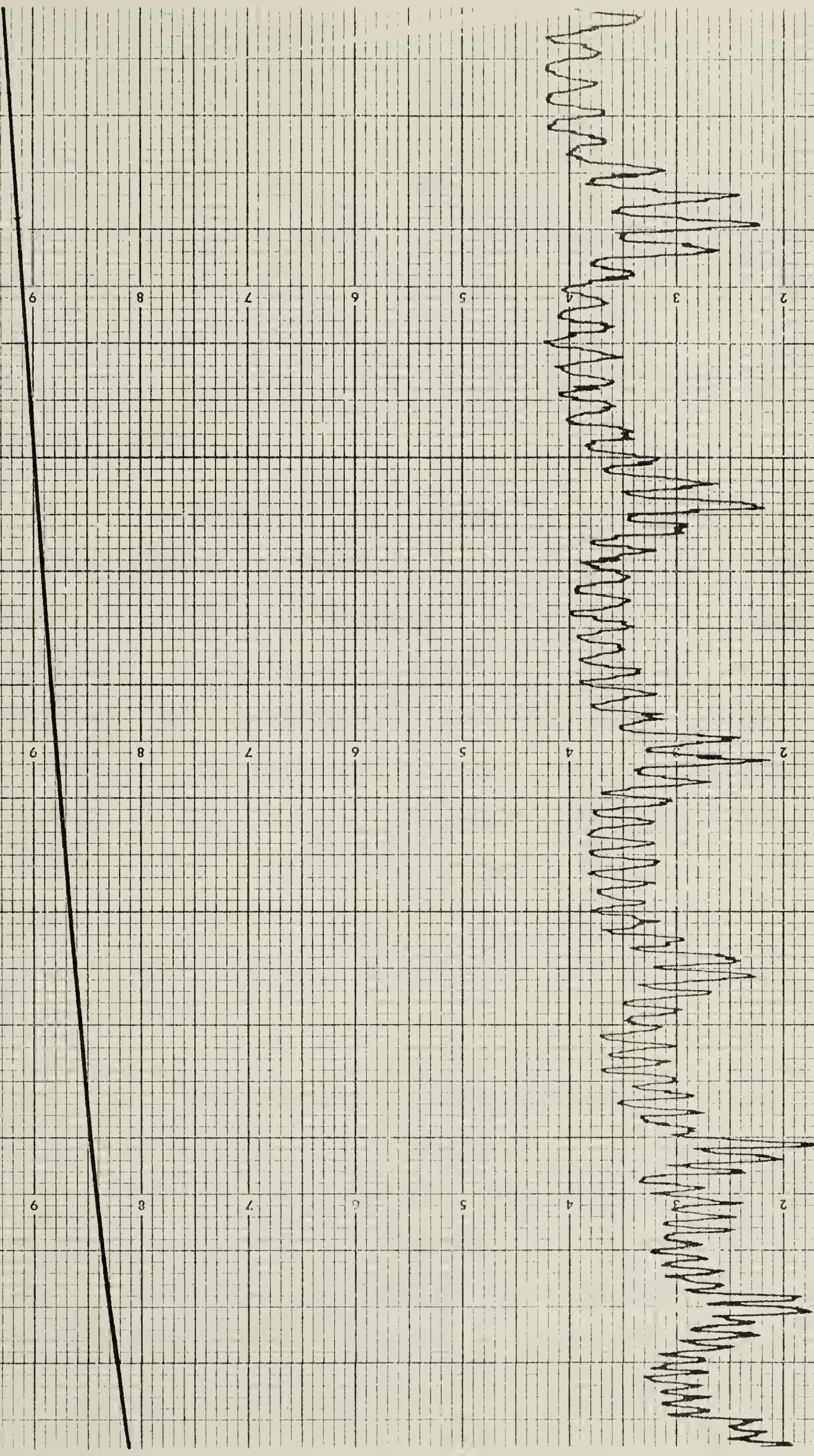
4

3

2

1

0



the periods with the sound wave-vector \vec{q} . Periods of the oscillations were observed to be the same for all four cases. The periods were found to vary with orientation of the magnetic field as shown in figures 6.9, 6.10, and 6.11 (most of the periods were obtained at a sound frequency of 63 megacycles/sec.).

Periods A, B, and C have been observed by Priestley²⁸ in measurements of the magnetic susceptibility (de Haas-van Alphen effect). Priestley identified these periods with the orbits α , β , and λ of figure 6.12, which shows the Fermi surface of magnesium in the double zone scheme. The accuracy of the measurements is not quite so great as in Priestley's work, however within the experimental uncertainty the periods are identical with those he obtained. The extremal areas of the Fermi surface corresponding to these oscillations are discussed at length by Priestley and will not be discussed here.

A fourth set of periods, denoted by D, have been observed in susceptibility measurements by Gordon, Joseph and Eck²⁹. These oscillations have been identified with arms of the multiply connected hole surface in the second Brillouin zone. Variation of the periods with direction of the magnetic field is difficult to determine since for some orientations

FIGURE 6.9

$$\Delta(1/H) \text{ vs. } \theta'$$

Periods of the B-oscillations in magnesium with magnetic field \vec{H} in the $(11\bar{2}0)$ plane.

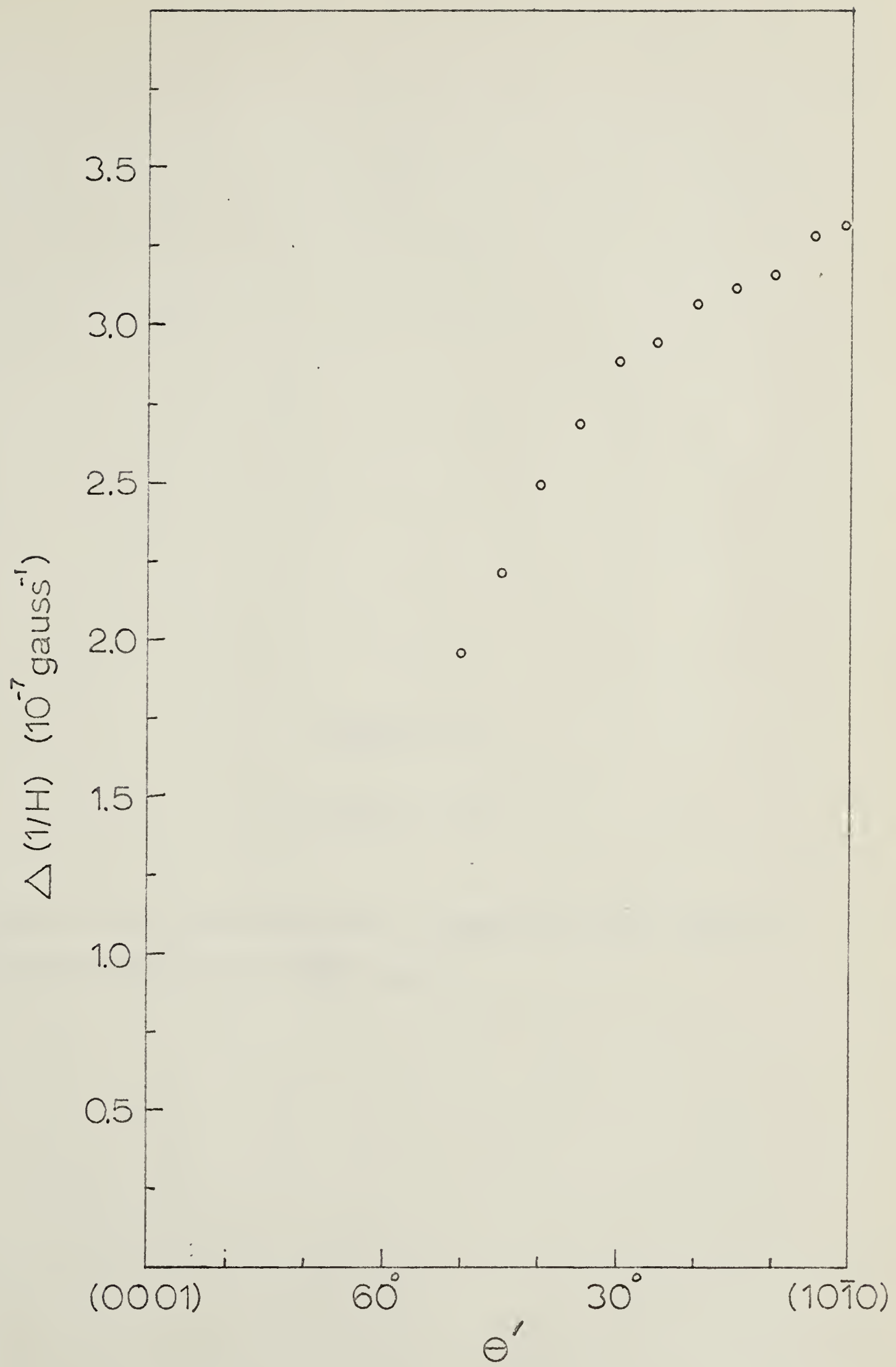


FIGURE 6.10

 $\Delta(1/H)$ vs. θ'

Periods of the D-oscillations in magnesium with magnetic field vector \bar{H} in the $(11\bar{2}0)$ plane.

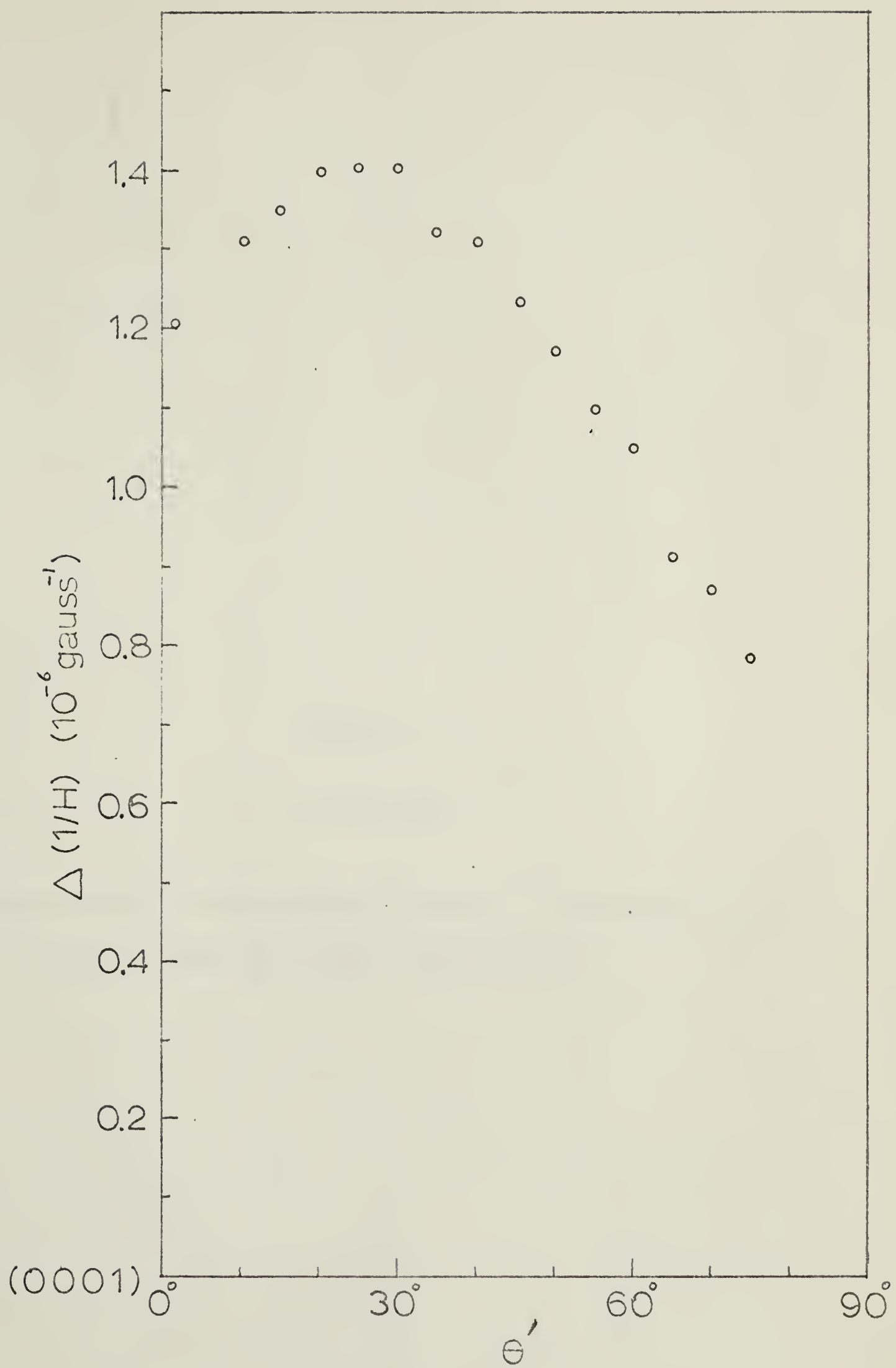


FIGURE 6.11

$$\Delta(1/H) \text{ vs. } \theta'$$

Periods of the A, B and C-oscillations in magnesium with magnetic field vector \bar{H} in the $(10\bar{1}0)$ plane.

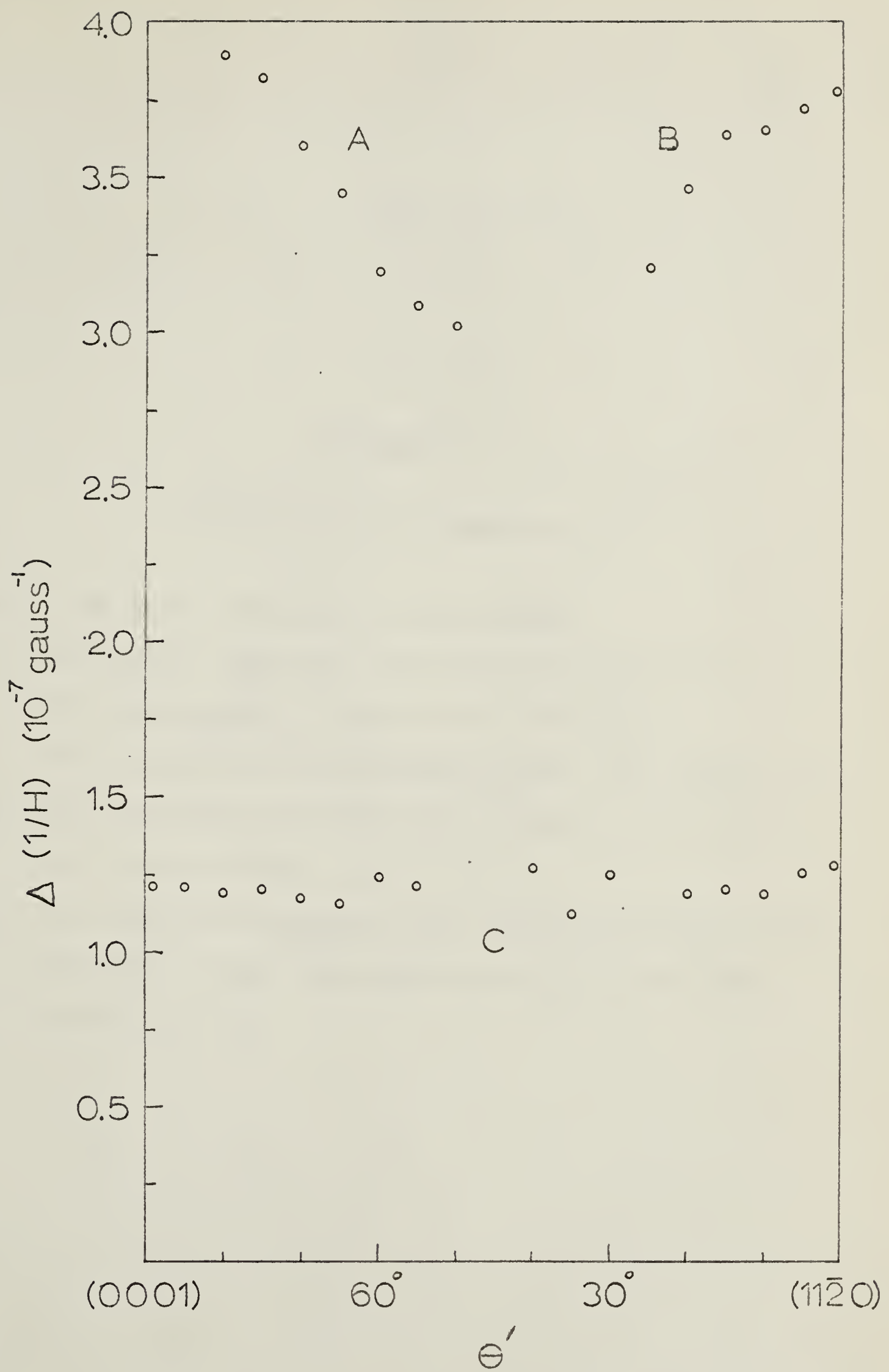


FIGURE 6.12

Fermi Surface of Magnesium.

Shown in the double Brillouin zone scheme.

(a) The double Brillouin zone used for magnesium.

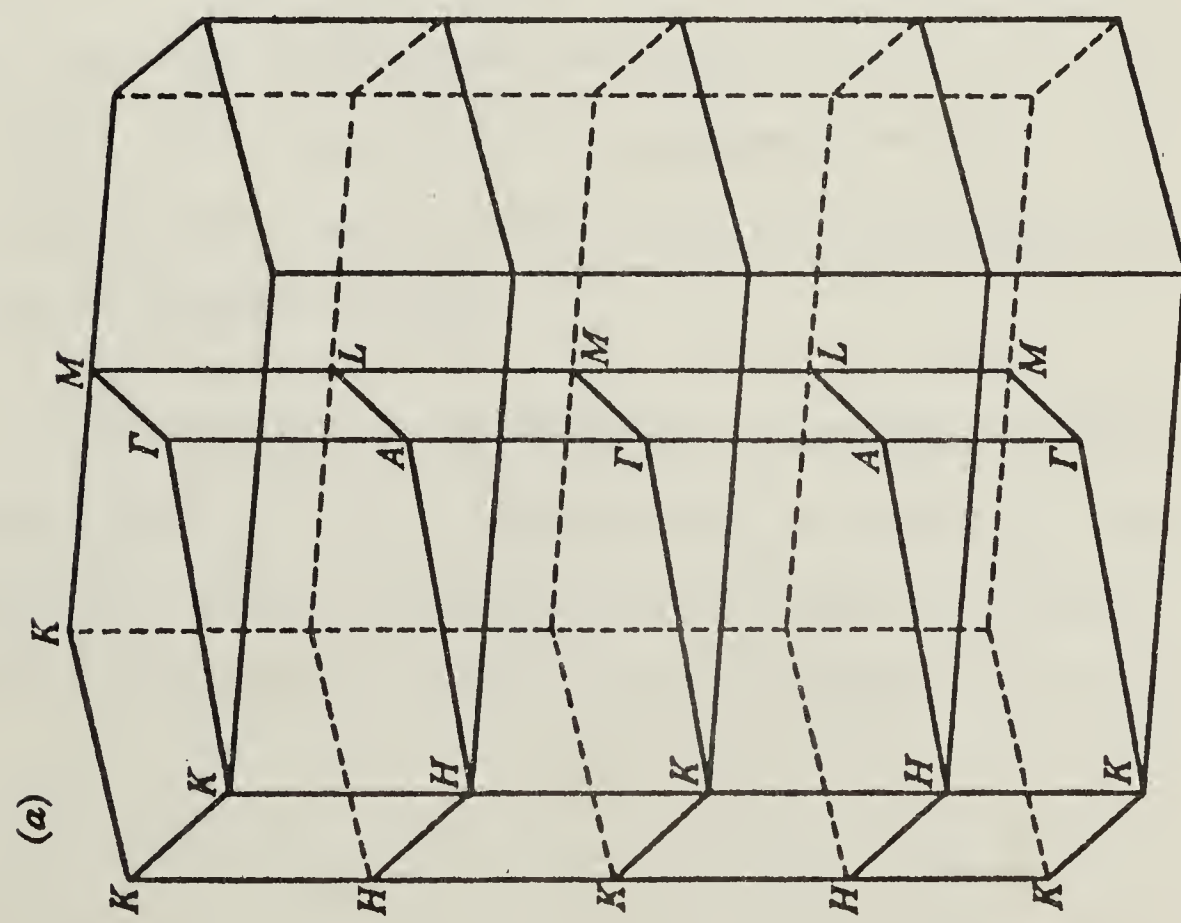
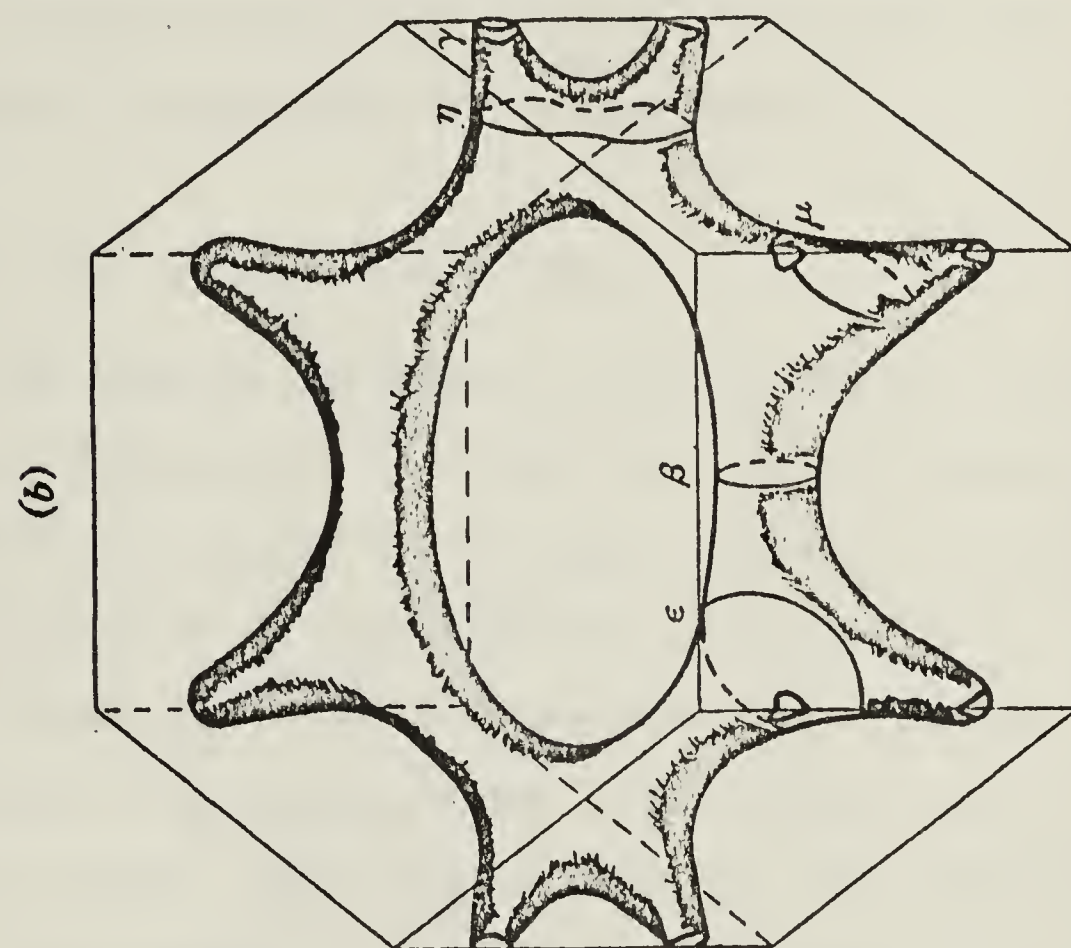
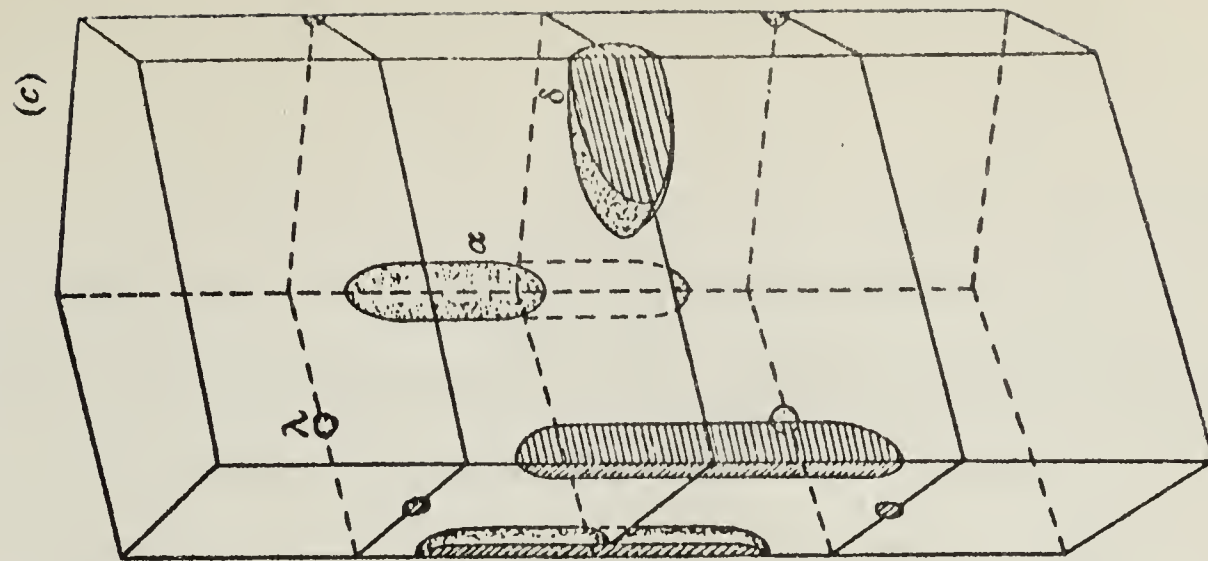
The dimensions of the zone at 0°K are:

$\Gamma A = 0.3211$ a.u., $\Gamma M = 0.6021$ a.u., $\Gamma K = 0.6951$ a.u.

(b) The multiply connected hole surface in the first and second zones.

(c) The electron surfaces in the third and fourth zones.

The part of the zone shown here is the lettered portion of (a).



there are many component periods arising from the twelve arms, and at other orientations the D oscillations disappear entirely. This latter feature is not characteristic of the results of Gordon et al and may occur because of distinctive features of the electron-phonon interaction which do not affect magnetic susceptibility measurements.

(ii) Amplitudes of the oscillations.

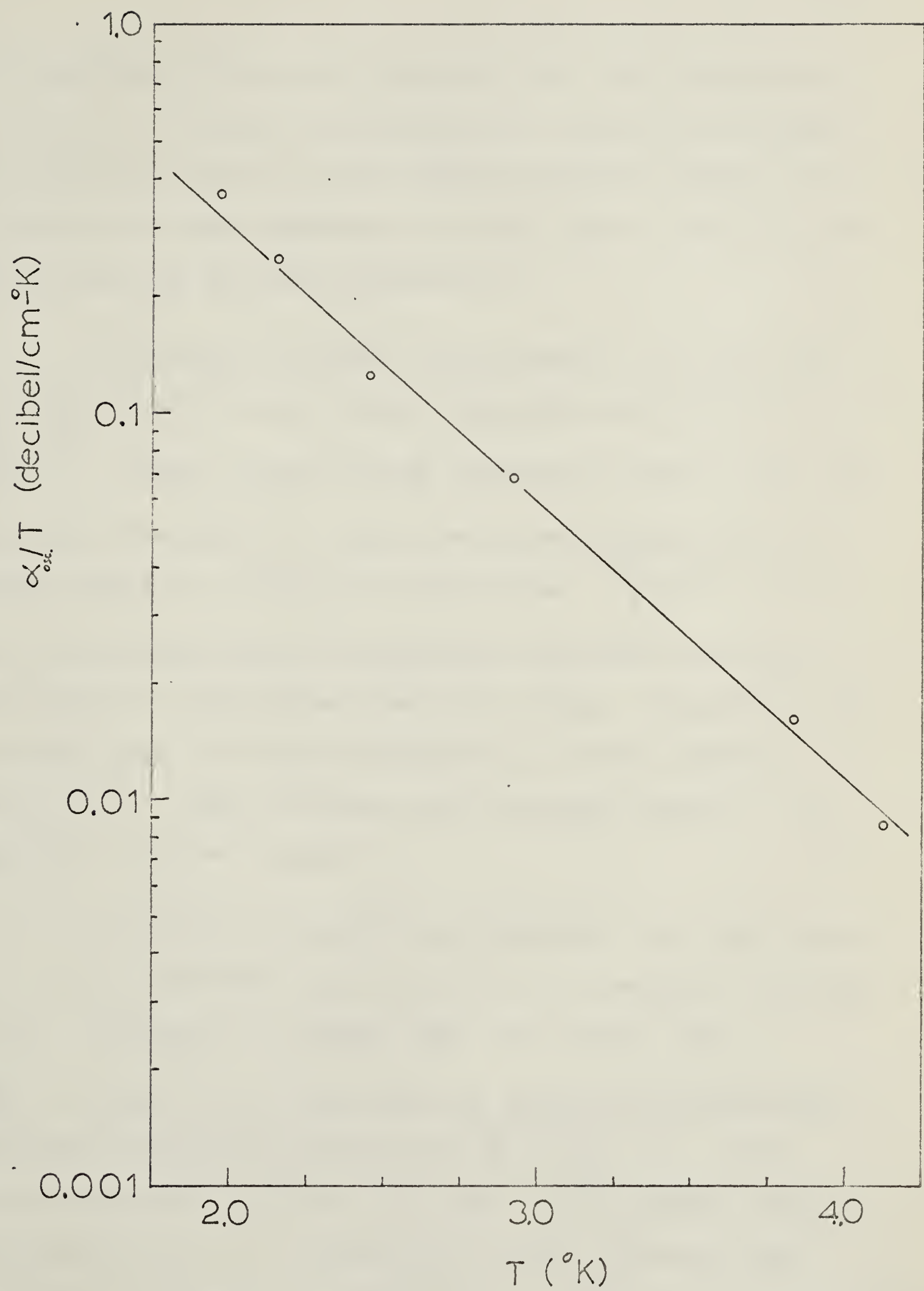
The maximum amplitude of the A, B and C oscillations is approximately 0.8 decibel/cm. This compares with a zero-field attenuation at the same ultrasonic frequency (63 megacycles/sec) of approximately 18 decibels/cm. (Since only the first and second pulse echoes were observed, and the second had very low amplitude, this figure is only accurate to $\sim 50\%$). The amplitude of the oscillations increases approximately linearly with the sound frequency (which is also the dependence exhibited by the zero-field attenuation). This result is in agreement with the Skobov theory. Oscillation amplitude also increases approximately linearly with magnetic field.

The temperature dependence of amplitude divided by temperature (α/T vs. T) is exponential as shown by figure 6.13. This behaviour is characteristic of de Haas-van Alphen oscillations where many Landau levels take part in the absorption

FIGURE 6.13

 α/T vs. T

Temperature dependence of the amplitude of a β -orbit oscillation in magnesium. \bar{H} is in the $(11\bar{2}0)$ plane, 5 degrees from the $(10\bar{1}0)$ axis.



simultaneously (equations 4.37 and 4.39). The temperature variation of α allows a calculation of the effective mass, which yields a value for the results shown in figure 6.13 of 0.20 m, in close agreement with the value 0.22 m obtained by Priestley at the same orientation.

According to Quinn and Rodriguez¹⁶, at 0°K, for this type of oscillatory effect the amplitude will be $(\frac{\hbar\omega_c}{E_f})^{3/2}$ times the zero-field attenuation when $\vec{q} \perp \vec{H}$, and negligible when $\vec{q} \parallel \vec{H}$. Since the effective mass of the example above is 0.20 m, at 20 kilogauss $(\frac{\hbar\omega_c}{E_f})^{3/2} \sim 10^{-3}$.

The observed amplitude in comparison with the zero-field attenuation is much higher than this ratio. In addition the amplitude does not become negligible, or even decrease, when $\vec{q} \parallel \vec{H}$. Thus the Quinn and Rodriguez theory is not supported by these results.

The Skobov theory¹⁷ also considers the case where many Landau cyclinders contribute to the absorption simultaneously. According to Skobov, when $kT \ll \hbar\omega_c$ and $(\frac{E_f}{\hbar\omega_c}) \gg (q_z \ell)^2 \gg 1$, the ratio of oscillation amplitude to zero field attenuation should be $\frac{q_z \ell}{\pi} (\frac{\hbar\omega_c}{E_f})^{1/2}$. The observed amplitude of the A, B, and C oscillations indicates a $q_z \ell$ factor of ~ 1 . Assuming an average effective mass $m^* = 0.2$ m and using the expression $\sigma = \frac{ne^2\tau}{m^*}$ for the zero-field

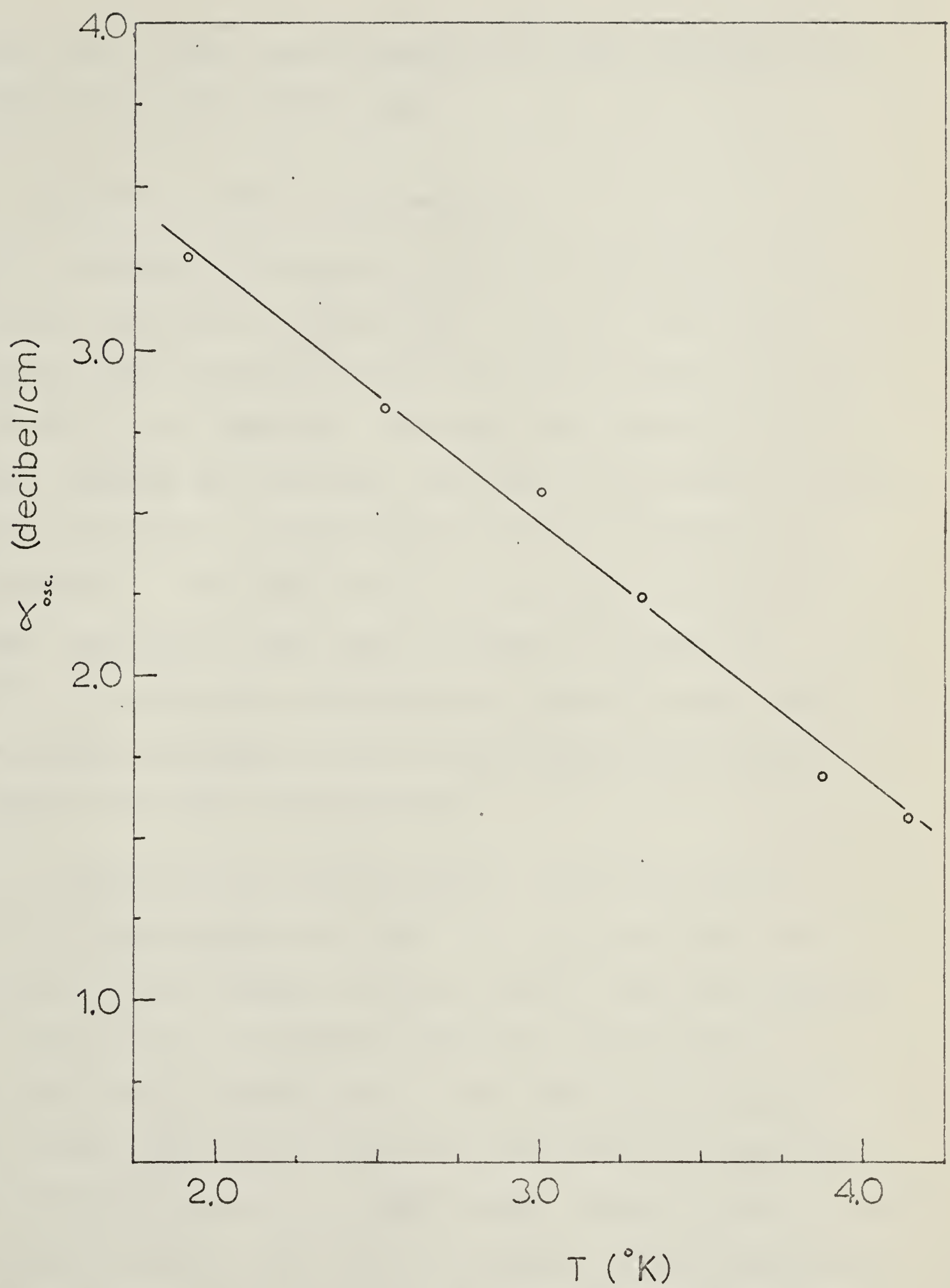
d.c. conductivity, the residual resistance ratio stated previously yields a rough estimate of $q\ell \sim 1$. Although the condition $(q_z\ell)^2 \gg 1$ is not satisfied, the amplitude is in reasonable agreement with the Skobov theory when $\bar{q} \parallel \bar{H}$. However the amplitude could decrease as θ approaches 90° and q_z decreases. Measurements were taken of the amplitude at 0.1 degree intervals with θ near 90° , and at 5 or 10 degree intervals for other orientations. The amplitude remained constant and angular variation of the amplitude as predicted by Skobov was not observed. Since the condition $(q\ell)^2 \gg 1$ is not satisfied this is not too surprising.

The maximum amplitude (at 63 megacycles) of approximately 4 decibels/cm observed for the D oscillations is much larger than for A, B or C oscillations. The D oscillations increase in amplitude linearly with ultrasonic frequency and field strength, as do the A, B and C oscillations. The D oscillations do not show a de Haas-van Alphen type of temperature dependence. Instead, as shown by figure 6.14, in the range 2 to 4°K the amplitude varies reciprocally with temperature, in agreement with the Gurevitch theory for giant quantum oscillations¹⁵ and the results of Shapira and Lax for gallium at ~ 100 kilogauss¹⁹. The magnitude and temperature dependence of the amplitude indicate that the D oscillations are more similar to giant quantum oscillations than to de Haas-van Alphen oscillations. Maximum amplitude was observed with

FIGURE 6.14

 α vs. T

Temperature dependence of the amplitude of a D-oscillation in magnesium. \bar{H} is in the $(11\bar{2}0)$ plane, 30 degrees from the (0001) axis.



H in the $(11\bar{2}0)$ plane, approximately 60° from the direction of \bar{q} and 20° from the (0001) axis.

(iii) Character of the D oscillations:

According to equation 4.35, in conjunction with the residual resistivity ratio $\frac{R_{4.2}}{R_{300}} \sim 7 \times 10^{-4}$, in these experiments the $q\ell$ factor is much too low for giant quantum oscillations to be observed. Although the D oscillations are not giant quantum oscillations, they are not de Haas-van Alphen oscillations either, and are characteristic of some intermediate regime. Oscillations of the intermediate regime have been observed in zinc and in bismuth by Toxen and Tansal³⁰. In both cases the $q\ell$ factor is much larger than in the present experiments, and it is difficult to explain the character of the D oscillations.

However, the D oscillations, following Gordon et al²⁹, are identified with arms of a multiply connected hole surface in the second Brillouin zone. With the magnetic field inclined 20 to 30 degrees from the (0001) axis to correspond with the orientation of the hole surface arms, it can be seen that if the arms are nearly regular cylinders and the field orientation is sufficiently close to the cylinder axis, only one Landau level will contribute to the absorption. In fact, the results of Gordon et al show that whatever the

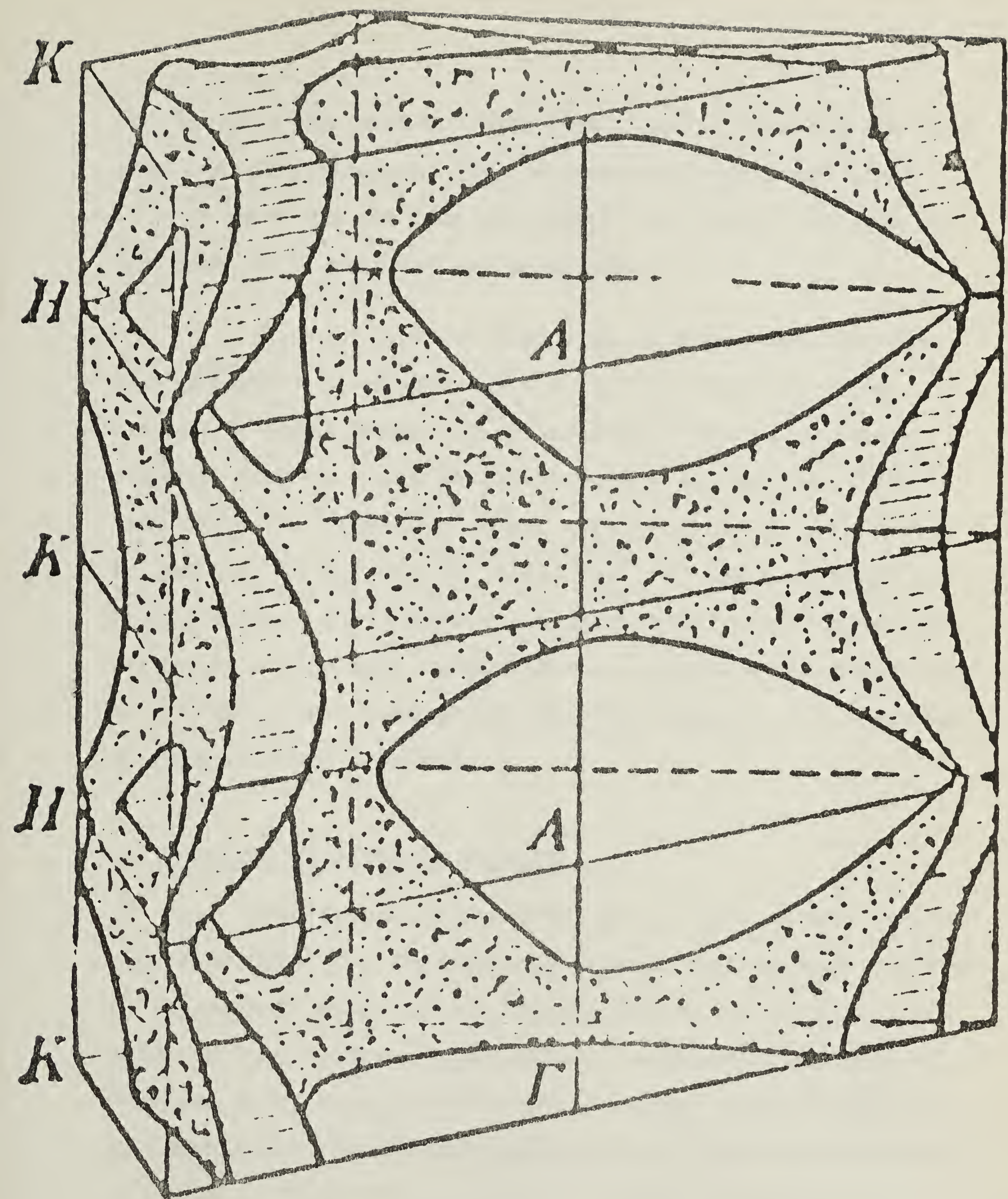
cross-section of the arms, it remains constant for a considerable distance along their length.

Of course, in the case discussed above absorption will only occur for values of the magnetic field such that $(E_f - n \hbar \omega_c)$ is in the range zero to approximately ΔE (for some integer n), where ΔE is the uncertainty of the electron energy. According to the uncertainty principle, ΔE is $\sim \frac{\hbar}{\tau}$. If the condition $\omega_c \tau > 1$ is satisfied, large oscillations in the sound attenuation similar to giant quantum oscillations will be observed.

Contributions to the attenuation from Landau levels intersecting the Fermi surface in regions of the hole surface other than the arms must be considered. According to Falicov and Cohen³¹, the degeneracy of electron energy levels at the hexagonal face of the Brillouin zone may be removed by spin-orbit coupling. If this is the case, the hole surface will be multiply connected in the (0001) direction as shown in figure 6.15. Then sound attenuation due to absorption at Landau levels intersecting the hole surface other than along the arms will oscillate with a very short period, since the areas of intersection will be much larger than the cross-sections of the arms. This contribution to the attenuation will then appear as a monotonic background plus a low amplitude, short period oscillation. Thus the large amplitude of the D

FIGURE 6.15

Fermi surface of a divalent hexagonal close-packed metal in the second band when spin-orbit coupling is taken into account (after Falicov and Cohen³¹).



oscillations may indicate spin-orbit splitting where the hole arms meet the hexagonal face of the Brillouin zone, since if this were not the case a tapered region near the ends of the arms would decrease the amplitude.

The variation of amplitude of the D oscillations with the angle θ between \bar{q} and \bar{H} is not expected to be typical of giant quantum oscillations or the intermediate regime. However these oscillations are an example of the fact that the topology of Fermi surfaces must be considered in addition to $q_z \ell$ and the ratio $\frac{\hbar\omega}{E_f}$ in discussing quantum oscillations. The character of quantum oscillations depends primarily on how many Landau levels contribute simultaneously to the ultrasonic absorption, and this number in turn depends on Fermi surface topology.

C. Quantum Oscillations in Zinc.

Experiments were carried out on four single crystal zinc specimens. No magnetoacoustic oscillations were observed in experiments conducted on two specimens, one of them spark machined from a large single crystal purchased from Research Crystals Inc., and the other from a single crystal supplied by Consolidated Mining and Smelting Co. This was interpreted as evidence that the $q\ell$ factor for these specimens was too low for oscillations to be observed (possibly much less than one),

although a spectrographic analysis of the latter specimen showed the purity to be 99.999%. Two specimens spark machined from a second single crystal obtained from CMS showed large amplitude oscillations of the ultrasonic attenuation coefficient.

Four successful experiments were conducted on one of these specimens. Unfortunately, this specimen was apparently contaminated in some way between the third and fourth experiments, since the amplitude of the oscillations was considerably reduced. Due to experimental difficulties, it was not possible to take amplitude vs. temperature measurements in the first three experiments, which meant that when such measurements were conducted during the fourth experiment, they yielded results considerably less accurate than if they had been obtained earlier. In addition, since the $q\ell$ factor had been considerably reduced, any measurements made were not typical of the phenomena observed in the first three experiments, since the nature of quantum oscillations depends strongly on the magnitude of $q\ell$. Subsequently a second specimen was spark machined from the same large single crystal as the first had been, however oscillations of the attenuation were not so great in amplitude as the earlier results. Both specimens were annealed several times to improve the $q\ell$ factor, however all attempts to effect an increase in the electron mean free path were unsuccessful.

A total of seven successful experiments were run on the two specimens. The direction of sound propagation for both specimens was within five degrees of the (0001) axis. The magnetic field vector was rotated in (10 $\bar{1}$ 0) and (11 $\bar{2}$ 0) planes, and rotated about the (0001) axis. In the third case, an angle of about 85 degrees was preserved between \bar{q} (or the (0001) axis) and \bar{H} for all orientations. Figures 6.16, 6.17, and 6.18 show chart recordings typical of the results. The magnetic field was varied continuously and automatically from zero to 20 kilogauss, however for most orientations of \bar{H} the observations were confined to the 10 to 20 kilogauss range.

Large amplitude quantum oscillations (~ 2 decibels/cm) were observed in zinc by Korolyuk and Prushchak³³, with $\bar{q} \parallel \bar{H}$. They made no study of the oscillations other than to remark that the amplitude decreased with increasing temperature.

Gibbons³⁴ has observed smaller amplitude quantum oscillations in zinc with the magnetic field direction, sound polarization vector and sound propagation vector mutually perpendicular. Again the only information obtained was that the amplitude decreased at higher temperatures.

(i) Periods of the oscillations:

Three sets of oscillations periodic in $1/H$ were observed. Measurements were taken at two or three orientations of the magnetic field, with ultrasonic frequencies 27, 45, 63, and

FIGURE 6.16

Chart recording showing oscillations of the acoustic attenuation in zinc. The magnetic field is approximately 20 kilogauss when the Hall probe trace is full scale. The magnetic field vector \bar{H} is in the $(10\bar{1}0)$ plane, 10 degrees from the $(11\bar{2}0)$ axis, and 80 degrees from the direction of the sound wave-vector \bar{q} . The longer period A-oscillation arises from the α or "cigar" orbits, and the shorter period B-oscillation arises from the β -orbits, as shown in figure 6.23.

L & N No 742

L & N No 742

10

9 8 7 6 5 4 3 2 1 0

L & N No 742

10

9 8 7 6 5 4 3 2 1 0

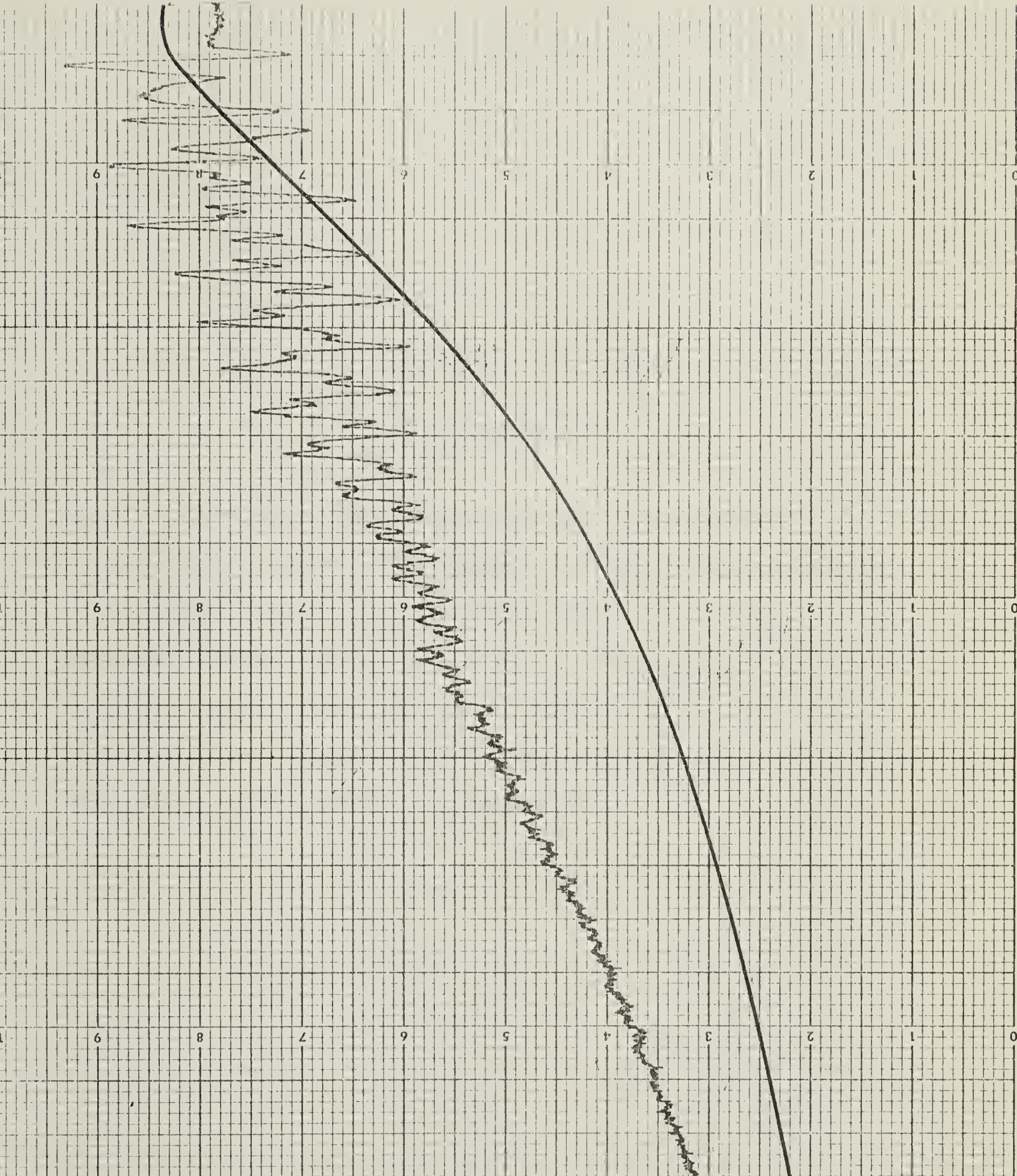


FIGURE 6.17

Chart recording showing oscillations of the acoustic attenuation in zinc. The magnetic field is approximately 20 kilogauss when the Hall probe trace is full scale. The magnetic field vector \bar{H} is in the $(11\bar{2}0)$ plane, 20 degrees from the (0001) axis and the direction of \bar{q} . The beat pattern arises from C-oscillations corresponding to the twelve γ -orbits shown in figure 6.23.

Lead No 742

10

9

8

7

6

5

4

3

2

1

0

Lead No 742

10

9

8

7

6

5

4

3

2

1

0

Lead No 742

10

9

8

7

6

5

4

3

2

1

0

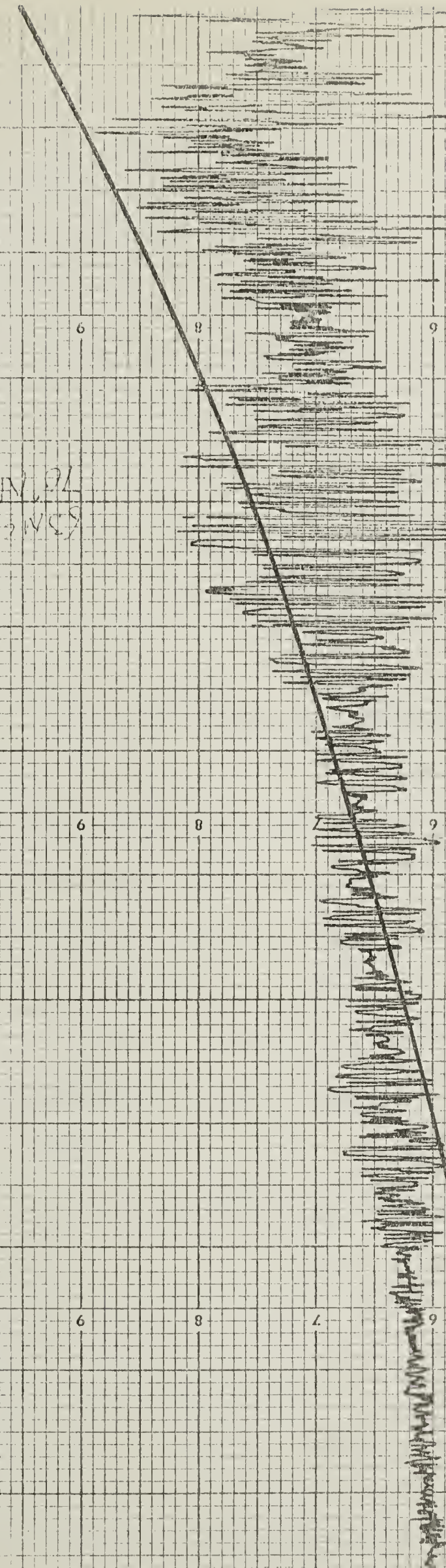
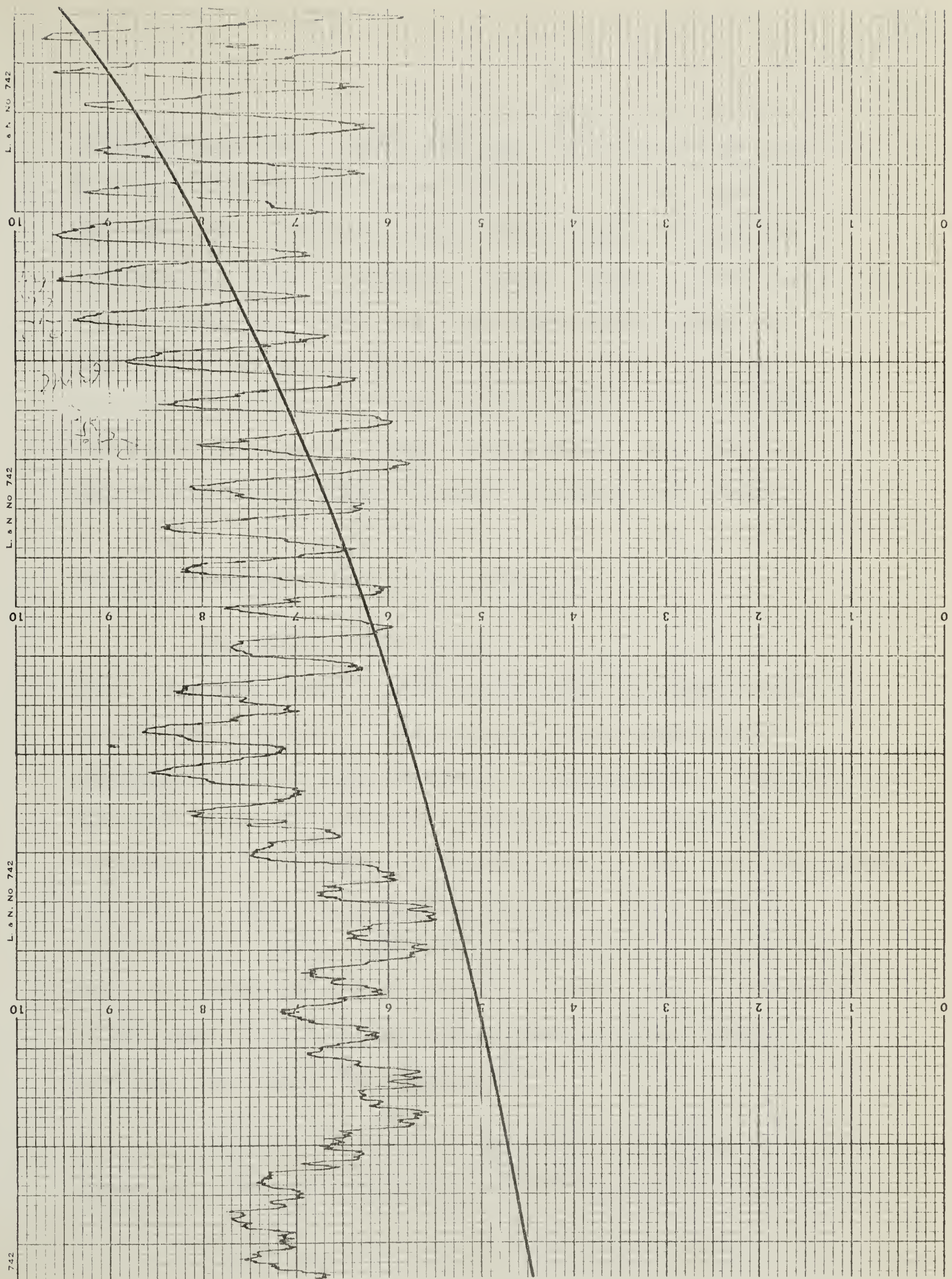


FIGURE 6.18

Chart recording showing oscillations of the acoustic attenuation in zinc. The magnetic field is approximately 20 kilogauss when the Hall probe trace is full scale. The magnetic field vector \bar{H} is in the $(11\bar{2}0)$ plane, 20 degrees from the $(10\bar{1}0)$ axis, and 70 degrees from the direction of the sound wave-vector \bar{q} . The long period A-oscillations originate from the α or "cigar" orbit and the shorter period B-oscillations originate from the β -orbit, as shown in figure 6.23. The A-oscillation shows the effect of spin-orbit splitting of the absorption maxima (echo-pulse minima).



81 megacycles/sec, to determine any variation of the oscillation periods with sound wave-vector \bar{q} . No such variation was observed. Variation of the periods with orientation of the magnetic field is shown in figures 6.19, 6.20 and 6.21. Periods denoted by A, B and C in these figures have been observed by Joseph and Gordon³² and identified with the periods α , β and γ of figure 6.22, which shows the Fermi surface of zinc in the single zone scheme. The results agree closely with those obtained by Joseph and Gordon.

(ii) Amplitudes of the oscillations:

The maximum amplitudes of the A, B, and C oscillations were each about 5 decibels/cm with the sound frequency at 63 megacycles/sec. This compares with a zero-field attenuation at the same frequency of approximately 8 decibel/cm. Thus the ratio of oscillation amplitude to zero-field attenuation is much greater than the ratio observed in magnesium for the A, B and C oscillations (0.8/18), and for the D oscillations (4/18). (The ratio observed for the D oscillations in magnesium only occurred for particular orientations of the magnetic field, and the $q\ell$ factor was not nearly so great as this ratio might suggest).

As was the case for magnesium, the maximum amplitude agrees with the predictions of Skobov¹⁷ within the experimental

FIGURE 6.19

$$\Delta(l/H) \text{ vs. } \theta'$$

Periods of the A-oscillation in zinc. The x's refer to observations with H in the $(10\bar{1}0)$ plane, the 0's to observations with H in the $(11\bar{2}0)$ plane.

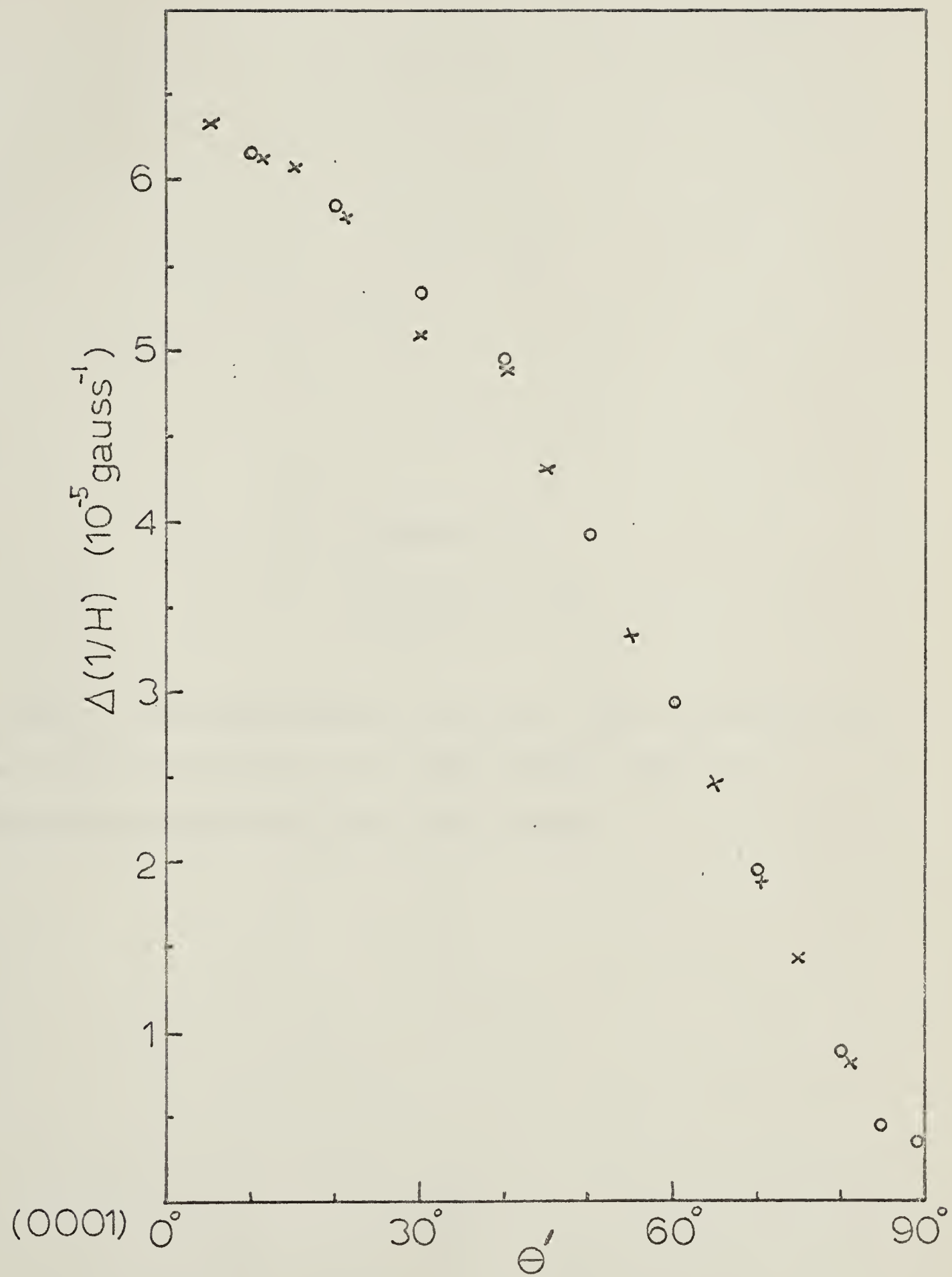


FIGURE 6.20

$$\Delta(1/H) \text{ vs. } \theta'$$

Periods of the B-oscillation in zinc. The x's refer to observations with H in the $(10\bar{1}0)$ plane, the 0's to observations with H in the $(11\bar{2}0)$ plane.

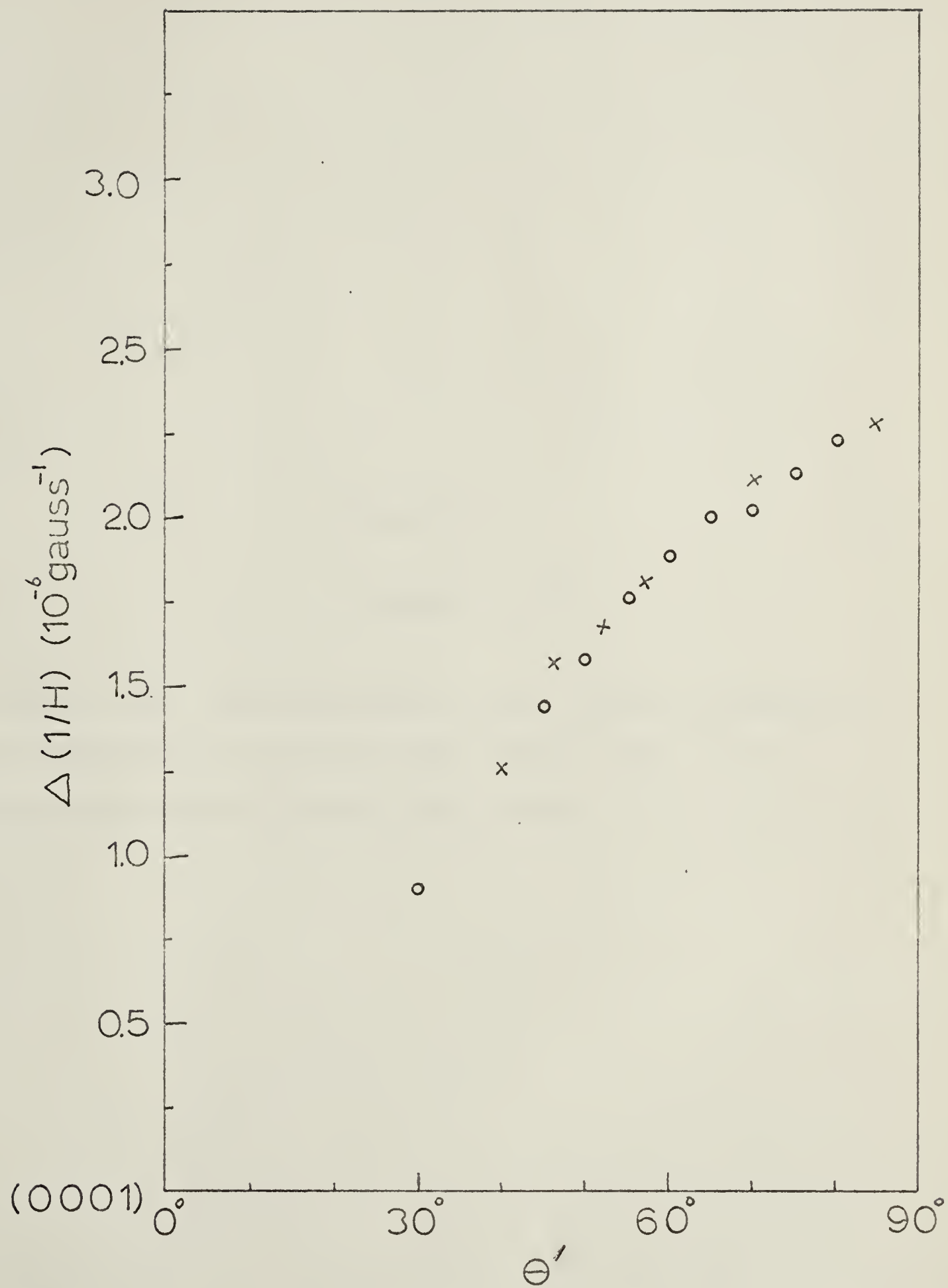


FIGURE 6.21

$$\Delta(l/H) \text{ vs. } \theta'$$

Periods of the C-oscillations in zinc. The x's refer to observations with H in the $(10\bar{1}0)$ plane, the o's to observations with H in the $(11\bar{2}0)$ plane.

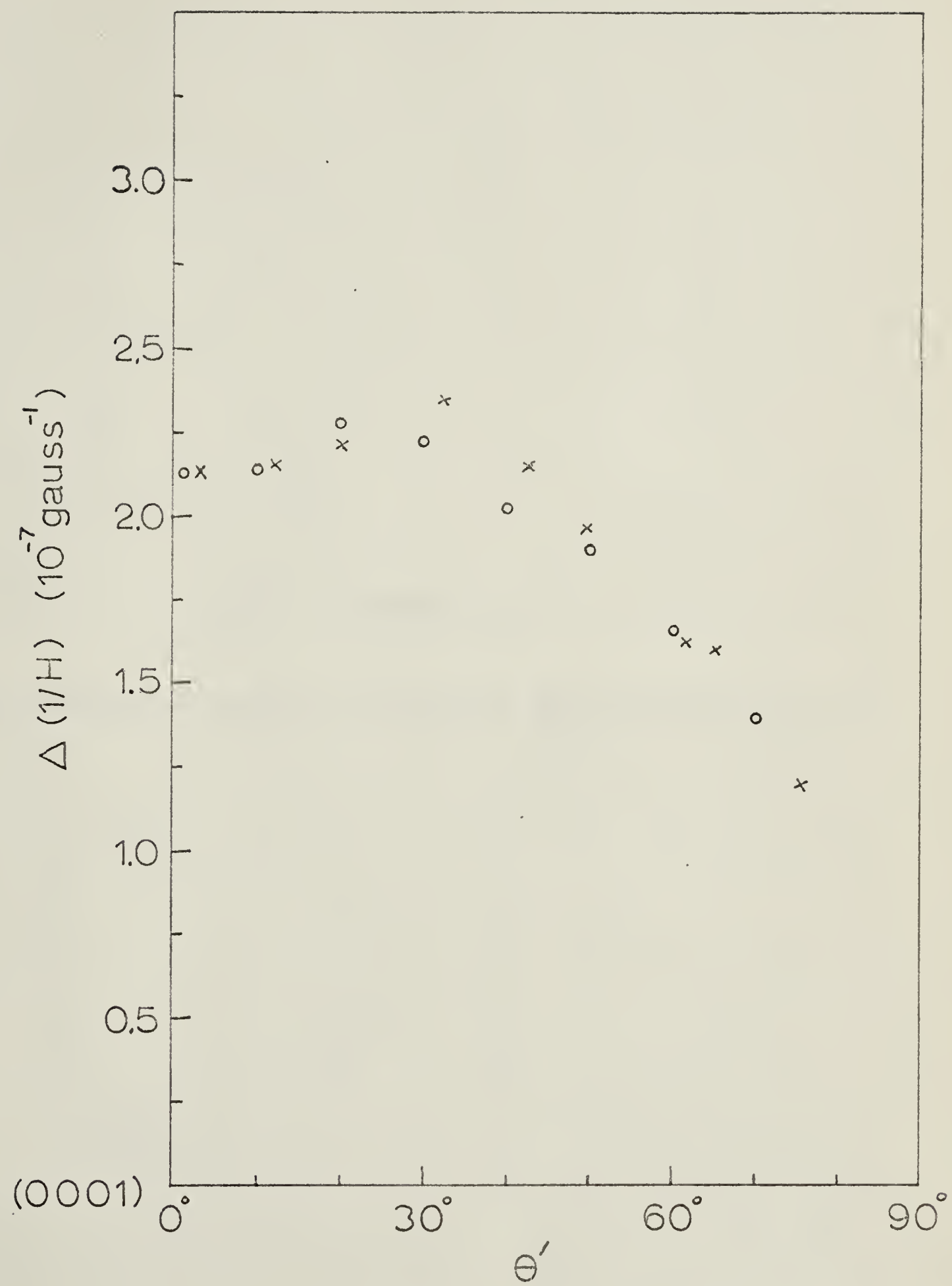
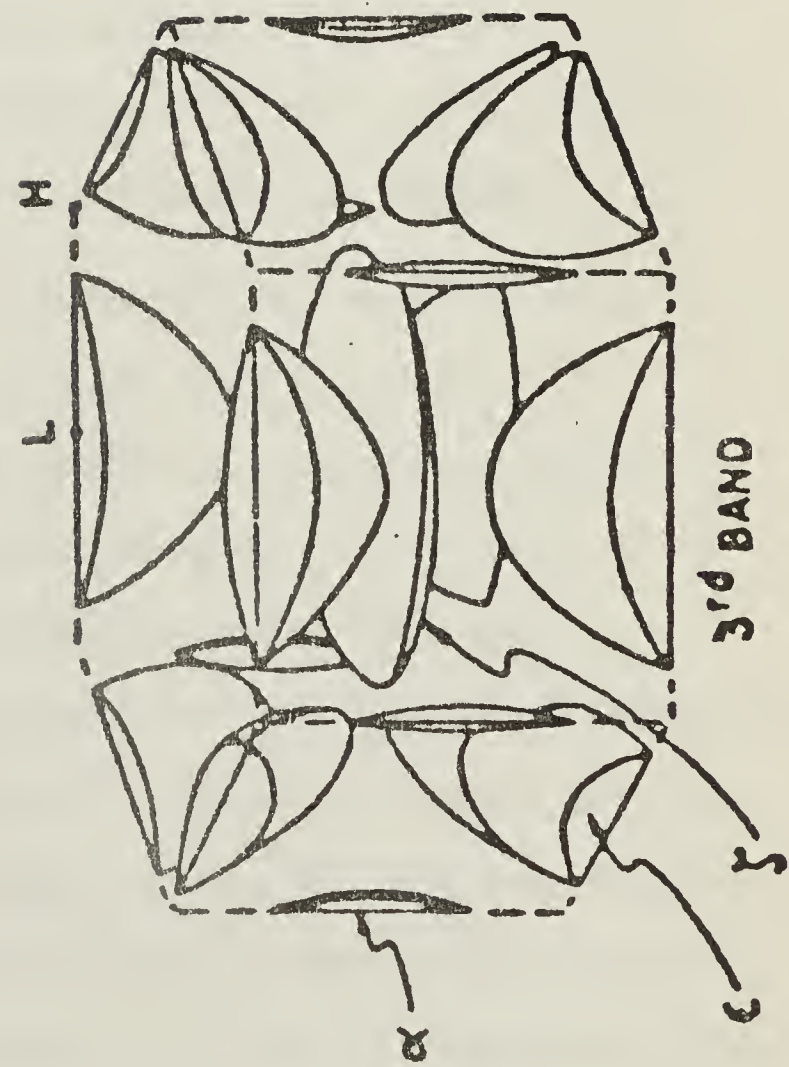
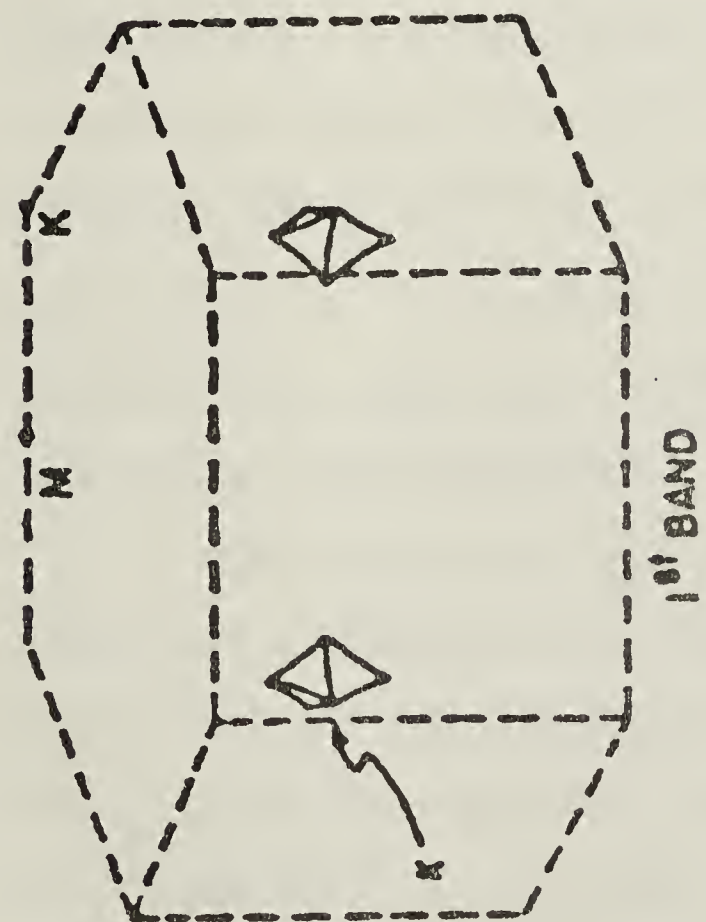
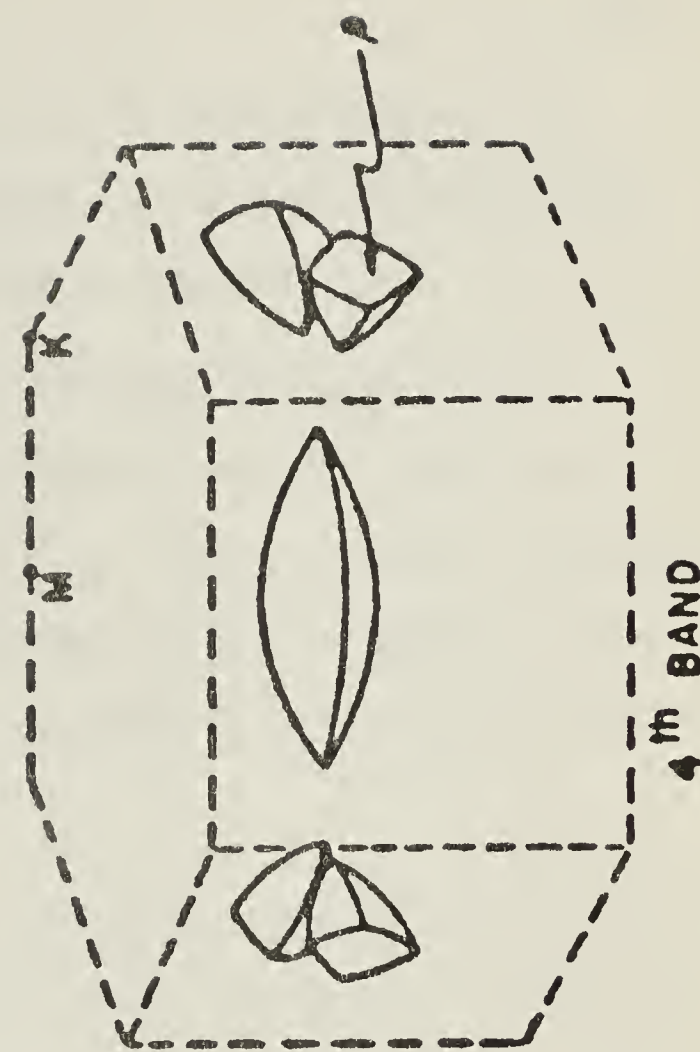
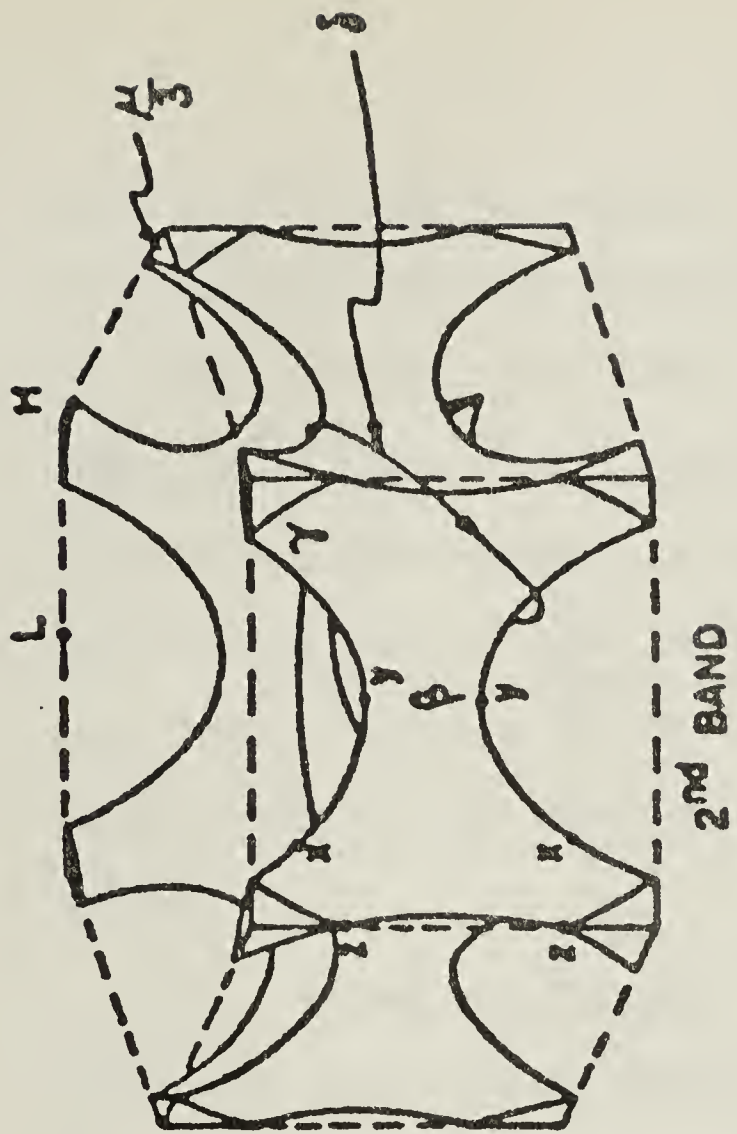


FIGURE 6.22

Fermi Surface of Zinc in the Single Brillouin Zone Scheme.



uncertainty. As an example, consider a B oscillation at 20 kilogauss, with an effective mass 0.2 m and an amplitude of 5 decibel/cm. Then using Skobov's result,

$$\frac{\alpha_{\text{osc}}}{\alpha_0} \sim \frac{q_Z \ell}{\pi} \left(\frac{\hbar \omega_c}{E_f} \right)^{1/2}, \text{ an estimate is obtained } q_Z \ell \sim 15.$$

A rough estimate of $q\ell$ can be obtained from the residual resistivity ratio $\frac{R_{4.2}}{R_{300}} = 3 \times 10^{-5}$. The $q\ell$ factor obtained from this source is 15 if the average effective mass in the conduction band is taken as ~ 0.2 m, which is a reasonable value.

Toxen and Tansal³⁰ have obtained results in bismuth where the oscillation amplitude is twice as great as the zero-field attenuation, which compares with the 2/3 ratio in these experiments. In both cases the oscillations cannot be regarded as giant or as the de Haas-van Alphen type, but are actually characteristic of an intermediate $q\ell$ regime. Since $q_Z \ell \sim \left(\frac{E_f}{\hbar \omega_c} \right)^{1/2}$, neither the expression of equation 4.37 (describing α when many Landau levels participate in the absorption simultaneously), nor Skobov's integral expression for α , applicable when $q_Z \ell$ is much larger, can be used with certainty to describe the sound absorption. However, in both cases the amplitude is expected to depend on the magnitude of $q_Z \ell$ according to Toxen and Liu¹⁸, and should thus vary as $\cos \theta$, where θ is the angle between \vec{q} and \vec{H} . The experimental results do not support this prediction in bismuth³⁰ or in zinc. (The results obtained for magnesium can not be considered here

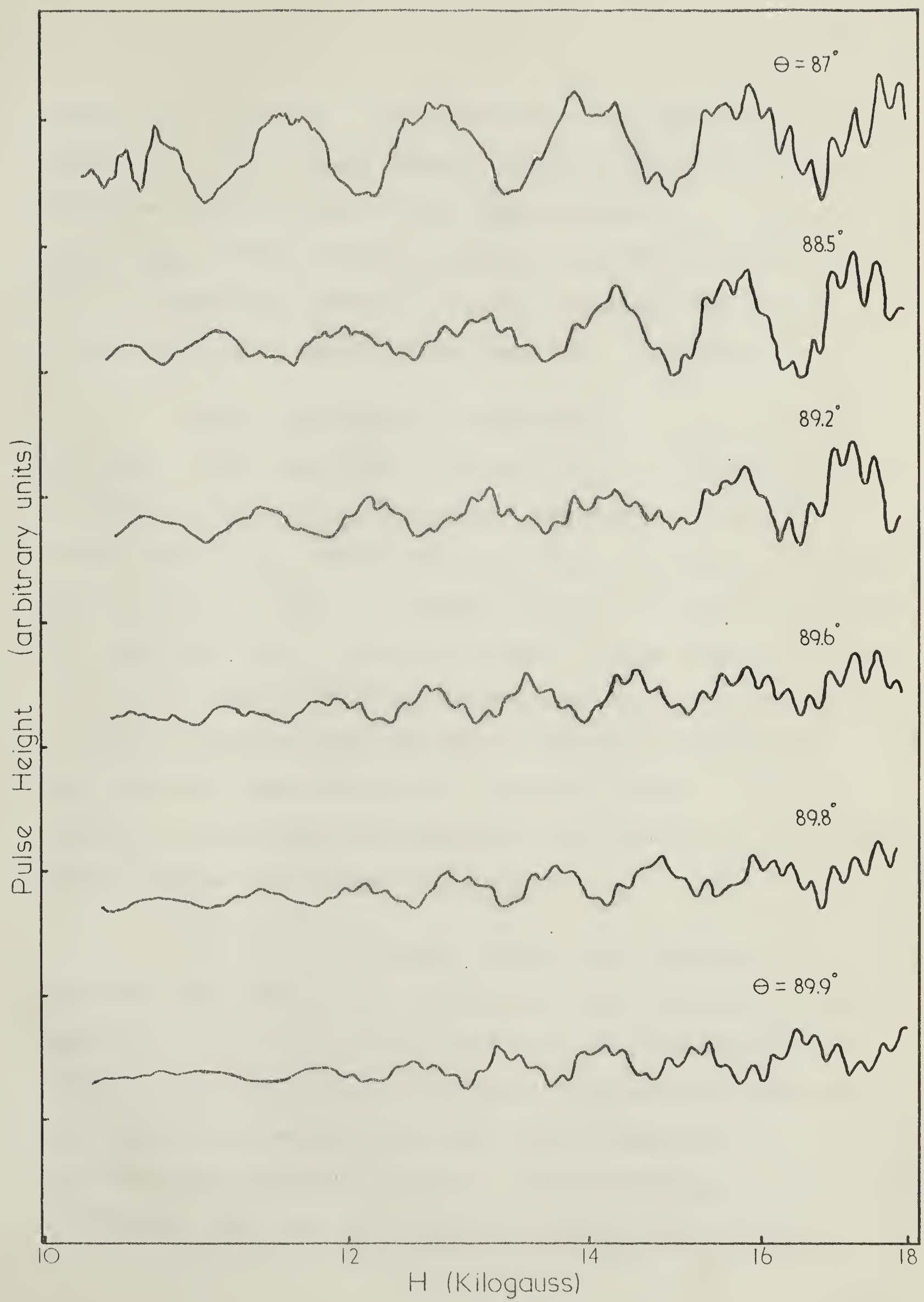
since the condition $(q\ell)^2 \gg 1$ is not satisfied). Instead, the amplitude of the oscillations remains constant when θ is in the range between zero and 87 degrees, and in the range from 87 to 90 degrees decreases as shown in figure 6.23, (shown also for bismuth in reference 30).

A possible explanation for this behaviour is outlined as follows. The amplitude of the oscillations decreases as the number of Landau levels participating simultaneously in the absorption increases. In accordance with the argument advanced on pages 46 and 47, the number will depend on $\omega\tau$ and the topology of the Fermi surface in the regions where the group velocity of the electrons satisfies $v_{gz} = v_s/\cos \theta$, rather than on the magnitude of $q_z \ell$ alone. As $\cos \theta$ decreases, v_{gz} increases. When $\cos \theta \sim 1/20$, then $v_{gz} \sim 20v_s$, and because $v_s = (1/200)v_f$, $v_{gz} \sim 1/10 v_f$. At this point, the plane in \bar{k} -space perpendicular to the magnetic field where the condition $v_{gz} = v_s/\cos \theta$ is satisfied has moved from a region where the Fermi surface tangent is nearly parallel to the Landau cylinders, to a region where there is an appreciable angle between the two. Since the phonon energy and the uncertainty of electron energies remain the same, the uncertainty Δv_{gz} of the electron group velocity is unchanged (neglecting $1/q_z \ell$ in comparison with $1/\omega\tau$). However, due to the changed topology of the Fermi surface in regions

FIGURE 6.23

Decrease in amplitude of oscillations in zinc as the angle θ between \bar{q} and \bar{H} approaches 90 degrees. \bar{H} is in the $(10\bar{1}0)$ plane, and \bar{q} is 3° from the (0001) axis. Full scale reading of the magnetic field trace is approximately 20 kilogauss. The long period arises from an α or "cigar" orbit, and the short period arises from a β -orbit, as shown in figure 6.23.

A similar decrease in amplitude occurs when θ approaches 90 degrees in the range above 90 degrees.



where $v_{gz} = v_s / \cos \theta$, the uncertainty Δv_{gz} may be sufficiently great that an increased number of Landau levels will intersect the Fermi surface in the range between $v_{gz} - \Delta v_{gz}$ and $v_{gz} + \Delta v_{gz}$. Thus for some orientation of \bar{H} and \bar{q} such that $\theta \sim 87$ degrees, and $\cos \theta \sim 1/20$, the amplitude of the oscillations will begin to decrease as θ increases.

Toxen and Tansal³⁰ attempted to relate a similar decrease of the amplitude in bismuth to the group velocity required to satisfy $v_{gz} = v_s / \cos \theta$ increasing beyond the Fermi velocity v_f . This would only occur when $\cos \theta \sim 1/200$, that is for $\theta \sim (90-0.1)$ degrees, whereas the amplitude change was observed when θ was much farther from 90 degrees. Toxen and Tansal suggest that the discrepancy could be reconciled if Skobov's theory were modified to include variation of the effective mass through the conduction band. It is difficult to see how any reasonable modification of this kind would achieve the necessary result.

As stated previously, it was not possible to determine the temperature variation of the oscillations with amplitude 2 to 5 decibel/cm which have been described above. Results were obtained only for oscillations with a maximum amplitude ~ 0.5 decibel/cm, which can be expected to be qualitatively different as well. (Measurements at 1.8 and 4.2°K do indicate that the large amplitude oscillations vary in

amplitude reciprocally with temperature, however they are not numerous enough to be conclusive). The amplitude of the small-amplitude oscillations was observed to vary with temperature in the same manner as de Haas-van Alphen oscillations, although the experimental uncertainty of the measurements is large. Figure 6.24 shows the temperature dependence of an A-oscillation (α or "cigar" orbit) when the magnetic field vector is approximately 85 degrees from the (0001) axis. A calculation of the effective mass yields the value 0.13 m, which is compatible with the value ~ 0.1 obtained by Joseph and Gordon³¹ at the same orientation. At this orientation it should be noted that the effective mass varies rapidly with field direction.

Measurements at 27, 45, and 63 magacycles/sec show that the amplitude of A, B and C oscillations increases linearly with sound frequency and thus with $q\ell$, in agreement with Skobov¹⁷ and with Toxen and Liu¹⁸. The amplitude of the oscillations was also observed to vary linearly with the magnetic field, as was the case for lower amplitude oscillations (de Haas-van Alphen) in magnesium. The Skobov theory predicts $H^{1/2}$ dependence when the condition $(\frac{E_f}{\hbar\omega})^c \gg (q_z\ell)^2 \gg 1$ is satisfied, and linear dependence when $(q_z\ell)^2 \gg (\frac{E_f}{\hbar\omega})^c$. For the oscillations observed for zinc, the former condition is satisfied, and thus the experimental behaviour does not support the Skobov prediction. For the results in magnesium, $q\ell \sim 1$, and this regime is not treated by the Skobov theory.

(iii) Effect of electron spin:

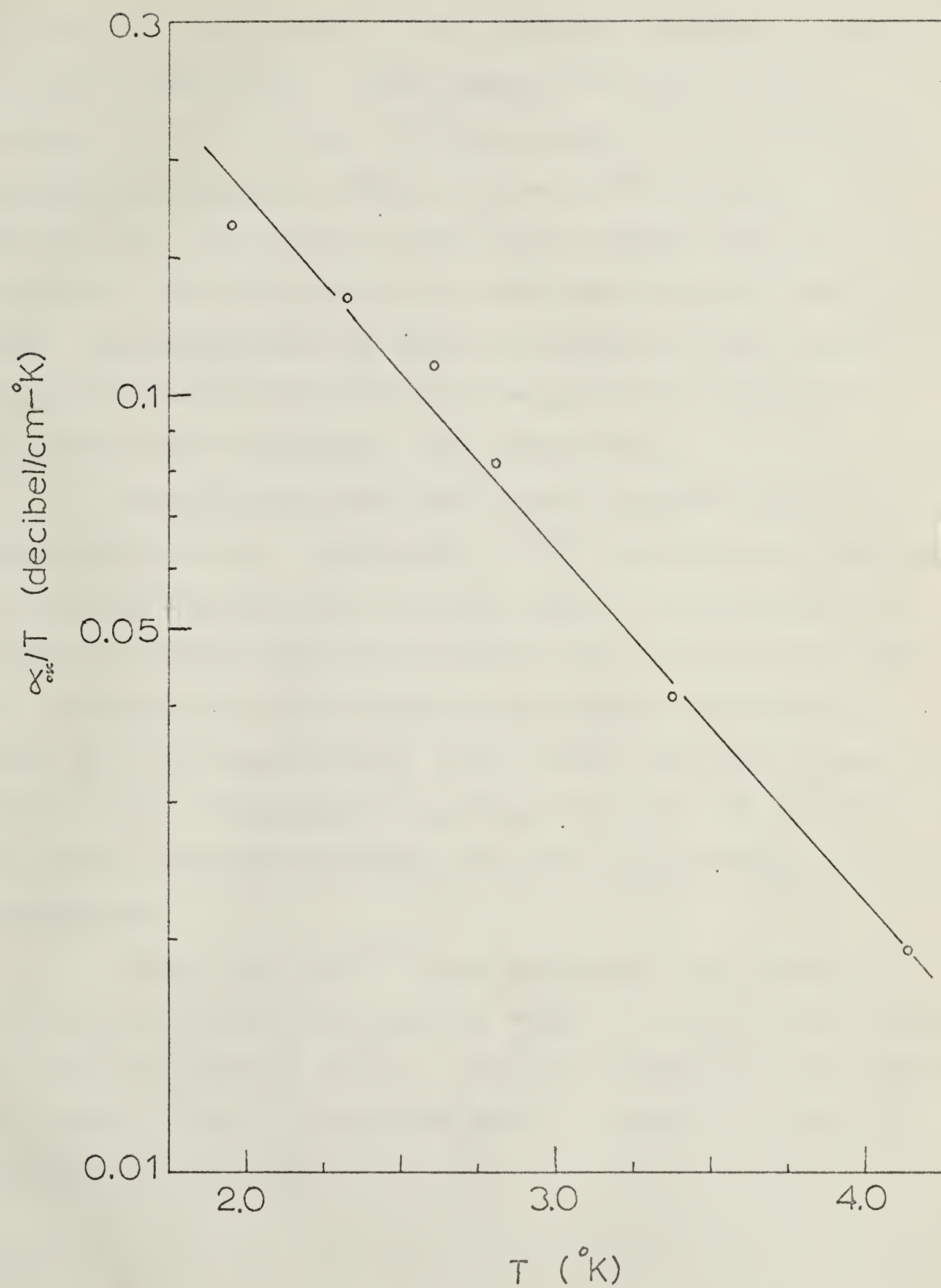
Several chart recordings show splitting of absorption maxima of the α -orbit oscillations in a very clear manner as in figure 6.18. This effect has been attributed to spin-splitting of the electron states. For the range of orientations of the magnetic field where the effect is observed, the effective mass for the α -orbit is ~ 0.01 m. In this case, the condition $(q_z \ell)^2 \gg \left(\frac{E_f}{h\omega_c}\right)$ is well satisfied, and the absorption pattern should be typical of quantum oscillations where at most electrons of a single Landau level participate.

Using equation 4.40, the g-factor calculated for the case shown in figure 6.18 is approximately 37, if the two sub-peaks of each absorption maximum coorespond to the same Landau level. Due to low amplitudes of the A-oscillations and large amplitudes of B and C oscillations, the absorption maxima can be accurately calculated only through a 30 degree range of the field orientation and even in this case the experimental uncertainty is fairly great. Within this range the spin-splitting remains constant. Bennett and Falicov⁽³⁵⁾ have calculated a theoretical g-value of 89 for the α -orbit with $\bar{H} \parallel (0001)$. For orientations of H within 70 degrees of the (0001) axis, Bennett and Falicov predict that the g-value will be the value $\bar{H} \parallel (0001)$ times $\cos \theta$, where θ is the angle between \bar{H} and the (0001) axis. Myers and Bosnell⁽³⁶⁾ have calculated the g-factor from spin-

FIGURE 6.24

 α/T vs. T

Temperature dependence of the amplitude of an α or "cigar" orbit oscillation in zinc. \bar{H} is 5 degrees from the (0001) axis.



splitting of oscillations of the ultrasonic absorption with \bar{H} in the (10 $\bar{1}$ 0) plane. Their results confirm the $\cos \theta$ variation and the g-value of 89 calculated for $\theta = 5^\circ$ is the same as the Bennett and Falicov value for $\bar{H} \parallel (0001)$. When $\theta = 60^\circ$, the g-value is 46, which compares with the g-value of 37 calculated for the spin-splitting of figure 6.18. (The discrepancy is within experimental error since uncertainty of the effective mass measurements required in the calculation is large at this orientation).

Since the effective mass of the α -orbit varies approximately as $\sec \theta$ ($\theta \neq 90^\circ$),^{32,35} the spin-splitting observed by Myers and Bosnell with θ in the range 0 to 70 degrees is constant (although they do not state this), which agrees with the behaviour observed in these experiments with θ in the range 60 to 90 degrees and \bar{H} in the (10 $\bar{1}$ 0) and 11 $\bar{2}$ 0 planes. Stark³⁷ has calculated the g-value to be 90, 180 or 360 for $\bar{H} \parallel (0001)$ from spin-splitting observed in galvanomagnetic measurements.

Shapira and Lax⁽¹⁹⁾ have calculated the g-factor for electrons in gallium and obtain a value of 30 for an orbit where the effective mass is 0.06 m. Toxen and Tansal⁽³⁰⁾ have observed spin-splitting of an absorption peak in bismuth, but did not calculate the g-factor.

CHAPTER VIISUMMARY AND CONCLUSIONS

Oscillations of sound attenuation that are periodic in the reciprocal of the magnetic field have been observed in copper, magnesium and zinc. The geometric oscillations observed in copper agree in all respects with theory and with experimental results that have appeared in the literature. Quantum oscillations of sound attenuation have been observed in magnesium and zinc. Periods of these oscillations agree closely with those observed by other workers for oscillations of the magnetic susceptibility. There are no observations noted in the literature of quantum oscillations of the sound attenuation in magnesium (nor of geometric oscillations). Quantum oscillations in zinc have been noted by other researchers, but have not been studied in any detail.

According to current theory, two types of quantum oscillations of the sound attenuation may be observed in a metal (as well as cyclotron resonance), depending on the mean free path of the electrons:

- (a) giant quantum oscillations, in which at most electrons of a single Landau level participate in the absorption, and

(b) oscillations similar to de Haas-van Alphen oscillations of the magnetic susceptibility, in which electrons of many Landau levels participate simultaneously.

Experimental results obtained in magnesium and zinc indicate that the nature of quantum oscillations which occur depends not only on the mean free path of the electrons but markedly on Fermi surface topology as well, a factor ignored in the present theories. As well as certain agreement, other discrepancies have also been noted between experimental results and the theory.

Information obtained from the experiments was limited by three factors:

- (a) magnitude of the sound frequency,
- (b) magnitude of the magnetic field, and
- (c) purity of the single crystal specimens.

The sound frequency can be increased by a factor of three or four if the present experimental apparatus is modified to include a separate receiving transducer. Greater improvement can be obtained in the second and third factors. An increase of magnetic field by a factor of five or more might be achieved with a superconducting solenoid. Specimen purity and thus mean free path of the electrons can be increased considerably. This can most easily be accomplished by performing

experiments on tin, in which a mean free path approaching one centimeter can now be obtained.

If these improvements were made, a great deal more information could be obtained. Calculations of the effective mass and g-factor of the electrons could be obtained from the line shape of absorption maxima. An interesting study could be made of the variation of the strength of the electron-phonon interaction with direction of the magnetic field.

BIBLIOGRAPHY

1. W. J. de Haas and P. M. van Alphen, Leiden Comm., 208d, 212a, (1930).
2. L. Onsager, Phil. Mag. 43, 1006 (1952).
3. I. M. Lifschitz and A. M. Kosevich, Zhur. Eksptl. i Teoret. Fiz. 29, 730 (1955).
4. A. B. Pippard, Rep. Prog. Phys. 23, 176 (1960).
5. G. E. H. Reuter, and E. H. Sondheimer, Proc. Roy. Soc. A195, 336 (1948).
6. G. Dresselhaus, A. F. Kip and C. Kittel, Phys. Rev. 98, 368, (1955).
7. W. Shockley, Phys. Rev. 90, 491 (1953).
8. R. G. Chambers, Phil. Mag. 1, 459, (1956).
9. A. B. Pippard, Phil. Trans. Roy. Soc. A250, 325 (1957).
10. R. Peierls, Ann. Phys. (Leipzig) 10, 97 (1931).
11. A. B. Pippard, Phil. Mag. 2, 1147 (1957).
12. V. L. Gurevitch, Soviet Physics JETP 1, 51 (1960).
13. M. H. Cohen, M. J. Harrison, and W. A. Harrison, Phys. Rev. 117, 937 (1960).
14. R. G. Chambers, Proc. Phys. Soc. (London) A65, 458 (1952); A258, 344 (1957).
15. V. L. Gurevitch, V. G. Skobov, and Yu. A. Firsov, Soviet Physics JETP 13, 552 (1961).
16. J. J. Quinn and S. Rodriguez, Phys. Rev. 128, 2487 (1962).
17. V. G. Skobov, Soviet Physics JETP 13, 1014 (1961).
18. A. M. Toxen and S. H. Liu, Phys. Rev. 138, A487 (1965).

19. Y. Shapira and B. Lax, Phys. Rev. 138, A1191 (1965).
20. S. Rodriguez, Phys. Rev. 130, 929 (1963).
21. D. N. Langenberg, J. J. Quinn, and S. Rodriguez, Phys. Rev. Letters 12, 104 (1964).
22. J. Adler, "The Effect of the Martensitic Transformation on the Thermoelectric Power of Sodium," Thesis, University of Alberta, (1960).
23. R. W. Morse, "The Fermi Surface," Conference Proceedings, (1960).
24. R. W. Morse, A. Myers, and C. T. Walker, J. Acoust. Soc. Am. 33, 699 (1961).
25. H. V. Bohm and V. J. Easterling, Phys. Rev. 128, 1021, (1962).
26. T. Kjeldaas and T. Holstein, Phys. Rev. Letters 2, 340, (1959).
27. W. C. Overton and J. Gaffney, Phys. Rev. 98, 969, (1955).
28. M. G. Priestley, Proc. Phys. Soc. (London) A276, 258, (1963).
29. W. L. Gordon, A. S. Joseph and T. G. Eck, "The Fermi Surface," Conference Proceedings, (1960).
30. A. M. Toxen and S. Tansal, Phys. Rev. 137, A211 (1965).
31. L. M. Falicov and M. H. Cohen, Phys. Rev. 130, 92 (1963).
32. A. S. Joseph and W. L. Gordon, Phys. Rev. 126, 489 (1962).
33. A. P. Korolyuk and T. A. Prushchak, Soviet Physics JETP 14, 1201 (1962).
34. D. F. Gibbons, Phil. Mag. 6, 445 (1961).
35. A.J. Bennett and L.M. Falicov, Phys. Rev. 136, A998 (1964)
36. A. Myers and J.R. Bosnell, Physics Letters 17, 9 (1965)
37. R.W. Stark, Phys. Rev. 135, A1698 (1964)

